ABSTRACT

Title of dissertation: MANIPULATING AND SIMPLIFYING THE INTERMOLECULAR INTERACTIONS IN LIQUID MIXTURES

Ang Gao, Doctor of Philosophy, 2017

Dissertation directed by: Professor John D. Weeks
Department of Chemistry and Biochemistry
Institute for Physical Science and Technology

Long ranged intermolecular interactions have significant influence on the structure of the liquid and present serious challenges for computer simulations. In particular, the long ranged tail of Coulomb interaction usually needs to be calculated using Ewald summation or related techniques in computer simulation, which can be too time consuming to be carried out for large systems. Local Molecular Field(LMF) theory has been developed to simplify long-ranged Coulomb and Van der Waals interactions for nonuniform liquids by approximating these long ranged interactions as effective static single-particle fields. Despite the success LMF theory made in describing the structure of nonuniform liquids, it is not appropriate to use LMF theory to describe the structure of uniform liquid mixtures, since the dynamically moving

unbalanced forces produced in mixture can not be captured by the framework of LMF theory. In this thesis, we propose a new framework which approximates the unbalanced forces produced in a mixture as effective intermolecular interactions. This new framework can simplify the long ranged intermolecular interactions and produce a mimic system with short ranged solvent-solvent interactions, which is much easier to simulate or analyze. Based on this framework and other techniques introduced in this thesis, we have constructed a " Short Solvent Model", which has noticeable advantages compared to the explicit solvent model and implicit solvent model. This framework has also been used to simplify the interactions of phase-separating mixtures. The impact of using this framework on the diffusion dynamics of the solutes has also been discussed. Possible application of this framework and the Short Solvent Model to biopolymers folding problems is briefly discussed.

MANIPULATING AND SIMPLIFYING THE INTERMOLECULAR INTERACTIONS IN LIQUID MIXTURES

by

Ang Gao

Dissertation submitted to the Faculty of the Graduate School of the
University of Maryland, College Park in partial fulfillment
of the requirements for the degree of
Doctor of Philosophy
2017

Advisory Committee:
Professor John D. Weeks, Chair/Advisor
Professor Christopher Jarzynski
Professor Silvina R. Matysiak
Professor Garegin Papoian
Professor Sergei Sukharev

Acknowledgements

I want to begin by thanking my advisor, Professor John Weeks, for guiding and supporting me through the last five years. I am really inspired by his great physical intuition and always enjoy discussing science with him. His dedication to science inspires me to further pursue my science career.

I would also like to thank Professors Chris Jarzynski, Garyk Papoian, Silvina Matysiak and Sergei Sukharev for serving on my committee. Their effort and time is much appreciated. I additionally want to thank Professors Michael Coplan, Garyk Papoian and Chris Jarzynski for the guidance and help they have provided as Director and Associate Director of the Chemical Physics graduate program. I am also very grateful for the help Debbie Jenkins and Maritza Montelara have provided over the years.

I would also like to thank the current and past members of the Weeks group. In particular, Rick Remsing helped a lot for getting me started and is always really helpful during my graduate study. I also enjoy working with current Weeks group member Teddy Baker, and I am looking forward to future collaborations with him. I also want to thank Guang Shi, Jocelyn Rodgers and Zhonghan Hu for many inspiring discussions.

I also would like to thank Professor Lawrence Pratt and his students for the collaborations during the past years, which led to the work shown in Chapter 4. I also want to thank Chris Jarzynski and Robert Dorfman for the inspiring discussions

about my work on linear response theory, which led to the work shown in Appendix E.

I also would like to thank a past member of the Jarzynski group – Zhiyue Lu, especially for helping me settle down when I first came to Maryland.

Finally, I would like to thank my parents for supporting me through my life.

Funding from NSF (CHE1300993) is gratefully acknowledged.

Table of Contents

List of Figures vi

List of Abbreviations viii

1 Introduction and Overview 1

2 Local Molecular Field Theory 11
- 2.1 Motivation . . . 11
- 2.2 Exact Starting Point of LMF Theory . . . 13
- 2.3 Approximations to Yield the LMF Equation . . . 14
- 2.4 Strategies for Closing the Self-Consistent LMF Loop . . . 15
- 2.5 Separate Coulomb Interaction and Apply LMF Theory . . . 16
- 2.6 Conclusions . . . 20

3 Manipulating the Intermolecular Interactions of Dilute Solutions 21
- 3.1 Framework and Derivation . . . 22
  - 3.1.1 Framework . . . 22
  - 3.1.2 Derivation . . . 28
- 3.2 Manipulating the Van der Waals Attractions for Apolar Solutes in Water . . . 33
  - 3.2.1 C_{60} in water . . . 36
  - 3.2.2 Argon in Water, Pratt-Chandler Theory and Inverse Temperature Behavior . . . 42
  - 3.2.3 Hard-Sphere-Like Solutes in Water . . . 45
- 3.3 Manipulating the Coulomb Interactions . . . 51
- 3.4 Conclusions . . . 57

4 Effects of the Long Ranged Component of Solute-Solvent Interactions On the Association of Solutes 58
- 4.1 Derivations . . . 62
- 4.2 Conclusions . . . 68

5 A Short Solvent Model 69
- 5.1 Effective Solute-Solute Interactions For the SSM . . . 71
- 5.2 Na-Cl PMF in water . . . 79
- 5.3 Conclusions . . . 84

6 Finite Density Solutions 86
- 6.1 Simplifying The Interactions For Phase-Separating and Well-Mixed Solutions . . . 86
- 6.2 Conclusions . . . 94

7 Diffusion Dynamics of Solutes in the Target and Mimic System 95
7.1 Mathematical Framework for Describing the Diffusion Dynamics . . . 95
7.2 Short Time Behavior of Diffusion Dynamics 98
7.3 Conclusions 103

8 Conclusions and Future work 107

A The correspondence between the interactions and correlation functions for mixtures 113

B Deriving the interactions in the mimic system from a free energy perspective 122

C Linear response theory for nonequilibrium reference systems 129
C.1 Review of Linear Response Theory 130
C.2 Nonequilibrium Reference System And Local Equilibrium 132
C.3 Linear response theory for nonequilibrium reference system 134
C.4 Simulation Result 138
C.5 Conclusion 141

Bibliography 143

List of Figures

1.1 Particles near a hard wall 4
1.2 Illustration of the fixing technique 6

2.1 Separation of LJ interaction 12
2.2 Separation of Coulomb interaction 17
2.3 Comparison of RDFs of different water models 18

3.1 Illustration of the manipulated solute-solvent vdW interactions 37
3.2 Illustration of the manipulated solute-solute vdW interactions 38
3.3 Fullerene-water and fullerene-fullerene interaction in the target and mimic system 40
3.4 Structure of the fullerene-water solution in the target, mimic and repulsive-core system 41
3.5 Interactions of Argon-water solution 43
3.6 Structure of the Argon-water solution in the target, mimic and repulsive-core system 44
3.7 Inverse temperature behavior of Argon association in water 46
3.8 Interactions of WCA Argon-water solution 49
3.9 Structure of the WCA Argon-water solution in the target, mimic and repulsive-core system 50
3.10 Interactions of repulsive core fullerene-water solution 52
3.11 Structure of the repulsive core fullerene-water solution in the target, mimic and repulsive-core system 53
3.12 Illustration of the evaporation behavior between two repulsive-core fullerenes 54

4.1 Full solutes and reference solutes 60
4.2 PMF and the reversible work of turning on the solute-solvent long ranged interaction 61
4.3 Partially Coupled Solute Dissolved In Solvent 63
4.4 Verify linear approximation for perturbed densities 66
4.5 Effects of Argon-water attraction on Argon-Argon association 67

5.1 The Short Solvent Model 72
5.2 The two step process to get the effective ion-ion interactions 77
5.3 Effective Na-Cl interaction with Periodic Images Taken Into Account 81
5.4 Effective Na-Cl interaction with periodic boundary effects taken into account 83
5.5 Na-Cl PMF of the SSM 84

6.1 Phase separating mixture 88

6.2 Two step mapping for the phase separating mixture 91
6.3 The mimic phase separating mixture 92
6.4 Coulomb-like mixture 93

7.1 Velocity autocorrelation function of fullerene in water 102
7.2 Velocity autocorrelation function of the repulsive core of fullerene in water 104
7.3 Velocity autocorrelation function of Na and Cl ion in water 105

8.1 Polymer in water and free mobile monomers in water 109

B.1 Relationship of free energies and N-body potential of mean forces . . 125
B.2 Free energy cost of changing the interactions of bulk solvent 126

C.1 Drying potential 140
C.2 Time dependent density of the drying process 142

List of Abbreviations

LMF	Local Molecular Field
LJ	Lennard-Jones
WCA	Weeks-Chandler-Andersen
YBG	Yvon-Born-Green
HS	Hard-Sphere
HB	Hydrogen bond
SPC/E	Extended simple point charge
GT	Gaussian-truncated
GTRC	Gaussian-truncated repulsive-core
NPT	Isothermal-isobaric; constant number of particles, pressure, and temperature
NVT	Canonical; constant number of particles, volume, and temperature
NVE	Microcanonical; constant number of particles, volume and energy
MF	Mean Field
MD	Molecular dynamics
vdW/VDW	van der Waals
LRT	Linear Response Theory
PMF	Potential of mean force
RDF	Radial distribution function
VCF	Velocity autocorrelation function
PME	Particle mesh Ewald
SCA	Strong-coupling approximation

Chapter 1

Introduction and Overview

In 1873, van der Waals proposed the famous van der Waals(vdW) equation in his thesis [1]. The vdW equation,

$$P = \frac{Nk_BT}{V - Nb} - a\frac{N^2}{V^2}\,, \tag{1.1}$$

generalized the equation of state for ideal gas by taking the pair interactions between molecules into account. Remarkably, van der Waals separated the pair interaction into the short ranged harshly repulsive interaction and the long ranged slowly varying attractive interaction. According to the modern interpretation of vdW equation [2,3], the short ranged repulsive interactions determine the excluded volume of the molecule, described by the b parameter in the van der Waals equation of state, while the average effect of the long ranged attractive interactions merely contributed an uniform external field exerting no net force, whose strength was determined by the a parameter in the van der Waals equation. The vdW equation successfully predicted the liquid-vapor coexistence and even the existence of the critical point. Moreover, the philosophy of separating the interactions and regarding the long ranged interactions as an uniform field has a deep influence for the liquid theory afterwards, and it is called the vdW picture nowadays.

When studying the structure of simple liquids, Widom [2] pointed out that

the vdW picture should be especially accurate when the thermodynamic state of the liquid is near the triple point, where the fluid particles are densely packed. Widom made two observations to support his argument. First of all, in a dense liquid, the excluded volume of the particles mainly determines how they are packed. Secondly, the force cancellation argument, which claims that the attractive forces exerted on a particle come from all directions and thus tend to cancel with each other, should work better in the densely packed limit. Widom's argument was further exploited and tested by the Weeks-Chandler-Andersen(WCA) theory [3], which quantitatively confirmed that the short ranged harshly repulsive interaction alone is able to determine to a very good approximation the bulk structure of a simple liquid. Moreover, Widom's argument and WCA theory can also be very accurately generalized to deal with Coulomb interactions. It has been shown that with the Coulomb interaction appropriately separated into a rapidly varying short ranged part and a slowly varying long ranged part, the short ranged part itself is able to very accurately determine the structure of the liquid, and this has been verified for complex fluids such as liquid water and liquid acetonitrile [4, 5]. Some details will be given later in this thesis.

Although the slowly varying long ranged forces nearly cancel in typical uniform bulk configurations, they could produce a net unbalanced force in the nonuniform state. For example, LJ particles near a hard wall are subject to attractive forces from other particles in the bulk direction, which will form a net "drying" force pulling

these interfacial particles away from the wall. Therefore, at nonuniform state, the attractive force can no longer be neglected in the way proposed by WCA theory. This motivated the development of Local Molecular Field(LMF) theory [6–9], which quantitatively figured out that the unbalanced force produced in the nonuniform state can be replaced by a nonuniform effective single-particle external field. For example, in the LMF treatment, the drying force near the hard wall is envisioned as arising from a static effective external field associated with a "renormalized" wall, as illustrated in Figure 1.1. LMF theory has been used to describe the structure of nonuniform LJ fluid and water in many applications, which gives results with excellent accuracy [10–13]. The details about LMF theory can be found in Chapter 2.

Despite the success LMF theory made in describing the structure of nonuniform liquid, for uniform liquid it would seem to say the same thing as what vdW picture and WCA theory said, which is that the long ranged interactions have no effect on the structure of uniform liquids and can be replaced by a uniform external field.

However, for uniform liquid mixtures the long ranged interactions do have important influence on the structure. For example, it is well known that the vdW attractions could greatly affect the hydration of water molecules around the apolar solutes and the hydrophobic association of these solutes [14, 15]. In fact, even for uniform mixtures, *unbalanced forces* will be produced by long ranged interactions

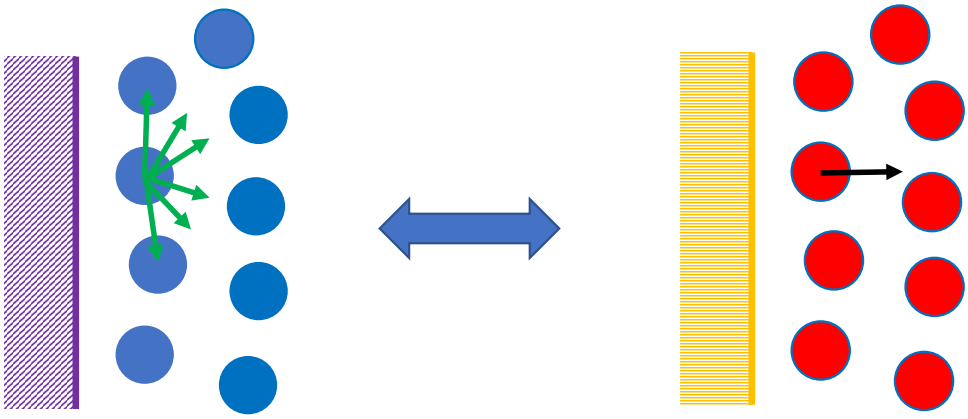

Figure 1.1: The left panel shows Lennard-Jones particles near a hard wall. The LJ particles near the wall feel attractions from other particles, denoted by the green arrow, which pull the particles away from the wall. The right panel shows harshly repulsive WCA particles near a "renormalized" wall. The renormalized wall potential not only includes the hard wall potential, but also includes a "drying" potential determined by LMF theory, which pushes the WCA particles away from the wall. The average force exerted on the particles as determined by LMF equations in the two panels is the same.

between different species. Consider the famous example of two mobile hard sphere solutes in water [14]. Here water molecules near the hard sphere solutes will always feel a net drying force produced by the water-water vdW attractions pulling water molecules away from the hard sphere solute, and most noticeably this drying force will move with the solutes as the solutes diffuse around. The *dynamic nature* of the unbalanced forces produced in mixture makes it impossible to describe them as static external fields. One trick to partially avoid this difficulty is to fix one of the solutes in space, and many previous applications of LMF theory [4, 16, 17] have used this idea. By doing this the uniform system is transformed into a nonuniform system. The unbalanced force associated with the fixed solute is also fixed along with it and can be described by an effective static external field using LMF theory. This solute has thus become a "wall-particle", like the hard wall we mentioned before. An illustration of the fixing technique is shown in Figure 1.2. Although by using this technique we can correctly describe the unbalanced force around the fixed solute using LMF theory, the unbalanced force around all the other mobile solutes still can not be correctly captured. This asymmetric treatment of mobile solute components shows one significant limitation of the current implementation of LMF theory, which is that within its framework the unbalanced forces have to be approximated as effective static external fields. However, for uniform mixtures, based on the observation that the unbalanced forces always move with particles, it is more appropriate to approximate these unbalanced forces as arising from *renormalized or effective pair*

interactions between particles. Based on this philosophy, we propose a new theory to describe the unbalanced force produced by long ranged interactions in uniform mixtures, and the rest of this thesis is focused on demonstrating this new theory.

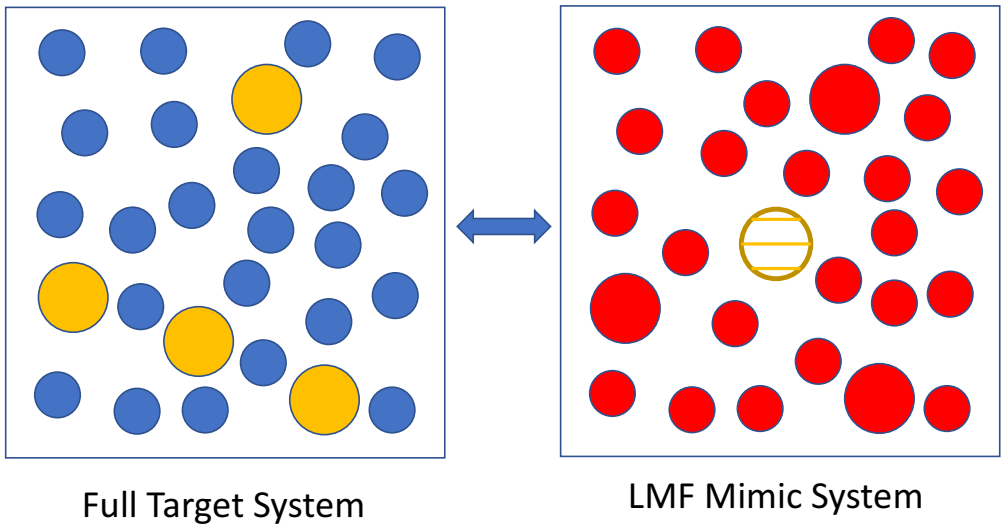

Figure 1.2: Asymmetric treatment of mobile solutes in the current version of LMF theory. The left panel shows an uniform LJ mixture with two mobile components. The large sphere is the solute and the small sphere is the solvent. In the right panel, one of the solutes is fixed at origin. The unbalanced forces around the fixed solute are approximated as an effective external field by LMF theory. All the other solutes and all the solvent particles are taken as WCA cores, denoted by the red sphere.

The new theory we want to propose can be formulated as a mathematical framework to manipulate the slowly varying long ranged pair interactions without significantly changing the structure of the mixture. These manipulations can potentially simplify the interactions between particles and provide insight about how the

long ranged interactions affect the structure of mixture. As an example to demonstrate our theory, let us consider a mixture composed of single-atom molecules. Suppose the interactions between these species are labeled as $u_{\mathrm{MM}'}(r)$, which can be separated into short and long ranged parts

$$u_{\mathrm{MM}'}(r) = u_{0,\mathrm{MM}'}(r) + u_{1,\mathrm{MM}'}(r). \tag{1.2}$$

We want to change the long tails of the $u_{\mathrm{MM}'}(r)$ in the following way

$$u_{\mathrm{MM}'}(r) = u_{0,\mathrm{MM}'}(r) + u_{1,\mathrm{MM}'}(r) \Longrightarrow u_{R,\mathrm{MM}'}(r) = u_{0,\mathrm{MM}'}(r) + u_{R1,\mathrm{MM}'}(r) \tag{1.3}$$

but keep the structure, or more precisely the radial distribution function of the mixture $g_{\mathrm{MM}'}(r)$ essentially unchanged.

This new set of interactions $\{u_{R,\mathrm{MM}'}(r)\}$ defines a new system, which we will call "mimic system" since it mimics the structure of the original or "target" system. At first glance, it might seem that we do not have any choice but to make

$$u_{R,\mathrm{MM}'}(r) = u_{\mathrm{MM}'}(r) \tag{1.4}$$

in order to keep the structure unchanged. However, we have shown that when there is a dominant solvent species, denoted as A, in the mixture, we can choose the long ranged interaction $u_{R1,\mathrm{AA}}(r)$ freely with almost no effect on the radial distribution function $g_{\mathrm{AA}}(r)$, since the force cancellation argument can be applied to the dominant solvent species. The other long ranged interactions in the mimic system, including the solute-solvent and solute-solute long ranged interactions, are

effective interactions which should be obtained by matching the unbalanced forces produced in the target and mimic system, similar to what is done in the current LMF theory. The detailed procedures are shown in Chapter 3.

The extra freedom in choosing $u_{R1,\mathrm{AA}}(r)$ makes it possible for us to find manipulations which could simplify the interactions to make both theoretical analysis and computer simulation easier. The simplest and often most useful choice is a *truncated solvent model* where $u_{R1,\mathrm{AA}}(r)$ is chosen to be 0. This can prove especially useful for solvents like water with long ranged Coulomb interactions, where standard treatments require costly Ewald sums [18]. A detailed discussion is given in Chapter 3.

By taking advantage of the slowly varying nature of the long ranged solute-solvent interactions, we have designed a method which can quantitatively determine the contribution from the solute-solvent long ranged interactions to the solute-solute PMFs. This method has been used to study the association of apolar solutes in water, which gives results that could clarify how the solute-solvent vdW attractions affect the hydrophobic associations [14, 15, 19], as discussed in Chapter 4.

By combining the method developed in Chapter 3 and 4, we are able to construct a "Short Solvent Model". In this Short Solvent Model, the solvent-solvent and solute-solvent Coulomb interactions are truncated, and the only long ranged interactions are between the solutes. Since solutes are usually the dilute species in most bio-environments, this model should be much faster to simulate than the

explicit solvent model. Also, since this model preserves local hydrogen bond structures, it should be much more accurate than an implicit solvent model [20] where dielectric screening is taken into account by models related to dielectric continuum theory.

For mixtures without a dominant species, such as a binary 50-50 mixture, we could not manipulate interactions as described above any more. Moreover, due to the more complicated coupling between structure and interactions, we believe that we can not make any changes to the interactions if we want to keep all pair correlation functions of the finite-density mixture essentially unchanged. However, if we just try to keep the structure of certain parts or components instead of the whole system unchanged, we are granted freedom to manipulate the long tails of interactions, and this extra degree of freedom makes it possible for us to find manipulations which could simply the analysis. This idea has been tested by applying it to model systems which have LJ-type interactions. Depending on the thermodynamic state and the interactions chosen, the model system may separate into several distinct phases. Using our framework, we could simplify the interactions of the model system and construct a mimic system exhibiting the same phase separating behavior. Remarkably, the mimic system has the same capillary wave fluctuations at phase boundaries as the target system, which is a feature not captured by LMF- or Density Functional Theory- based approaches [21, 22]. The details can be found in Chapter 6.

Our manipulation of interactions is designed to preserve the structure of the mixture. The influence of the manipulation on the dynamics of the liquid is also explored, and analytically we have shown that the short time behavior of the diffusion dynamics of the solutes is to a good approximation unaffected by our manipulation of interactions. Computer simulations are conducted to verify our argument. Detailed discussions can be found in Chapter 7.

Conclusions and possible applications of our theory to biopolymer folding problems are briefly discussed in Chapter 8.

Chapter 2

Local Molecular Field Theory

2.1 Motivation

The motivation of LMF theory comes from applying WCA theory to a nonuniform Lennard-Jones(LJ) liquid. For uniform LJ liquid, WCA theory has shown that it is beneficial to separate the LJ interaction into a short ranged, repulsive WCA interaction and a long ranged, attractive tail [3]. More precisely,

$$u(r) = 4\epsilon\{(\frac{\sigma}{r})^{12} - (\frac{\sigma}{r})^{6}\} \tag{2.1}$$

is separated into

$$u_0(r) = \begin{cases} u(r) + \epsilon & \text{if } r < r_0 \\ 0 & \text{otherwise} \end{cases} \tag{2.2}$$

and

$$u_1(r) = \begin{cases} -\epsilon & \text{if } r < r_0 \\ u(r) & \text{otherwise} \end{cases}, \tag{2.3}$$

where $r_0 = 2^{1/6}\sigma$ is the position of the minimum of the LJ potential. As shown in Figure 2.1 the corresponding WCA liquid is a very good approximation to the bulk structure of LJ liquid. The reason WCA theory works well is because long ranged attractive forces exerted on the particles come from all directions and thus cancel

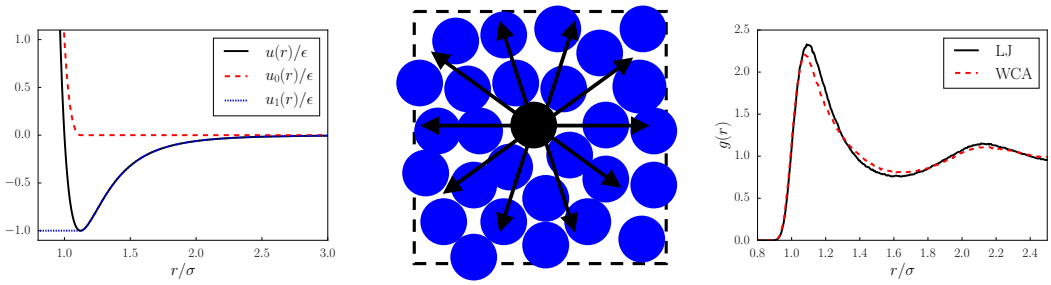

(a) **(b)** **(c)**

Figure 2.1: (a) Separate the LJ potential into short ranged harshly repulsive WCA interaction and long ranged attraction tail. (b) An illustration of the force cancellation argument. As one can see the attractive forces exerted on a particle cancel with each other. (c) Comparison of the radial distribution function for the LJ fluid and corresponding WCA fuild. The thermodynamic state of the fluid is $\rho\sigma^3 = 0.65$ and $k_BT/\epsilon = 1.0$.

with each other, as illustrated in Figure 2.1. Thus the repulsive core itself is enough to determine the structure of the liquid. However, for LJ liquids in nonuniform environments, net unbalanced forces could be produced by these attractive forces. For example, for LJ fluid confined by hard walls, the particles near the wall will be pulled toward the bulk by the long ranged attractive forces from other particles, thus forming a vapor-like interface near the wall. The corresponding WCA fluid does not have this property. LMF theory tries to solve this problem by introducing an effective external field to account for the unbalanced force produced by long ranged interactions. More precisely, for a nonuniform system with pair potential $u(r) = u_0(r) + u_1(r)$ and external field $\phi(\boldsymbol{r})$, LMF tries to map this target system to

a mimic system with the repulsive core interaction $u_0(r)$ and a renormalized external field $\phi_R(\boldsymbol{r})$. An illustration of this LMF mapping is

$$\left\{ \begin{array}{c} u(r) \\ \\ \phi(\boldsymbol{r}) \end{array} \right\} \Longrightarrow \left\{ \begin{array}{c} u_0(r) \\ \\ \phi_R(\boldsymbol{r}) \end{array} \right\}. \tag{2.4}$$

The renormalized potential $\phi_R(\boldsymbol{r}\,)$ is chosen such that the nonuniform singlet density of the target system matches that of the "mimic" system,

$$\rho(\boldsymbol{r};[\phi]) = \rho_R(\boldsymbol{r};[\phi_R])\,. \tag{2.5}$$

2.2 Exact Starting Point of LMF Theory

To find out the appropriate $\phi_R(\boldsymbol{r})$, our philosophy is to match the average forces exerted on the particles in the target and mimic system [11, 23]. We start from the Yvon-Born-Green hierarchy of equations [24] for both systems, which are

$$k_BT\nabla \ln \rho(\boldsymbol{r};[\phi]) = -\nabla\phi(\boldsymbol{r}) - \int d\boldsymbol{r}'\rho(\boldsymbol{r}'|\boldsymbol{r};[\phi])\nabla u(|\boldsymbol{r}-\boldsymbol{r}'|) \tag{2.6}$$

and

$$k_BT\nabla \ln \rho_R(\boldsymbol{r};[\phi_R]) = -\nabla\phi_R(\boldsymbol{r}) - \int d\boldsymbol{r}'\rho_R(\boldsymbol{r}'|\boldsymbol{r};[\phi_R])\nabla u_0(|\boldsymbol{r}-\boldsymbol{r}'|) \tag{2.7}$$

respectively. $\rho(\boldsymbol{r}'|\boldsymbol{r};[\phi])$ is the density at $\boldsymbol{r}'$ given a particle is fixed at $\boldsymbol{r}$. $-k_BT\nabla \ln \rho(\boldsymbol{r};[\phi])$ can be interpreted as the average force felt by the particle at position $\boldsymbol{r}$. The right hand side of both equations shows the sources of forces, which include the external field and the mutual interaction of particles.

We want to choose $\phi_R(\boldsymbol{r})$ such that the singlet density is the same in the target and mimic system. Assuming the existence of such a $\phi_R(\boldsymbol{r})$, we can subtract both equations and get the following formally exact equation

$$\begin{aligned}\nabla\phi_R(\boldsymbol{r}) = \nabla\phi(\boldsymbol{r}) &+ \int d\boldsymbol{r}'\rho_R(\boldsymbol{r}';[\phi_R])\nabla u_1(|\boldsymbol{r}-\boldsymbol{r}'|) \\ &+ \int d\boldsymbol{r}'(\rho(\boldsymbol{r}'|\boldsymbol{r};[\phi]) - \rho_R(\boldsymbol{r}'|\boldsymbol{r};[\phi_R]))\nabla u_0(|\boldsymbol{r}-\boldsymbol{r}'|) \\ &+ \int d\boldsymbol{r}'(\rho(\boldsymbol{r}'|\boldsymbol{r};[\phi]) - \rho(\boldsymbol{r}';[\phi]))\nabla u_1(|\boldsymbol{r}-\boldsymbol{r}'|)\,.\end{aligned} \tag{2.8}$$

2.3 Approximations to Yield the LMF Equation

Eq.(2.8) is still an exact equation, but it shows the terms to be approximated explicitly. LMF theory claims that the line 2 and 3 in Eq.(2.8) should be approximately 0. The validity of these approximations is explained as follows.

Line 2 probes the difference between the conditional density in the full and mimic system over the range of the short ranged potential $u_0(r)$. We claim this difference to be approximately 0. Since a good choice of $u_0(r)$ provides an accurate description of nearest neighbor interactions, combined with the fact that the singlet density is captured by construction in the mimic system, the conditional density should also be approximately captured in the mimic system.

The integrand of line 3 involves the difference between the conditional density and singlet density. This difference is not zero in general, but we are saved by the fact that it is integrated with the gradient of the long tail. Since $u_0(r)$ is chosen to encompass the repulsive core interactions, we will have $\nabla u_1(|\boldsymbol{r}-\boldsymbol{r}''|) \approx 0$ inside the

"hard core distance", which is exactly the range where the conditional density and the singlet density differ the most. Thus it is reasonable to expect the integrand in line 3 to be approximately 0.

These approximations yield the LMF equation

$$\phi_R(\boldsymbol{r}) = \phi(\boldsymbol{r}) + \int d\boldsymbol{r}' \rho_R(\boldsymbol{r}'; [\phi_R]) u_1(|\boldsymbol{r} - \boldsymbol{r}'|) + C\,. \tag{2.9}$$

C is an integral constant, which can be chosen such that $\phi_R(\boldsymbol{r}) \to 0$ when $r \to \infty$ and will give us

$$\phi_R(\boldsymbol{r}) = \phi(\boldsymbol{r}) + \int d\boldsymbol{r}' \big(\rho_R(\boldsymbol{r}'; [\phi_R]) - \rho_b\big) u_1(|\boldsymbol{r} - \boldsymbol{r}'|)\,. \tag{2.10}$$

ρ_b is the bulk density of the fluid.

2.4 Strategies for Closing the Self-Consistent LMF Loop

As shown in Eq.(2.10), one needs the knowledge about $\rho_R(\boldsymbol{r}'; [\phi_R])$ to determine $\phi_R(\boldsymbol{r})$. However, one also needs the knowledge about $\phi_R(\boldsymbol{r})$ to determine $\rho_R(\boldsymbol{r}'; [\phi_R])$. This means that Eq.(2.10) is a self consistent equation. To solve Eq.(2.10) one apparently needs to start from an initial guess and solve Eq.(2.10) iteratively. However, Hu and Weeks applied linear response method to do the iteration, which could greatly accelerate the whole process. The details can be found in [12].

The accuracy of Eq.(2.10) has been tested in many places. For example, Ref [12]compares the density of LJ fluid around a hard sphere cavity and the density

of the WCA fluid subject to the LMF external field defined in Eq.(2.10). The nonuniform density of these two systems shows excellent agreement. More examples can be found in [12].

2.5 Separate Coulomb Interaction and Apply LMF Theory

In previous sections we have discussed how to truncate LJ interactions and use LMF theory to account for the unbalanced forces coming from the truncated long tails. For more complex molecules, the mutual interaction usually includes not only LJ interaction, but also Coulomb interactions. Well known examples are the classical water models such as SPC/E [25] and TIP/5P [26]. Analogous to the separation of LJ interactions, previous research [4] has shown that it is useful to separate the Coulomb potential into short ranged and long ranged parts

$$v(r) = \frac{1}{r} = \frac{\mathrm{erfc}(r/\sigma)}{r} + \frac{\mathrm{erf}(r/\sigma)}{r} \equiv v_0(r) + v_1(r)\,, \tag{2.11}$$

where $\mathrm{erf}(r)$ and $\mathrm{erfc}(r) = 1-\mathrm{erf}(r)$ are the error and complementary error functions. The parameter σ is usually chosen on the order of the nearest neighbor distance between charges. Fig 2.2 shows the separation schematically. $v_1(r)$ can be viewed as the potential generated by a unit Gaussian charge distribution with width σ

$$v_1(r) = \frac{1}{\sigma^3\pi^{3/2}} \int d\boldsymbol{r}' \frac{e^{-(r'/\sigma)^2}}{|\boldsymbol{r}-\boldsymbol{r}'|}. \tag{2.12}$$

Similarly, $v_0(r)$ can be viewed as a unit point charge shielded by a negative unit Gaussian charge distribution

$$v_0(r) = \int d\boldsymbol{r}' \Big[\delta(r') - \frac{e^{-(r'/\sigma)^2}}{\sigma^3\pi^{3/2}}\Big] \frac{1}{|\boldsymbol{r} - \boldsymbol{r}'|} \,. \tag{2.13}$$

Short water models based on this Gaussian truncation scheme have been developed.

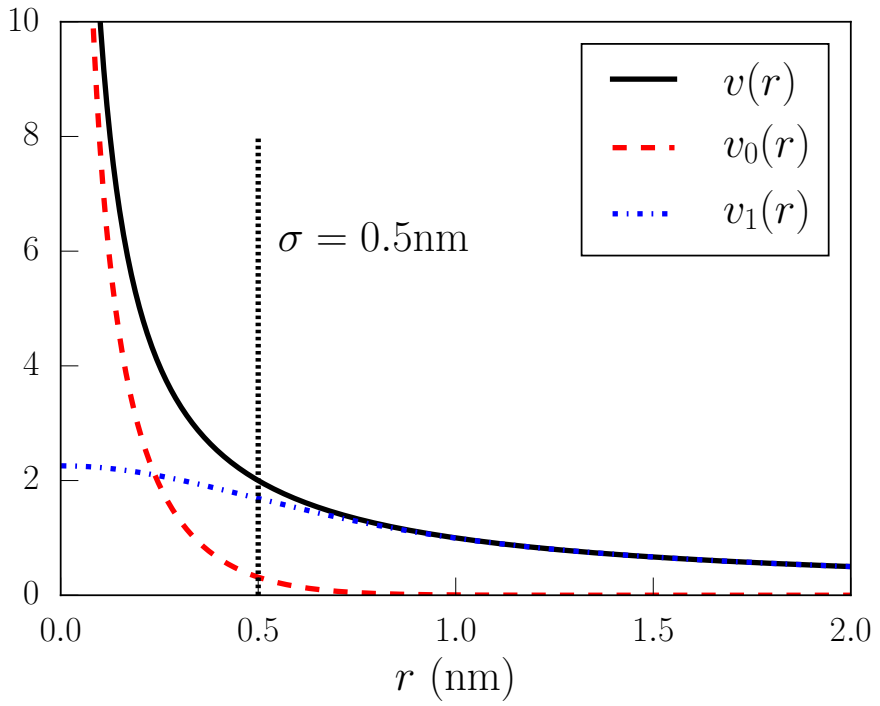

Figure 2.2: Separate the Coulomb interaction $v(r) = \frac{1}{r}$ into short ranged part $v_0(r) = \frac{\mathrm{erfc}(r/\sigma)}{r}$ and long ranged part $v_1(r) = \frac{\mathrm{erf}(r/\sigma)}{r}$. σ is chosen to be 0.5nm in this case.

The Gaussian Truncated (GT) water model [11] has Gaussian truncated electrostatic interaction and full LJ interaction between water molecules. The Gaussian Truncated Repulsive Core (GTRC) water model [27] has Gaussian truncated electrostatic

interaction and WCA interaction between water molecules. Previous research [11,27] has shown that both GT and GTRC water model can give a good description of the bulk properties of water, because that long ranged forces tend to cancel in uniform systems. The comparison of the the radial distribution function of these short water models with the full SPC/E water model is shown in Fig 2.3. In nonuniform

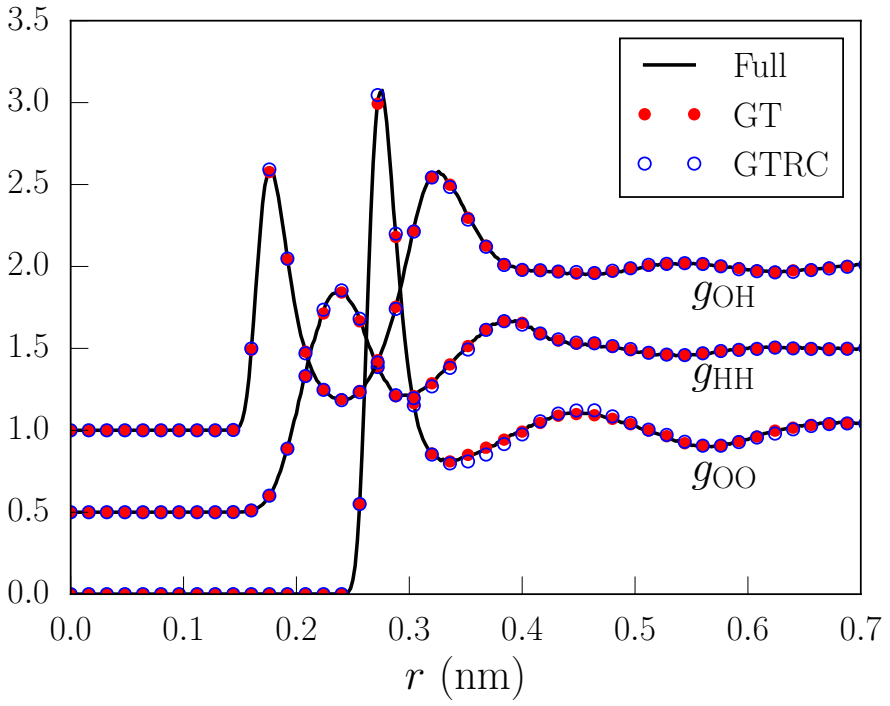

Figure 2.3: Comparison of the radial distribution function of SPC/E, GT and GTRC water. $g_{OO}(r)$ represents the RDF between Oxygen sites. $g_{OH}(r)$ represents the RDF between Oxygen and Hydrogen site. $g_{HH}(r)$ represents the RDF between Hydrogen sites. The Gaussian truncation parameter σ is chosen to be 0.5nm in this case.

systems, the long ranged tail of the Coulomb interaction could produce unbalanced

forces. For example, Ref [11] shows the Gaussian smoothed charge density, which is a useful quantity to characterize the dielectric properties of liquids, of SPC/E water and GT water confined between two hard walls. The SPC/E water model and the corresponding GT water model has obviously different Gaussian smoothed charge density, which indicates that the long ranged tail of the Coulomb interaction is vital for the dielectric properties of nonuniform liquid.

The effect of the long ranged tail of Coulomb interaction could also be taken into account by LMF theory. For a system interacting with Coulomb interaction $v(r)$ and external electric field $\mathcal{V}(\boldsymbol{r})$, LMF theory tries to map it to a system interacting with short ranged Coulomb interaction $v_0(r)$ and renormalized external electric field $\mathcal{V}_R(\boldsymbol{r})$. $\mathcal{V}_R(r)$ has the following expression

$$\mathcal{V}_R(\boldsymbol{r}) = \mathcal{V}(\boldsymbol{r}) + \int d\boldsymbol{r}' \rho_R^q(\boldsymbol{r}'; [\mathcal{V}_R]) v_1(|\boldsymbol{r} - \boldsymbol{r}'|)\,, \tag{2.14}$$

where $\rho_R^q(\boldsymbol{r}'; [\mathcal{V}_R])$ is the charge density of water, completely analogous to the uncharged LMF equation Eq.(2.10). Ref [11] also shows the Gaussian smoothed charge density of GT water confined between hard wall while simultaneously subject to the LMF electric field $\mathcal{V}_R(\boldsymbol{r})$, which agrees excellently with the Gaussian smoothed charge density of SPC/E water. More examples which verifies the accuracy of Eq.(2.14) can be found in [10, 27, 28].

2.6 Conclusions

In this chapter, we have reviewed the framework and several applications of LMF theory. As shown by previous researches, LMF theory can accurately describe the structure of nonuniform liquids.

Chapter 3

Manipulating the Intermolecular Interactions of Dilute Solutions

Long ranged intermolecular interactions could have significant influence on the structure of the mixture and present serious challenges for computer simulations. It is well known that the water-water vdW attraction contributes significantly to the hydrophobic interactions between large apolar solutes [14, 15], and that the long ranged tail of Coulomb interaction is important for the screening of charges in water [11]. Due to the importance of long ranged component of intermolecular interactions, they need to be taken into account in computer simulation if one desires accurate numerical results. In particular, the long ranged tail of Coulomb interaction, which decays slowly as $\frac{1}{r}$, is usually calculated using Ewald summation or related techniques in computer simulation [18,29,30]. The Ewald-related techniques are time consuming to be carried out for large systems and usually requires certain symmetry of the simulation box.

To simplify the calculation of the long ranged tails and improve the speed of simulation, in this chapter we will describe a framework which allow us to simplify the long ranged interactions but still keep the structure of the mixture unaffected by the simplification. Using our framework, we can construct a "mimic" system, which has the same short ranged components of intermolecular interactions as the

target system, but has simplified long ranged tails. The simplified long ranged interactions are chosen such that the radial distribution functions between all the species are unchanged in the mimic system. This framework can be used to manipulate and simplify vdW interactions, Coulomb interactions and other long ranged slowly-varying interactions.

In this chapter, we first describe the details of our framework in Chapter 3.1 and then use this framework to simplify the vdW attractions (Chapter 3.2) and Coulomb interactions (Chapter 3.3) for dilute solutions.

3.1 Framework and Derivation

This section contains two subsections. In Chapter 3.1.1, I will illustrate the framework of our theory by studying the LJ-type dilute binary solutions, and then further generalize the framework to work with more general multi-species dilute solutions composed of multi-sites particles. In Chapter 3.1.2 I will show the detailed derivations for the results obtained in Chapter 3.1.1.

3.1.1 Framework

In last chapter, we have shown that LMF theory can be applied successfully to nonuniform liquids. However, within the framework of LMF theory, the unbalanced forces produced by long ranged interactions can only be approximated as static effective single-particle fields. This makes it inappropriate to use LMF theory to

describe the dynamically moving unbalanced forces produced in uniform mixtures. In this section, we propose a new theory, which approximates the unbalanced forces produced by slowly varying long ranged interactions in uniform mixtures as effective pair interactions.

Our new theory can be formulated as a mathematical framework to manipulate the long ranged interactions without changing the structure of the mixture. The manipulations can potentially simplify the interactions between particles and provide insight about how the long ranged interactions affect the structure of mixture. As an example to demonstrate our theory, let us consider a mixture composed of two different types of single-atom molecules, denoted as A and B. The interactions are labeled as $u_{\mathrm{MM}'}(r)$, where $\mathrm{M}, \mathrm{M}' \in \{\mathrm{A}, \mathrm{B}\}$. $u_{\mathrm{MM}'}(r)$ can be separated into short and long ranged part

$$u_{\mathrm{MM}'}(r) = u_{0,\mathrm{MM}'}(r) + u_{1,\mathrm{MM}'}(r). \tag{3.1}$$

We want to change the long tails of the $u_{\mathrm{MM}'}(r)$ in the following way

$$\left\{ \begin{array}{l} u_{\mathrm{AA}}(r) = u_{0,\mathrm{AA}}(r) + u_{1,\mathrm{AA}}(r) \\ u_{\mathrm{AB}}(r) = u_{0,\mathrm{AB}}(r) + u_{1,\mathrm{AB}}(r) \\ u_{\mathrm{BB}}(r) = u_{0,\mathrm{BB}}(r) + u_{1,\mathrm{BB}}(r) \end{array} \right\} \Longrightarrow \left\{ \begin{array}{l} u_{R,\mathrm{AA}}(r) = u_{0,\mathrm{AA}}(r) + u_{R1,\mathrm{AA}}(r) \\ u_{R,\mathrm{AB}}(r) = u_{0,\mathrm{AB}}(r) + u_{R1,\mathrm{AB}}(r) \\ u_{R,\mathrm{BB}}(r) = u_{0,\mathrm{BB}}(r) + u_{R1,\mathrm{BB}}(r) \end{array} \right\} \tag{3.2}$$

where the long ranged tail is changed from u_1 to u_{R1} but the short part u_0 is kept the same. This new set of interactions $\{u_{R,\mathrm{AA}}(r), u_{R,\mathrm{AB}}(r), u_{R,\mathrm{BB}}(r)\}$ defines a new system, which we will call "mimic" system following the tradition of LMF theory.

Our new framework is designed to find accurate choices of $u_{R1,\mathrm{MM}'}(r)$ which will keep the structure of the mimic system close to the structure of the original or "target" system.

The similarity of the structure of the target and mimic system can be mathematically characterized by the similarity of the radial distribution functions. In our framework $\{u_{R1,\mathrm{AA}}(r), u_{R1,\mathrm{AB}}(r), u_{R1,\mathrm{BB}}(r)\}$ are chosen to match the radial distribution functions of the target and mimic system

$$\begin{aligned} g_{\mathrm{AA}}(r) &\approx g_{R,\mathrm{AA}}(r) \\ g_{\mathrm{BB}}(r) &\approx g_{R,\mathrm{BB}}(r) \\ g_{\mathrm{AB}}(r) &\approx g_{R,\mathrm{AB}}(r)\,, \end{aligned} \tag{3.3}$$

where $g_{\mathrm{MM}'}(r)$ denotes the radial distribution function of the target system while $g_{R,\mathrm{MM}'}(r)$ denotes the radial distribution function of the mimic system. The matching of radial distribution function can also be equivalently expressed as the matching of the potential of mean force

$$\omega_{\mathrm{MM}'}(r) = \omega_{R,\mathrm{MM}'}(r) \tag{3.4}$$

where $\omega_{\mathrm{MM}'}(r) = -k_B T \nabla g_{\mathrm{MM}'}(r)$ represents the potential of mean force between M and M$'$, or equivalently expressed as the matching of the pair correlation function

$$\rho_{\mathrm{M|M}'}(r|0) = \rho_{R,\mathrm{M|M}'}(r|0) \tag{3.5}$$

where $\rho_{\mathrm{M|M}'}(r|0) = \rho_{b,\mathrm{M}} g_{\mathrm{MM}'}(r)$ is the conditional density of M at distance r given that a M$'$ particle fixed at the origin. $\rho_{b,\mathrm{M}}$ is the bulk density of M.

As discussed in Appendix A, there is one-to-one mapping between pair interactions and radial distribution functions. Therefore, it seems that $u_{R1,\mathrm{MM}'}(r)$ has to be very close to $u_{1,\mathrm{MM}'}(r)$ in order for Eq.(3.3) to be true. But in the special limit where B is dilutely solvated in A, $g_{R,\mathrm{AA}}(r)$ is not sensitive to the choice of $u_{R1,\mathrm{AA}}(r)$, since the force cancelation argument still works for the densely packed solvent particles. Therefore

$$g_{\mathrm{AA}}(r) \approx g_{R,\mathrm{AA}}(r) \tag{3.6}$$

for all the choices of $u_{R1,\mathrm{AA}}(r)$ as long as it is slowly varying. This extra freedom of choosing $u_{R1,\mathrm{AA}}(r)$ makes it possible for us to find out meaningful choices for $\{u_{R1,\mathrm{AA}}(r), u_{R1,\mathrm{AB}}(r), u_{R1,\mathrm{BB}}(r)\}$, as shown below.

Although we have the freedom to choose $u_{R1,\mathrm{AA}}(r)$ as long as it is slowly varying, we do not have the freedom in choosing $u_{R1,\mathrm{AB}}(r)$ and $u_{R1,\mathrm{BB}}(r)$. They have to be chosen such that

$$\begin{aligned} g_{R,\mathrm{AB}}(r) &\approx g_{\mathrm{AB}}(r) \\ g_{R,\mathrm{BB}}(r) &\approx g_{\mathrm{BB}}(r)\,. \end{aligned} \tag{3.7}$$

Finding out $u_{R1,\mathrm{AB}}(r)$ and $u_{R1,\mathrm{BB}}(r)$ which will satisfy Eq.(3.7) is the core part of our theory. Physically speaking $u_{R1,\mathrm{AB}}(r)$ and $u_{R1,\mathrm{BB}}(r)$ are chosen by matching the unbalanced forces produced in the target and mimic system. The matching of the forces can be mathematically formulated by making use of the YBG hierarchy of equations, similar to what has been done in LMF theory. The detailed procedures

will be described in Chapter 3.1.2 and I will just list the conclusion here.

$$u_{R1,\mathrm{AB}}(r) = u_{1,\mathrm{AB}}(r) - \int d\boldsymbol{r}'(\rho_{R,\mathrm{A|B}}(r'|0) - \rho_{b,\mathrm{A}})(u_{R1,\mathrm{AA}}(|\boldsymbol{r} - \boldsymbol{r}'|) - u_{1,\mathrm{AA}}(|\boldsymbol{r} - \boldsymbol{r}'|))$$

$$u_{R1,\mathrm{BB}}(r) = u_{1,\mathrm{BB}}(r) - \int d\boldsymbol{r}'(\rho_{R,\mathrm{A|B}}(r'|0) - \rho_{b,\mathrm{A}})(u_{R1,\mathrm{AB}}(|\boldsymbol{r} - \boldsymbol{r}'|) - u_{1,\mathrm{AB}}(|\boldsymbol{r} - \boldsymbol{r}'|)) \tag{3.8}$$

It is worth noticing that the choice of $u_{R1,\mathrm{AB}}(r)$ and $u_{R1,\mathrm{BB}}(r)$ are coupled with the choice of $u_{R1,\mathrm{AA}}(r)$, which is not surprising since the choice of $u_{R1,\mathrm{AA}}(r)$ will affect the unbalanced forces produced in the mimic system.

To summarize briefly, to keep the structure of the example dilute solution unchanged, we can choose $u_{R1,\mathrm{AA}}(r)$ freely, but $u_{R1,\mathrm{AB}}(r)$ and $u_{R1,\mathrm{BB}}(r)$, which are dependent on the choice of $u_{R1,\mathrm{AA}}(r)$, has to be determined by Eq.(3.8).

The benefits of being able to manipulate these interactions is that we can create a mimic system which is easier to analyze or simulate than the original system. For example, we can choose $u_{R1,\mathrm{AA}}(r)$ to be 0. In that case the mimic system will not have long ranged interactions between the solvents, therefore both the computer simulation and the theoretical analysis of this mimic system will be much easier. In Section 3.2 and 3.3 we will focus on this special kind of mimic system and test our theory by using it to deal with vdW attractions and the long tail of Coulomb interactions.

Eq.(3.8) is only targeting binary dilute solutions composed of single-site molecules. Similar equations can be drawn for dilute solutions composed of multiple types of molecules, and these molecules can be rigid molecules composed of several sites.

The solvent in this solution, which is the dominant species, is still denoted by A. The solute species, which are dilutely solvated, are denoted by B, C, D and so on. The sites in a molecule are represented by Greek letters such as ξ, α and η. ξM represents site ξ of molecule specie M, where $\mathrm{M} = \{\mathrm{A}, \mathrm{B}, \mathrm{C}, \cdots\}$. The intermolecular interactions between site ξM and $\alpha\mathrm{M}'$ are denoted by $u_{\xi\mathrm{M}\alpha\mathrm{M}'}(r)$, which can be separated into short ranged and long ranged part as follows

$$u_{\xi\mathrm{M}\alpha\mathrm{M}'}(r) = u_{0,\xi\mathrm{M}\alpha\mathrm{M}'}(r) + u_{1,\xi\mathrm{M}\alpha\mathrm{M}'}(r). \tag{3.9}$$

We want to manipulate the long tails of the intermolecular interactions as we did previously

$$u_{\xi\mathrm{M}\alpha\mathrm{M}'}(r) = u_{0,\xi\mathrm{M}\alpha\mathrm{M}'}(r) + u_{1,\xi\mathrm{M}\alpha\mathrm{M}'}(r) \Longrightarrow u_{R,\xi\mathrm{M}\alpha\mathrm{M}'}(r) = u_{0,\xi\mathrm{M}\alpha\mathrm{M}'}(r) + u_{R1,\xi\mathrm{M}\alpha\mathrm{M}'}(r)\,. \tag{3.10}$$

$u_{R1,\xi\mathrm{M}\alpha\mathrm{M}'}(r)$ is chosen such that the site-site correlation function is unchanged under the manipulation

$$g_{R,\xi\mathrm{M}\alpha\mathrm{M}'}(r) \approx g_{\xi\mathrm{M}\alpha\mathrm{M}'}(r)\,. \tag{3.11}$$

Since A is the dominant species, we can still choose the long tail of A-A intermolecular interaction $u_{R1,\xi\mathrm{A}\alpha\mathrm{A}}(r)$ freely. The other long tails, or more precisely the long tails of solvent-solute and solute-solute interactions, can be determined by

$$\begin{aligned} &u_{R1,\xi\mathrm{A}\alpha\mathrm{M}}(r) \\ =&u_{1,\xi\mathrm{A}\alpha\mathrm{M}}(r) - \sum_{\eta\mathrm{A}} \int d\boldsymbol{r}'(\rho_{R,\eta\mathrm{A}|\alpha\mathrm{M}}(r'|0) - \rho_{b,\eta\mathrm{A}})(u_{R1,\eta\mathrm{A}\xi\mathrm{A}}(|\boldsymbol{r} - \boldsymbol{r}'|) - u_{1,\eta\mathrm{A}\xi\mathrm{A}}(|\boldsymbol{r} - \boldsymbol{r}'|)) \end{aligned} \tag{3.12}$$

and

$$u_{R1,\xi \mathrm{M}'\alpha \mathrm{M}}(r)$$
$$= u_{1,\xi \mathrm{M}'\alpha \mathrm{M}}(r) - \sum_{\eta \mathrm{A}} \int d\boldsymbol{r}' (\rho_{R,\eta \mathrm{A}|\alpha \mathrm{M}}(r'|0) - \rho_{b,\eta \mathrm{A}})(u_{R1,\eta \mathrm{A}\xi \mathrm{M}'}(|\boldsymbol{r} - \boldsymbol{r}'|) - u_{1,\eta \mathrm{A}\xi \mathrm{M}'}(|\boldsymbol{r} - \boldsymbol{r}'|)) \,. \tag{3.13}$$

In both equations above, $\mathrm{M}, \mathrm{M}' = \{\mathrm{B}, \mathrm{C}, \mathrm{D}, \cdots\}$. $\rho_{R,\eta \mathrm{A}|\alpha \mathrm{M}}(r|0)$ is the density of site ηA at distance r given a αM site is placed at the origin in the mimic system. $\sum_{\eta \mathrm{A}}$ sums over all the sites of specie A. We will not show how to derive Eq.(3.12) and (3.13) here. The procedures are similar to what will be shown in Chapter 3.1.2, while the only complication here is that we now have intramolecular interactions. However, the intramolecular interactions are unchanged in the mimic system and would not contribute to $u_{R1,\xi \mathrm{A}\alpha \mathrm{M}}(r)$ and $u_{R1,\xi \mathrm{M}'\alpha \mathrm{M}}(r)$.

It is worth noticing that sometimes we just want to keep certain parts of the structure unchanged under the manipulation. For example, in many cases, the solute-solute radial distribution function is the only thing we are interested in. In that case, we only need to preserve solute-solute RDF in the mimic system. This does give us extra freedom in manipulating the interactions, and this scenario will further explored in Chapter 4 and 6.

3.1.2 Derivation

In this section I will derive Eq.(3.8). The procedure is very much similar to the derivation of the LMF equation (See Eq.(2.10)). Let us derive the expression

for $u_{R1,\mathrm{AB}}(r)$ first. The exact YBG equations for $\rho_{\mathrm{A|B}}(r|0)$ and $\rho_{R,\mathrm{A|B}}(r|0)$ are

$$-k_B T\nabla \ln \rho_{\mathrm{A|B}}(r|0) = \nabla u_{\mathrm{AB}}(r) + \int d\boldsymbol{r}' \rho_{\mathrm{A|AB}}(\boldsymbol{r}'|\boldsymbol{r},\boldsymbol{0})\nabla u_{\mathrm{AA}}(|\boldsymbol{r}-\boldsymbol{r}'|) \tag{3.14}$$

and

$$-k_B T\nabla \ln \rho_{R,\mathrm{A|B}}(r|0) = \nabla u_{R,\mathrm{AB}}(r) + \int d\boldsymbol{r}' \rho_{R,\mathrm{A|AB}}(\boldsymbol{r}'|\boldsymbol{r},\boldsymbol{0})\nabla u_{R,\mathrm{AA}}(|\boldsymbol{r}-\boldsymbol{r}'|) \tag{3.15}$$

$u_{R1,\mathrm{AB}}(r)$ is chosen such that $\rho_{\mathrm{A|B}}(r|0) = \rho_{R,\mathrm{A|B}}(r|0)$. Subtract both equations and we get exactly

$$\begin{aligned}
\nabla u_{R1,\mathrm{AB}}(r) = {} & \nabla u_{1,\mathrm{AB}}(r) \\
& + \int d\boldsymbol{r}' \rho_{R,\mathrm{A|B}}(r'|0)\nabla(u_{1,\mathrm{AA}}(|\boldsymbol{r}-\boldsymbol{r}'|) - u_{R1,\mathrm{AA}}(|\boldsymbol{r}-\boldsymbol{r}'|)) \\
& + \int d\boldsymbol{r}' (\rho_{\mathrm{A|AB}}(\boldsymbol{r}'|\boldsymbol{r},\boldsymbol{0}) - \rho_{\mathrm{A|B}}(r'|0))\nabla u_{1,\mathrm{AA}}(|\boldsymbol{r}-\boldsymbol{r}'|) \\
& - \int d\boldsymbol{r}' (\rho_{R,\mathrm{A|AB}}(\boldsymbol{r}'|\boldsymbol{r},\boldsymbol{0}) - \rho_{R,\mathrm{A|B}}(r'|0))\nabla u_{R1,\mathrm{AA}}(|\boldsymbol{r}-\boldsymbol{r}'|) \\
& + \int d\boldsymbol{r}' (\rho_{\mathrm{A|AB}}(\boldsymbol{r}'|\boldsymbol{r},\boldsymbol{0}) - \rho_{R,\mathrm{A|AB}}(\boldsymbol{r}'|\boldsymbol{r},\boldsymbol{0}))\nabla u_{0,\mathrm{AA}}(|\boldsymbol{r}-\boldsymbol{r}'|)\,.
\end{aligned} \tag{3.16}$$

Eq.(3.16) is still an exact equation, but it shows the terms to be approximated explicitly. We claim that line 3, 4 and 5 of Eq.(3.16) should be approximately 0. By making these approximations, three-body correlation functions $\rho_{\mathrm{A|AB}}(\boldsymbol{r}'|\boldsymbol{r},\boldsymbol{0})$ and $\rho_{R,\mathrm{A|AB}}(\boldsymbol{r}'|\boldsymbol{r},\boldsymbol{0})$, which are really hard to get numerically or analytically, do not appear any more. The validity of these approximations is shown in the following part.

Line 3 and 4 of Eq.(3.16) involves the difference between the three-body correlation functions and pair correlation functions. This difference is not zero in general,

but we are saved by the fact that it is integrated with the gradient of the long tail. We can choose $\nabla u_{R1,\mathrm{AA}}(|\boldsymbol{r}-\boldsymbol{r}'|)$ and $\nabla u_{1,\mathrm{AA}}(|\boldsymbol{r}-\boldsymbol{r}'|)$ to be approximately zero inside the effective hard core distance, which is exactly the range where the conditional density and the singlet density differ the most. Thus it is reasonable to expect the integrand in line 3 and 4 to be approximately 0.

Line 5 probes the difference between the three-body correlation function in the target and mimic system via convolution with $\nabla u_{0,\mathrm{AA}}(r)$. We claim this line to be approximately 0 based on the the following arguments.

- The integrand in line 5 is quickly forced to zero at larger $|\boldsymbol{r}-\boldsymbol{r}'|$ by the vanishing gradient of the short ranged $u_{0,\mathrm{AA}}(r)$. Since both the target and mimic system have the same strong short range core forces with appropriately chosen $u_0(r)$s, which should mainly determine the short-ranged part of the correlation functions, it seems plausible that with proper choice of $u_0(r)$s, line 5 can be neglected.

- The pair correlation functions are designed to be the same in the full and mimic system. The close resemblance of the pair correlation functions in dense full and mimic systems is an indication that the three-body correlation functions are also close in the full and mimic system, since three-body correlation functions are functions of pair correlation functions as shown in Appendix A.

After the approximations, Eq.(3.16) become

$$\nabla u_{R1,\mathrm{AB}}(r) = \nabla u_{1,\mathrm{AB}}(r) + \int d\boldsymbol{r}' \rho_{R,\mathrm{A|B}}(r'|0) \nabla (u_{1,\mathrm{AA}}(|\boldsymbol{r}-\boldsymbol{r}'|) - u_{R1,\mathrm{AA}}(|\boldsymbol{r}-\boldsymbol{r}'|)) \,. \tag{3.17}$$

After integrating over the gradient and fixing the integration constant such that $u_{R1,\mathrm{AB}}(r)$ is 0 at infinity, we can get

$$u_{R1,\mathrm{AB}}(r) = u_{1,\mathrm{AB}}(r) + \int d\boldsymbol{r}' (\rho_{R,\mathrm{A|B}}(r'|0) - \rho_{b,\mathrm{A}}) (u_{1,\mathrm{AA}}(|\boldsymbol{r}-\boldsymbol{r}'|) - u_{R1,\mathrm{AA}}(|\boldsymbol{r}-\boldsymbol{r}'|)) \,. \tag{3.18}$$

The derivations to get $u_{R1,\mathrm{BB}}(r)$ is similar. The YBG equation for $\rho_{\mathrm{B|B}}(r|0)$ and $\rho_{R,\mathrm{B|B}}(r|0)$ are

$$-k_B T \nabla \ln \rho_{\mathrm{B|B}}(r|0) = \nabla u_{\mathrm{BB}}(r) + \int d\boldsymbol{r}' \rho_{\mathrm{A|BB}}(\boldsymbol{r}'|\boldsymbol{r},\boldsymbol{0}) \nabla u_{\mathrm{AB}}(|\boldsymbol{r}-\boldsymbol{r}'|) \tag{3.19}$$

and

$$-k_B T \nabla \ln \rho_{R,\mathrm{B|B}}(r|0) = \nabla u_{R,\mathrm{BB}}(r) + \int d\boldsymbol{r}' \rho_{R,\mathrm{A|BB}}(\boldsymbol{r}'|\boldsymbol{r},\boldsymbol{0}) \nabla u_{R,\mathrm{AB}}(|\boldsymbol{r}-\boldsymbol{r}'|) \tag{3.20}$$

respectively. $u_{R1,\mathrm{BB}}(r)$ is chosen such that $\rho_{\mathrm{B|B}}(r|0) = \rho_{R,\mathrm{B|B}}(r|0)$. Subtract both equations and rearrangement. We get

$$\begin{aligned}
\nabla u_{R1,\mathrm{BB}}(r) = \nabla u_{1,\mathrm{BB}}(r) & \\
&+ \int d\boldsymbol{r}' \rho_{R,\mathrm{A|B}}(r'|0) \nabla (u_{1,\mathrm{AB}}(|\boldsymbol{r}-\boldsymbol{r}'|) - u_{R1,\mathrm{AB}}(|\boldsymbol{r}-\boldsymbol{r}'|)) \\
&+ \int d\boldsymbol{r}' (\rho_{\mathrm{A|BB}}(\boldsymbol{r}'|\boldsymbol{r},\boldsymbol{0}) - \rho_{\mathrm{A|B}}(r'|0)) \nabla u_{1,\mathrm{AB}}(|\boldsymbol{r}-\boldsymbol{r}'|) \\
&- \int d\boldsymbol{r}' (\rho_{R,\mathrm{A|BB}}(\boldsymbol{r}'|\boldsymbol{r},\boldsymbol{0}) - \rho_{R,\mathrm{A|B}}(r'|0)) \nabla u_{R1,\mathrm{AB}}(|\boldsymbol{r}-\boldsymbol{r}'|) \\
&+ \int d\boldsymbol{r}' (\rho_{\mathrm{A|BB}}(\boldsymbol{r}'|\boldsymbol{r},\boldsymbol{0}) - \rho_{R,\mathrm{A|BB}}(\boldsymbol{r}'|\boldsymbol{r},\boldsymbol{0})) \nabla u_{0,\mathrm{AB}}(|\boldsymbol{r}-\boldsymbol{r}'|) \,.
\end{aligned} \tag{3.21}$$

Now we can make approximations similar to what we did before. Notice that in order for Line 4 of Eq.(3.21) to vanish, $u_{R1,\mathrm{AB}}(r)$ needs to be slowly varying inside the effective hard core distance. $u_{R1,\mathrm{AB}}(r)$ is determined by Eq.(3.18), which will be slowly varying inside the core when $u_{1,\mathrm{AA}}(r) - u_{R1,\mathrm{AA}}(r)$ is slowly varying enough. When $u_{1,\mathrm{AA}}(r) - u_{R1,\mathrm{AA}}(r)$ is not slowly varying enough, $u_{R1,\mathrm{AB}}(r)$ could vary substantially inside the hard core distance, and this has been practically verified when $u_{1,\mathrm{AA}}(r) - u_{R1,\mathrm{AA}}(r)$ corresponds to the vdW attraction. However, in that case we have the freedom to force $u_{R1,\mathrm{AB}}(r)$ to be slowly varying inside the hard core without affecting the structure, since $u_{R1,\mathrm{AB}}(r) \ll u_{0,\mathrm{AB}}(r)$ inside the hard core distance. In this way we obtain a core corrected version of Eq.(3.21)

$$
\begin{aligned}
& u_{R1,\mathrm{AB}}(r) \\
=& \begin{cases} u_{1,\mathrm{AB}}(r) - \int dr'(\rho_{R,\mathrm{A|B}}(r'|0) - \rho_{b,\mathrm{A}})(u_{R1,\mathrm{AA}}(|r-r'|) - u_{1,\mathrm{AA}}(|r-r'|)) & r \geq d_{\mathrm{AB}} \\ u_{R1,\mathrm{AB}}(d_{\mathrm{AB}}) & r < d_{\mathrm{AB}} \end{cases},
\end{aligned}
\tag{3.22}
$$

which certainly will make Line 4 of Eq.(3.21) vanish. d_{AB} denotes the effective hard core distance. For $r < d_{\mathrm{AB}}$, $u_{0,\mathrm{AB}}(r) \gg k_B T$. Notice that any physically reasonable choice for $d_{\mathrm{AB}}(r)$ will give essentially the same results.

After making the approximations, we have

$$
\nabla u_{R1,\mathrm{BB}}(r) = \nabla u_{1,\mathrm{BB}}(r) + \int d\boldsymbol{r}' \rho_{R,\mathrm{A|B}}(r'|0) \nabla (u_{1,\mathrm{AB}}(|\boldsymbol{r} - \boldsymbol{r}'|) - u_{R1,\mathrm{AB}}(|\boldsymbol{r} - \boldsymbol{r}'|)) \,.
\tag{3.23}
$$

After integrating over the gradient and fixing the integration constant, we can get

$$u_{R1,\mathrm{BB}}(r) = u_{1,\mathrm{BB}}(r) + \int d\boldsymbol{r}'(\rho_{R,\mathrm{A|B}}(r'|0) - \rho_{b,A})(u_{1,\mathrm{AB}}(|\boldsymbol{r} - \boldsymbol{r}'|) - u_{R1,\mathrm{AB}}(|\boldsymbol{r} - \boldsymbol{r}'|))\,. \tag{3.24}$$

which is just what is shown in Eq.(3.8).

3.2 Manipulating the Van der Waals Attractions for Apolar Solutes in Water

The vdW attractions could have important influences on the association of apolar solutes in water, and the solute-solute, solute-water and water-water vdW attractions influence the PMF between solutes through different mechanisms [15]. The solute-solute attraction adds directly to the PMF between solutes when the solutes are dilutely solvated. The effects of the solute-water and water-water attraction on the solute-solute PMF are more subtle. Qualitatively speaking, the water-water attraction produces a drying force on the interfacial water molecules, which effectively increases the energy of the interfacial water and thus favors the association of the solutes. The solute-water attraction produces an attractive force on the interfacial water molecules, which lowers the energy of interfacial water and thus favors the dissociation of the solutes. Many theories have been devoted to provide a quantitative description for the effects of the solute-water and water-water vdW attractions [14,31–33], however, most of these theories are numerically not very accurate. To tackle this problem, in this section we use the framework described

in Chapter 3.1 to map the solution of apolar solutes and water to a mimic system which has the water-water vdW attraction truncated but still possesses the same structure as the original target system. Thus, we are saved with the necessity to theoretically describe the effects of the water-water vdW attractions by studying the mimic system as an alternative. We also described a new and surprisingly accurate theory dealing with the effects of the solute-water attractions, which will be shown in Chapter 4.

Let us first discuss the mathematical labels needed. We will use A to label the water molecules and B to label the apolar solutes. The water-solute and solute-solute interaction are denoted as $u_{\rm AB}(r)$ and $u_{\rm BB}(r)$ respectively. The water-water interaction are composed of Coulomb part and vdW part. In this section we will only focus the vdW part, denoted by $u_{\rm AA}(r)$, and the Coulomb part will not be manipulated or changed in the mimic system. The Coulomb interaction is able to be manipulate using our framework, as will be shown in Chapter 3.3. In practice we have found that the long ranged tail of Coulomb interactions have almost no influence on the association of apolar solutes. Therefore for conceptual simplicity we do not manipulate the Coulomb interaction here. $\{u_{\rm AA}(r), u_{\rm AB}(r), u_{\rm BB}(r)\}$ can all be separated into the repulsive core interaction $u_{0,{\rm MM'}}(r)$ and the long ranged attractive interaction $u_{1,{\rm MM'}}(r)$.

For the mimic system to be constructed, we will choose the water-water interaction to be just the repulsive-core interaction, or in other words, $u_{R1,{\rm AA}}(r) = 0$. By

truncating the water-water attraction, the mimic Hamiltonian is simplified. Based on our discussions in Chapter 3.1.2, $u_{R1,\mathrm{AB}}(r)$ and $u_{R1,\mathrm{BB}}(r)$ have the following expressions

$$u_{R1,\mathrm{AB}}(r) = \begin{cases} u_{1,\mathrm{AB}}(r) + \int dr'(\rho_{R,\mathrm{A|B}}(r'|0) - \rho_{b,\mathrm{A}})u_{1,\mathrm{AA}}(|r-r'|) & \text{for } r \geq d_{\mathrm{AB}} \\ u_{R1,\mathrm{AB}}(d_{\mathrm{AB}}) & \text{for } r < d_{\mathrm{AB}} \end{cases}, \tag{3.25}$$

and

$$u_{R1,\mathrm{BB}}(r) = u_{1,\mathrm{BB}}(r) - \int dr'(\rho_{R,\mathrm{A|B}}(r'|0) - \rho_{b,\mathrm{A}})(u_{R1,\mathrm{AB}}(|r-r'|) - u_{1,\mathrm{AB}}(|r-r'|)) \,. \tag{3.26}$$

Notice that we forced $u_{R1,\mathrm{AB}}(r)$ to be constant inside the effective hard core distance d_{AB}. The reason of doing this can be found in Section 3.1.2.

Fig 3.1 and 3.2 qualitatively shows the physical meaning of Eq.(3.25) and Eq.(3.26) respectively. The integral term in Eq.(3.25) and Eq.(3.26) can be interpreted as the effective interactions used to compensate the truncation of water-water attraction $u_{1,\mathrm{AA}}(r)$. As shown in Figure 3.1, the water molecules near the surface of the solute feel vdW attractions from other water molecules, which forms a "drying" force pulling the interfacial water towards the bulk direction. This "drying force" corresponds to the integral term in Eq.(3.25). This drying force along with the solute-water vdW attraction are incooperated into $u_{R1,\mathrm{AB}}(r)$. As illustrated in Fig 3.1, $u_{R1,\mathrm{AB}}(r)$ should be less attractive than $u_{1,\mathrm{AB}}(r)$. As shown in Figure 3.2, when two solutes are close to each other, the water molecules in between the two solutes

have different structure compared to the water molecules outside, so the forces exerted on the solutes coming from these water molecules are different from inside and outside, thus producing an unbalanced force along the solute-solute direction. The difference of this unbalanced force between the target and mimic system correspond to the integral term in Eq.(3.26), which along with the direct solute-solute vdw attraction are incooperated into $u_{R1,\mathrm{BB}}(r)$. Since $u_{R1,\mathrm{AB}}(r)$ is less attractive than $u_{1,\mathrm{AB}}(r)$, $u_{R1,\mathrm{BB}}(r)$ also needs to be less attractive than $u_{1,\mathrm{BB}}(r)$ such that the total force on the solute are the same in the full and mimic system, as illustrated in Figure 3.2.

In the following subsections we will manipulate the vdW attractions for the fullerene-water solution (Chapter 3.2.1), Argon-water solution (Chapter 3.2.2) and Hard Sphere-water solution (Chapter 3.2.3) using the method prescribed here.

3.2.1 C_{60} in water

We first test our theory by studying fullerenes in solution with water. We used a coarse grained model for fullerene [34, 35], with the fullerene-water and the fullerene-fullerene interaction defined as

$$\begin{aligned} u_{\mathrm{AB}}(r) =& 4N\epsilon_{\mathrm{AB}}\frac{\sigma_{\mathrm{AB}}^2}{r\eta}\left\{\frac{1}{20}\left[\left(\frac{\sigma_{\mathrm{AB}}}{\eta-r}\right)^{10}-\left(\frac{\sigma_{\mathrm{AB}}}{\eta+r}\right)^{10}\right]\right. \\ &\left.-\frac{1}{8}\left[\left(\frac{\sigma_{\mathrm{AB}}}{\eta-r}\right)^{4}-\left(\frac{\sigma_{\mathrm{AB}}}{\eta+r}\right)^{4}\right]\right\} \end{aligned} \tag{3.27}$$

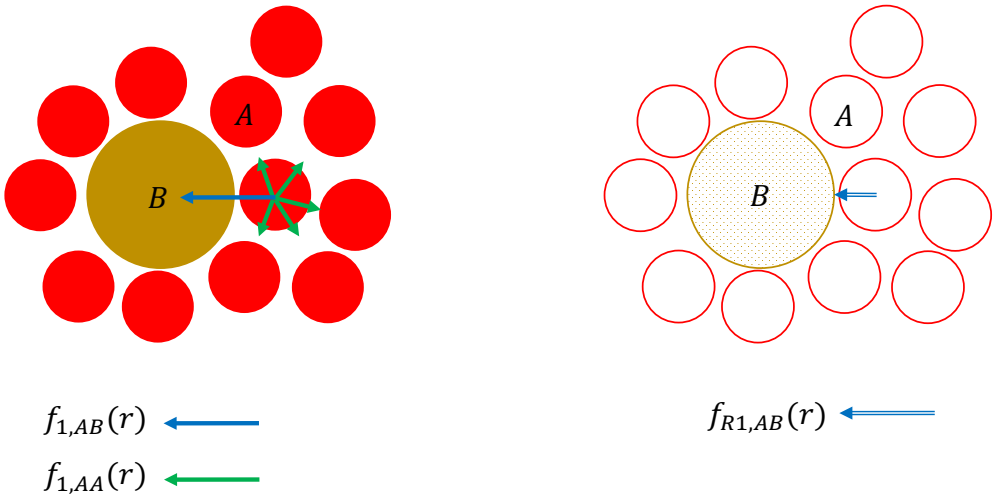

Figure 3.1: In this figure A stands for solvent. B stands for solute. The left panel corresponds to the target system. The right panel corresponds to the mimic system. In the target system, a solvent particle feels vdw attractive forces from the solute and the surrounding solvent, denoted by $f_{1,\mathrm{AB}}(r) = -\nabla u_{1,\mathrm{AB}}(r)$ and $f_{1,\mathrm{AA}}(r) = -\nabla u_{1,\mathrm{AA}}(r)$ respectively. These forces are incooperated into $f_{R1,\mathrm{AB}}(r) = -\nabla u_{R1,\mathrm{AB}}(r)$, as shown in the right panel. Physically speaking the total force exerted on the solvent particles are the same in both system. But notice that the force matching happens in the sense of an ensemble average, while this figure only shows one typical configuration.

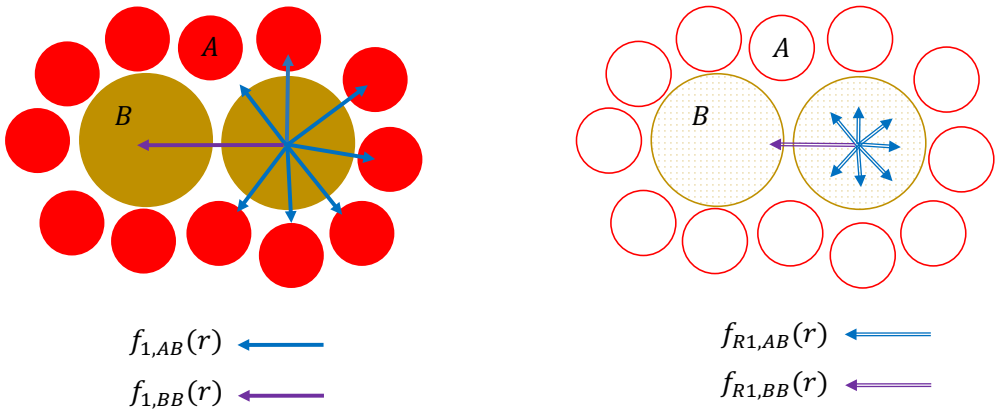

Figure 3.2: In this figure A stands for solvent. B stands for solute. The left panel corresponds to the target system. The right panel corresponds to the mimic system. The left panel shows the vdW attractive forces acted on the solute particle, including the solute-solvent vdW attractive force $f_{1,\mathrm{AB}}(r) = -\nabla u_{1,\mathrm{AB}}(r)$ and the solute-solute attractive force $f_{1,\mathrm{BB}}(r) = -\nabla u_{1,\mathrm{BB}}(r)$. The right panel shows the long ranged part of the solute-solvent and solute-solute interaction acted on the solute, denoted by $f_{R1,\mathrm{AB}}(r) = -\nabla u_{R1,\mathrm{AB}}(r)$ and $f_{R1,\mathrm{BB}}(r) = -\nabla u_{R1,\mathrm{BB}}(r)$ respectively. The total force acted on the solute coming from these long ranged interactions should be basically the same in both system. As illustrated in this figure, the $u_{R1,\mathrm{BB}}(r)$ should less attractive than $u_{1,\mathrm{BB}}(r)$.

and

$$\begin{aligned} u_{\mathrm{BB}}(r) = &- \alpha\Big[\frac{1}{s(s-1)^3} + \frac{1}{s(s+1)^3} - \frac{2}{s^4}\Big] \\ &+ \zeta\Big[\frac{1}{s(s-1)^9} + \frac{1}{s(s+1)^9} - \frac{2}{s^{10}}\Big] \end{aligned} \tag{3.28}$$

where A stands for water, B stands for fullerene, $N = 60$, $\sigma_{\mathrm{AB}} = 3.19\,\text{Å}$, $\epsilon_{\mathrm{AB}} = 0.392\,\mathrm{kJ/mol}$, $\alpha = 4.4775\,\mathrm{kJ/mol}$, $\zeta = 0.0081\,\mathrm{kJ/mol}$ and $\eta = 0.355\,\text{Å}$. Both $u_{\mathrm{AB}}(r)$ and $u_{\mathrm{BB}}(r)$ can be separated into short ranged repulsive interaction and long ranged attractive interaction, as illustrated in Figure 3.3. The water-water interaction is defined by the SPC/E water model, which contains both Coulomb interactions and LJ interactions.

In the corresponding mimic system, the vdW attraction between water is truncated and the fullerene-water, fullerene-fullerene interaction, which are shown in Figure 3.3, are obtained according to Eq.(3.25) and Eq.(3.26) respectively. The comparison of the structure of the target and mimic system is shown in Figure 3.4. The structure of the target and mimic system closely resembles each other, which justifies the approximations made in our derivation. To gain better insight about how much the vdW attractions alters the structure of the solution, Figure 3.4 also shows the structure of a "repulsive-core" system, where the vdW attractions between all the species are truncated.

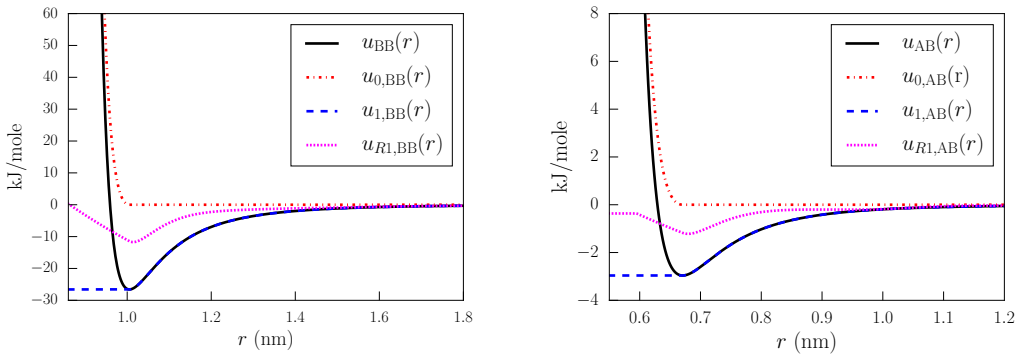

(a) **(b)**

Figure 3.3: B stands for the fullerene. A stands for the water. In (a), $u_{0,\mathrm{BB}}(r)$ is the short ranged repulsive component of the fullerene-fullerene interaction. $u_{1,\mathrm{BB}}(r)$ is the long range attractive component of the fullerene-fullerene interaction. $u_{\mathrm{BB}}(r) = u_{0,\mathrm{BB}}(r) + u_{1,\mathrm{BB}}(r)$ is the fullerene-fullerene interaction in the target system. $u_{R1,\mathrm{BB}}(r)$ is the long ranged component of the fullerene-fullerene interaction in the mimic system. In (b), $u_{0,\mathrm{AB}}(r)$ is the short ranged repulsive component of the fullerene-water interaction. $u_{1,\mathrm{AB}}(r)$ is the long range attractive component of the fullerene-water interaction. $u_{\mathrm{AB}}(r) = u_{0,\mathrm{AB}}(r) + u_{1,\mathrm{AB}}(r)$ is the fullerene-water interaction in the target system. $u_{R1,\mathrm{AB}}(r)$ is the long ranged component of the fullerene-water interaction in the mimic system.

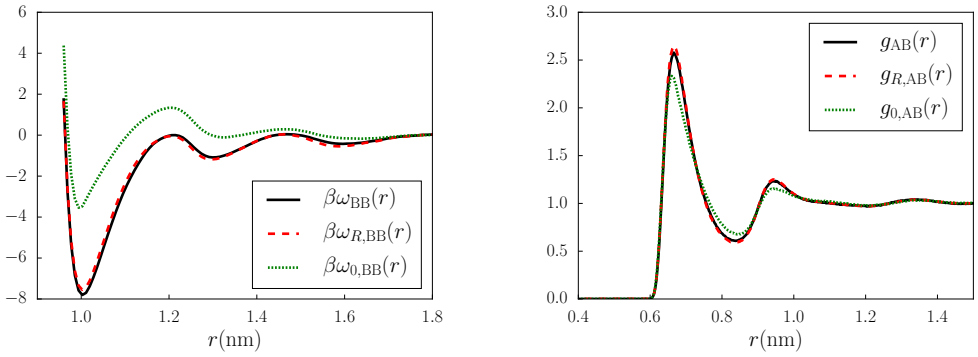

(a) **(b)**

Figure 3.4: (a) compares the fullerene-fullerene PMF of the target, mimic and repulsive-core system, represented by $\omega_{\mathrm{BB}}(r)$, $\omega_{R,\mathrm{BB}}(r)$ and $\omega_{0,\mathrm{BB}}(r)$ respectively. (b) compares the fullerene-water RDF of the target, mimic and repulsive-core system, represented by $g_{\mathrm{AB}}(r)$, $g_{R,\mathrm{AB}}(r)$ and $g_{0,\mathrm{AB}}(r)$ respectively. All the data is obtained at $T = 300\mathrm{K}$ and $P = 1\mathrm{atm}$ by computer simulation.

3.2.2 Argon in Water, Pratt-Chandler Theory and Inverse Temperature Behavior

We further test our theory by studying Argon particles dissolved in water. This system has been studied by many people and still being actively studied [36–38]. The most well-know theory studying Argon associations is the Pratt-Chandler theory [36], which used integral equations to determine the association between Argon particles in water. However, it is now believed that the Pratt-Chandler theory has neglected the contribution of solute-water and solute-solute vdW attractions [14]. Or in other words, the Pratt-Chandler theory was targeting "repulsive-core" solutes.

By manipulating the vdW interactions following the procedures shown before, we can quantitatively show that the vdW attractions do not contribute strongly to the hydrophobic association of Argon. According to Ref [15], the hydrophobic interaction between Argon comes from the two different effects. First is the vdW attractions, as we already discussed. The second physical reason behind the Argon association is that the orientational fluctuation of water molecules near the Argon is restricted, which thus favors the association of Argon in order to reduce the number of interfacial water molecules and increase the entropy of the whole system. By showing that the vdW attraction does not contribute strongly, we have verified that the hydrophobic association of Argon should be due to the restraint of the orientational fluctuation of interfacial water, which is a purely entropic effect.

The interaction between Argon-Argon and Argon-water are modeled as LJ

interactions. The water-water interaction is still defined by the SPC/E water model. Again, we use B to denote the solute Argon and A to denote the solvent water. In the mimic system, the water-water vdW attraction is truncated, or in other words, $u_{R1,\mathrm{AA}}(r) = 0$. $u_{R1,\mathrm{AB}}(r)$ and $u_{R1,\mathrm{BB}}(r)$ are determined based on Eq.(3.25) and Eq.(3.26). Figure 3.5 shows $u_{R1,\mathrm{AB}}(r)$ and $u_{R1,\mathrm{BB}}(r)$ obtained at $T = 300\mathrm{K}$ and $P = 1\mathrm{atm}$. According to Figure 3.5 both $u_{R1,\mathrm{AB}}(r)$ and $u_{R1,\mathrm{BB}}(r)$ are very small

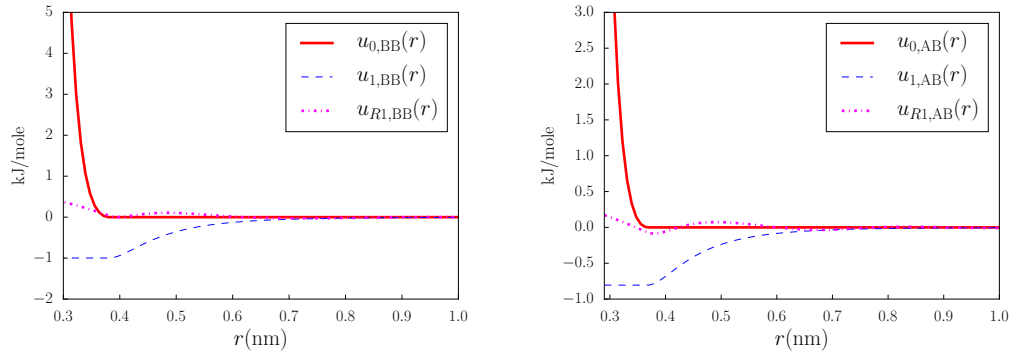

(a) **(b)**

Figure 3.5: In this figure, B stands for Argon, A stands for water. In figure (a), $u_{R1,\mathrm{BB}}(r)$ is the long ranged part of the Argon-Argon interaction in the mimic system. $u_{1,\mathrm{BB}}(r)$ is the long ranged attractive part of Argon-Argon interaction in the target system. $u_{0,\mathrm{BB}}(r)$ is the short ranged repulsive part of Argon-Argon interaction in the target system. In figure (b), $u_{R1,\mathrm{AB}}(r)$ is the long ranged part of the Argon-water interaction in the mimic system. $u_{1,\mathrm{AB}}(r)$ is the long ranged attractive part of Argon-Water interaction in the target system. $u_{0,\mathrm{AB}}(r)$ is the short ranged repulsive part of Argon-Water interaction in the target system.

compared to $u_{1,\mathrm{AB}}(r)$ and $u_{1,\mathrm{BB}}(r)$ outside the repulsive core. Also, given that $k_BT = 2.5\mathrm{kJ/mole}$ for $T = 300\mathrm{K}$, $u_{R1,\mathrm{AB}}(r)$ and $u_{R1,\mathrm{BB}}(r)$ are negligible compared

to k_BT, which means that

$$\begin{aligned} u_{R,\mathrm{AB}}(r) \approx & u_{0,\mathrm{AB}}(r) \\ u_{R,\mathrm{BB}}(r) \approx & u_{0,\mathrm{BB}}(r) \end{aligned} \tag{3.29}$$

in this mimic system. Therefore the interactions in the mimic system obtained are very close to the repulsive-core system, showing the accuracy of the LJ force cancellation picture in this case. This explains the similarity of the structure between the target system and the repulsive-core system, as shown in Figure 3.6.

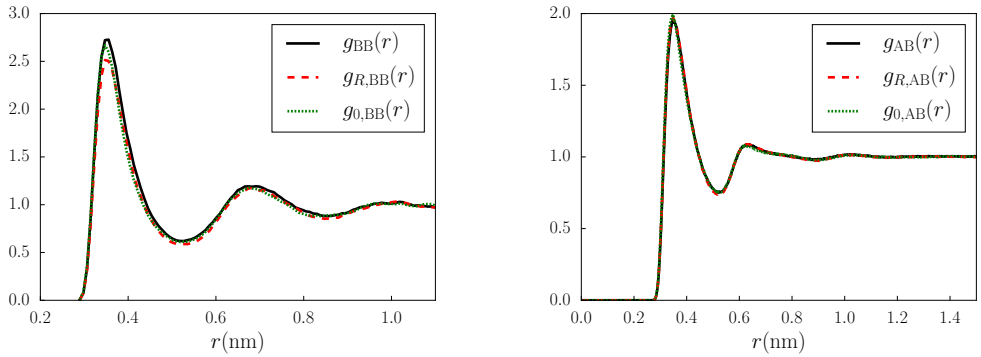

(a) **(b)**

Figure 3.6: In Figure (a), $g_{\mathrm{BB}}(r)$ is the Argon-Argon RDF of the target system. $g_{R,\mathrm{BB}}(r)$ is the Argon-Argon RDF of the mimic system. $g_{0,\mathrm{BB}}(r)$ is the Argon-Argon RDF of the repulsive-core system where the vdW attractions between all the species are turned off. In Figure (b), $g_{\mathrm{AB}}(r)$ is the Argon-water RDF of the target system. $g_{R,\mathrm{AB}}(r)$ is the Argon-water RDF of the mimic system. $g_{0,\mathrm{AB}}(r)$ is the Argon-water RDF of the repulsive-core system.

Our conclusion that the Argon association should be an entropic effect also explains the inverse temperature behavior. It is found out that in a certain tem-

perature range the association strength between Argons grows stronger when the temperature increases [38], which is demonstrated in Figure 3.7a. There has been speculations that the inverse temperature behavior comes from the solute-water vdW attractions [39]. But our work already shows that the vdW attractions do not affect the hydrophobic association of Argon. Thus, the inverse temperature behavior should be an entropic effect. This is further verified by examining the temperature dependence of Argon-Argon association in the repulsive-core system, where the vdW attractions between all the species are truncated. As shown in Figure 3.7b, we find out that the same inverse temperature behavior exists in the repulsive core system, which confirms that the inverse temperature behavior is an entropic effect. A qualitative explanation for this inverse temperature behavior can be given here. When the temperature increases, the fluctuation, especially the orientational fluctuation, of bulk water molecules are also increased. However, the structure of the interfacial water molecules is restricted by the geometry of the solute, thus being less sensitive to the temperature increase. Therefore, when temperature increases, the entropy difference between the bulk water and interfacial water molecules becomes higher, which as a result induces stronger hydrophobic association.

3.2.3 Hard-Sphere-Like Solutes in Water

In previous sections we have studied the fullerene-water and Argon-water solutions. In both cases, there is no obvious "drying" around an isolated solute. As

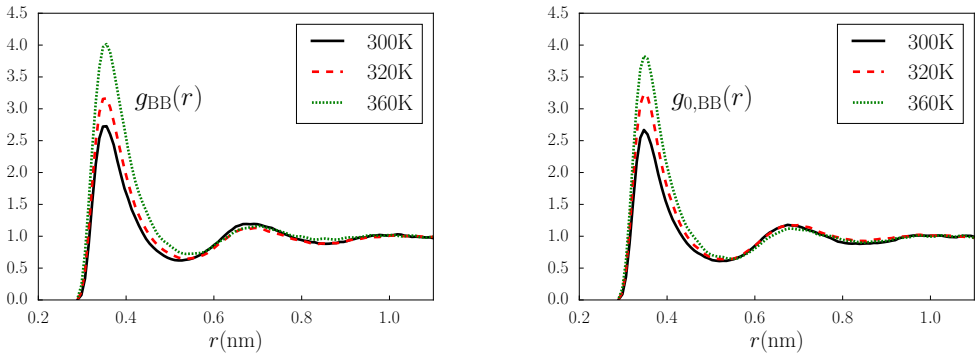

(a) **(b)**

Figure 3.7: Figure (a) shows the inverse temperature behavior of the Argon-Argon RDF $g_{\mathrm{BB}}(r)$. Figure (b) shows the inverse temperature behavior of the Argon-Argon RDF in the repulsive core system, denoted by $g_{0,\mathrm{BB}}(r)$. All the data are obtained at $P = 1\mathrm{atm}$.

we mentioned at beginning of Chapter 3.2, the drying behavior results from the breaking of the hydrogen bonding network near the solute and from the unbalanced force produced by the water-water vdW attractions. For Argon and fullerene in water, the water-water attraction is balanced by the solute-water attraction, as we have shown in Figure 3.3 and 3.5, thus even the repulsive-core system has almost correct solute-water RDF as shown in Figure 3.4 and 3.6. To test the accuracy and find the limits of our theory, it is beneficial to find systems where vdW attractions have a significant influence on the structure. In this section, we try to study harshly repulsive hard-sphere-like solutes. By "hard-sphere-like" we mean that both the solute-water and solute-solute interaction are harshly repulsive interactions like the WCA core potential of the LJ fluid. We try to study these hard-sphere-like solutes

instead of real hard spheres because it is hard to use the discontinuous hard sphere potential in standard MD simulation packages. These hard-sphere-like solutes are used as a computationally useful alternative exhibiting the same physics.

Noticeably there exist many theories discussing the hydrophobic hydration and association of hard spheres in water, which makes the hard sphere solvation problem even more interesting. The most famous one is the Lum-Weeks-Chandler theory [14], which uses Gaussian Fluctuation Theory to take into account the repulsive-core contribution to the hydrophobicity and uses mean field theory to take into account the water-water attraction contribution. The Lum-Weeks-Chandler theory qualitatively works really well and is able to predict the "length scale transition behavior" of hydrophobic hydration, which means that the drying of water happens only when the hard sphere solute is large enough(about 1nm diameter). This length scale transition is related to the breaking of hydrogen bonds and was first suggested by Stillinger [40] and we are also going to show it using simulation data later.

In the target system, the hard-sphere-like solute is denoted by B and the water is denoted by A. The solute-water and solute-solute interaction in the target system is denoted by $u_{0,\mathrm{AB}}(r)$ and $u_{0,\mathrm{BB}}(r)$, which are short ranged harshly repulsive interaction. The water-water interaction in the target system still follows the interaction of SPC/E water, and the LJ part is denoted by $u_{\mathrm{AA}}(r)$. We manipulate these interaction and construct the mimic system, which has interaction $\{u_{R,\mathrm{AA}}(r), u_{R,\mathrm{AB}}(r), u_{R,\mathrm{BB}}(r)\}$. The water-water attraction is chosen to be truncated

in the mimic system, namely $u_{R1,\mathrm{AA}}(r) = 0$. $u_{R1,\mathrm{AB}}(r)$ and $u_{R1,\mathrm{BB}}(r)$ are determined following Eq.(3.25) and Eq.(3.25). In this particular situation, $u_{R1,\mathrm{AB}}(r)$ can be effectively interpreted as the unbalanced potential produced by the water-water vdW attraction, which is a repulsive potential pushing water away from the solute. The $u_{R1,\mathrm{BB}}(r)$ will also be a repulsive potential, whose main role is to balance the additional solute-solute effective attraction produced by $u_{R1,\mathrm{AB}}(r)$. One can better understand this point by looking at Figure 3.1 and 3.2.

Our first model for the hard-sphere-like solute is the repulsive core of Argon. The diameter of the core is 0.34 nm, which is below the transition length and hence there is no obvious drying near the solute, as shown in Figure 3.9b. The interactions in the target and mimic system are shown in Figure 3.8. $u_{R1,\mathrm{AB}}(r)$ and $u_{R1,\mathrm{BB}}(r)$ are repulsive as expected. The solute-water and solute-solute RDF of the target and mimic system are shown in Figure 3.9, as one can see the RDFs in the mimic system closely match the RDFs in the target system, which verifies the accuracy of our theory. The RDFs in the repulsive-core system, where vdW attractions between all the species are truncated, are also shown in Figure 3.9. The solute-solute RDF in the repulsive-core system is obviously different, which shows that the water-water attractions have an obvious influence on the hydrophobic association. However, the solute-water RDF in the repulsive core system is quite close to the solute-water RDF in the target and mimic system, because the water-water vdW attraction is not strong enough to break the hydrogen bonds and pull the water molecules away

from the solute.

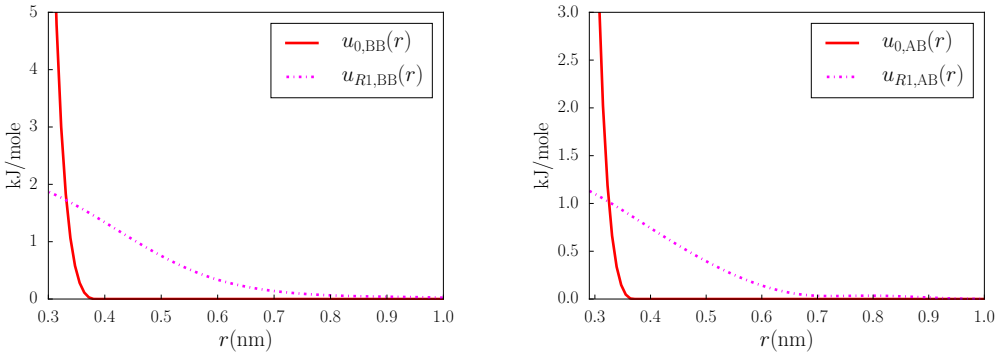

(a) **(b)**

Figure 3.8: In this figure, B stands for the repulsive core of Argon, A stands for water. In figure (a), $u_{R1,\mathrm{BB}}(r)$ is the long ranged part of the solute-solute interaction in the mimic system. $u_{0,\mathrm{BB}}(r)$ is the short ranged repulsive core solute-solute interaction. In figure (b), $u_{R1,\mathrm{AB}}(r)$ is the long ranged part of the solute-water interaction in the mimic system. $u_{0,\mathrm{AB}}(r)$ is the short ranged repulsive core solute-water interaction.

Our second model for the hard-sphere-like solute is the repulsive core of fullerene. The coarse grained model of fullerene is already defined in Chapter 3.2.1. The diameter of the core is about 1 nm, which is just about the transition length and we do see obvious drying near the solute, as shown in Figure 3.11b. So this is a really good case to test the limit of our theory. The interactions in the target and mimic system are shown in Figure 3.10. $u_{R1,\mathrm{AB}}(r)$ and $u_{R1,\mathrm{BB}}(r)$ are strongly repulsive in this case. The solute-water RDF and solute-solute PMF of the target and mimic system are shown in Figure 3.11, as one can see the RDF and PMF in the mimic

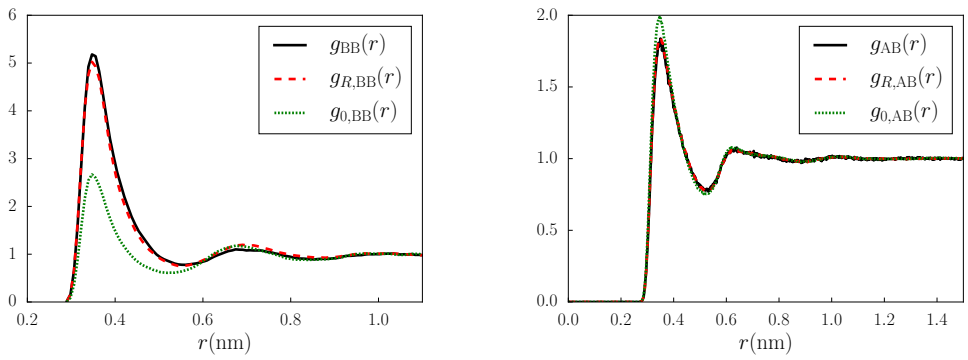

(a) **(b)**

Figure 3.9: In this figure, B stands for the repulsive core of Argon, A stands for water. Figure (a) shows the solute-solute RDF in the target, mimic and repulsive-core system, represented by $g_{\mathrm{BB}}(r)$, $g_{R,\mathrm{BB}}(r)$ and $g_{0,\mathrm{BB}}(r)$ respectively. Figure (b) shows the solute-water RDF in the target, mimic and repulsive-core system, represented by $g_{\mathrm{AB}}(r)$, $g_{R,\mathrm{AB}}(r)$ and $g_{0,\mathrm{AB}}(r)$ respectively.

system basically match the corresponding ones in the target system, although the matching of the solute-solute PMF is not as good as what we have seen in before, which is not surprising considering the huge drying needed to be taken care of. The RDFs in the repulsive-core system, where vdW attractions between all the species are truncated, are also shown in Figure 3.11. One feature of the target system which is correctly captured in the mimic system is the "evaporation phenomena". As shown in Figure 3.11a, the solute-solute PMF in the repulsive-core system has a local minimum at about $r = 1.2$nm, which corresponds to the configuration that one water molecule is placed in between the two fullerenes. However, this minimum does not exist in the PMF of the target and mimic system, since the drying force is too strong and a vacuum layer is formed between the fullerenes. An illustration of the evaporation behavior is shown in Figure 3.12. As one can see, even in this case where obvious drying happens, our theory still works pretty well, which proves that the approximations we made are physically valid.

3.3 Manipulating the Coulomb Interactions

Calculating the Coulomb interactions in computer simulations using Ewald summation or related techniques can be really time consuming when the size of the system becomes large. To speed up the simulation speed, we use the framework shown in Chapter 3.1 to simplify the Coulomb interactions. In the mimic system constructed by us, the "effective range" of the interactions, defined as the range

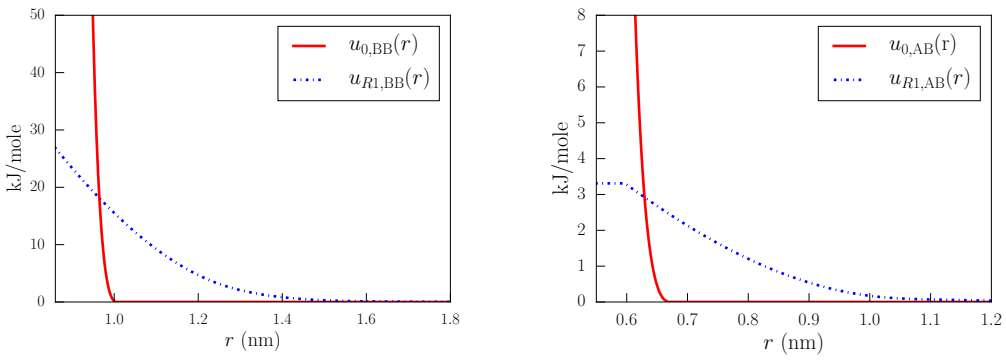

(a) **(b)**

Figure 3.10: In this figure, B stands for the repulsive core of Fullerene, A stands for water. In figure (a), $u_{R1,\mathrm{BB}}(r)$ is the long ranged part of the solute-solute interaction in the mimic system. $u_{0,\mathrm{BB}}(r)$ is the short ranged repulsive core solute-solute interaction. In figure (b), $u_{R1,\mathrm{AB}}(r)$ is the long ranged part of the solute-water interaction in the mimic system. $u_{0,\mathrm{AB}}(r)$ is the short ranged repulsive core solute-water interaction.

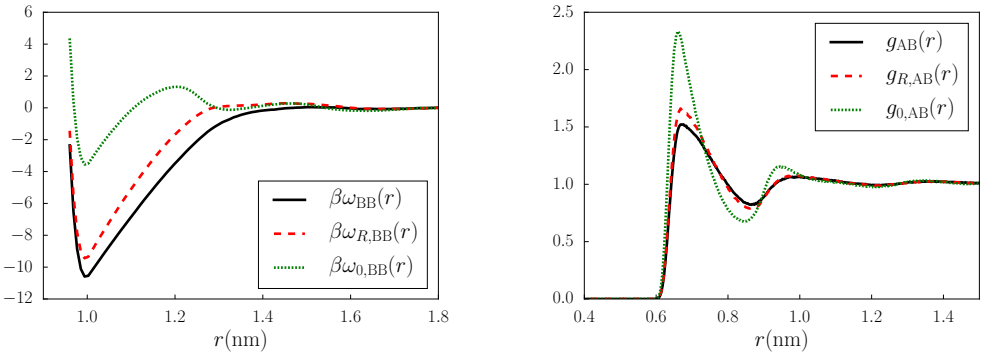

(a) **(b)**

Figure 3.11: In this figure, B stands for the repulsive core of Fullerene, A stands for water. Figure (a) shows the solute-solute RDF in the target, mimic and repulsive-core system, represented by $u_{\mathrm{BB}}(r)$, $u_{R,\mathrm{BB}}(r)$ and $u_{0,\mathrm{BB}}(r)$ respectively. Figure (b) shows the solute-water RDF in the target, mimic and repulsive-core system, represented by $u_{\mathrm{AB}}(r)$, $u_{R,\mathrm{AB}}(r)$ and $u_{0,\mathrm{AB}}(r)$ respectively.

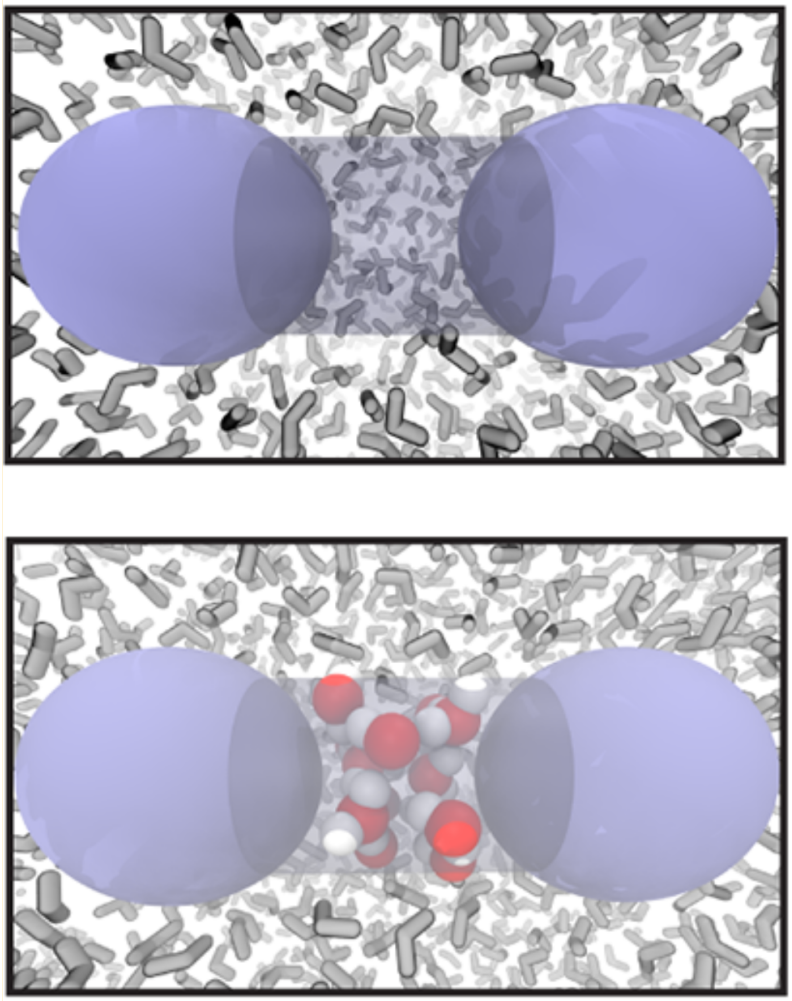

Figure 3.12: This figure illustrates the evaporation phenomena between two repulsive-core fullerenes. The top panel illustrates the evaporation phenomena. As one can see a vacuum region forms between the two solutes. As a comparison, the bottom panel illustrates the case where water molecules fill in between the solutes. This figure is taken from Ref [17] with permission.

within which the strength of the interactions are larger or comparable to kT, are significantly shorter, as will be shown later.

The model system we are going to study is dilute solution with single-site ions as solutes. We will use A to denote the solvent and Greek letters ξ, α to denote the ion solutes. Coulomb interactions, no matter between ion-solvent, solvent-solvent or ion-ion, always have the same form $\frac{1}{r}$, which can be separated into short ranged $v_0(r)$ and long ranged part $v_1(r)$ as discussed in Chapter 2.5. We can manipulate the long ranged tail of Coulomb interactions using our framework. In the mimic system constructed by us, the manipulated Coulomb potential, which are denoted as $v_{R,\mathrm{MM}'}(r) = v_0(r) + v_{R1,\mathrm{MM}'}(r)$, can have different long tails between species. The mapping of the interactions is summarized as follows

$$\left\{\begin{array}{c} v_{\mathrm{AA}}(r) = v_0(r) + v_1(r) \\ v_{\xi\mathrm{A}}(r) = v_0(r) + v_1(r) \\ v_{\xi\alpha}(r) = v_0(r) + v_1(r) \end{array}\right\} \Longrightarrow \left\{\begin{array}{c} v_{R,\mathrm{AA}}(r) = v_0(r) + v_{R1,\mathrm{AA}}(r) \\ v_{\xi\mathrm{A}}(r) = v_0(r) + v_{R1,\xi\mathrm{A}}(r) \\ v_{\xi\alpha}(r) = v_0(r) + v_{R1,\xi\alpha}(r) \end{array}\right\}. \tag{3.30}$$

$v_{R1,\mathrm{AA}}(r)$ can be chosen freely without affecting $g_{R,\mathrm{AA}}(r)$. $v_{R1,\xi\mathrm{A}}(r)$ and $v_{R1,\alpha\xi}(r)$ are chosen according to the following formula

$$v_{R1,\xi A}(r) = v_1(r) - \frac{1}{q_\xi}\int d\boldsymbol{r}' \rho^q_{R,A|\xi}(r'|0)(v_{R1,AA}(|\boldsymbol{r}-\boldsymbol{r}'|) - v_1(|\boldsymbol{r}-\boldsymbol{r}'|)) \tag{3.31}$$

and

$$v_{R1,\xi\alpha}(r) = v_1(r) - \frac{1}{q_\alpha}\int d\boldsymbol{r}' \rho^q_{R,A|\alpha}(r'|0)(v_{R1,\xi A}(|\boldsymbol{r}-\boldsymbol{r}'|) - v_1(|\boldsymbol{r}-\boldsymbol{r}'|)) \tag{3.32}$$

respectively. q_ξ stands for the charge of ion ξ. $\rho^q_{A|\xi}(r|0)$ stands for the charge density

of solvent A around the ion ξ. These two equations can be derived based on Eq.(3.12) and (3.13), and the straightforward derivations will not be shown here.

A particularly useful choice of $v_{R1,\mathrm{AA}}(r)$ is to make it equal zero, which means that the Coulomb interaction between solvent molecules are truncated. In this case, $v_{R1,\xi\mathrm{A}}(r)$ obtained using Eq.(3.31) asymptoticly goes to $\frac{1}{\epsilon r}$, and $v_{R1,\xi\alpha}(r)$ obtained using Eq.(3.32) asymptotically goes to $\frac{2}{\epsilon r} - \frac{1}{\epsilon^2 r}$ when r is large. ϵ is the dielectric constant of the solvent. Therefore, in the mimic system, the ion-solvent and ion-ion Coulomb interaction still have long ranged tails, but screened by ϵ.

The presence of the long tails in the mimic system is not surprising considering the fact that the screening of the ion charges has to be preserved in the mimic system. Thanks to the screening, the long tails in the mimic system have much shorter effective range when the solvent has high dielectric constant, which could lower the computational cost. More importantly, the long tails are only within ion-solvent and ion-ion, which means that the computational cost for calculating these long tails using Ewald summation will be $O(N_B N_A + N_B^2)$, where N_B is the number of the solvated ions. This computational cost is much smaller compared to the cost of using Ewald summation $O((N_B + N_A)^2)$ or the cost of using Particle Mesh Ewald method $O((N_B + N_A)\log(N_B + N_A))$ in the target system, when the concentration of the ions is low.

In Chapter 5, we will show that we can further simplify the mimic system to a new system where the only long ranged tails are between the ions. For that new

system, the computational cost for calculating the long tails will be $O(N_B^2)$, which is even much smaller compared to the computational cost for the mimic system constructed here.

3.4 Conclusions

In this chapter, we have presented the framework to manipulate and simplify the intermolecular interactions of liquid mixtures. This framework has been used to simplify the vdW attractions in neutral solutes-water solutions, which provides a convenient way to quantitatively understand the contribution from water-water attractions to the hydrophobic hydration and association of solutes. This framework has also been used to simplify the Coulomb interactions in ion-water solutions. The mimic system constructed has truncated Coulomb interaction between solvents and is much easier and faster to simulate, and potentially this mimic system can be used in bio-simulations and greatly increase the simulation efficiency.

Chapter 4

Effects of the Long Ranged Component of Solute-Solvent Interactions On the Association of Solutes

The PMF between solutes can be greatly altered by the long ranged component of the solute-solvent interactions. This is due to the fact that the solute-solute PMF is closely related to the solvation free energies of solutes, which are very sensitive to the long ranged solute-solvent interactions such as the vdW attraction and Coulomb interaction [15, 41]. More precisely, the PMF between solutes can be interpreted as the difference of solvation free energy for a pair of solutes separated infinitely far away and a pair separated at distance r. The contribution from the solute-solvent long ranged interactions to the solvation free energy of the solute pair generally depends on the separation of the pair, thus contributing an effective term to the solute-solute PMF. Several theories have been developed focusing on how the solute-water vdW attraction affects the association of the solutes [31–33], but the numerical predictions of these theories are generally speaking not very accurate. To tackle this problem, in this chapter, we develop a method to quantitatively describe the effects of the long ranged component of solute-solvent interactions on the PMF between solutes. This method only makes use of the slowly varying nature of the long ranged solute-solvent interaction and therefore can be used to deal with both vdW

and Coulomb interactions.

The contribution from the long ranged solute-solvent interaction to the solute-solute PMF is quantitatively defined as the difference of the PMF between two full solutes and the PMF between two "reference" solutes. For the reference solutes, the solute-water interactions are truncated and the solute-solute interaction is still the full interaction. Notice that our choice of the interaction between reference solutes is difference from the conventional way of choosing the interaction between reference solutes as the truncated interaction [31]. With our choice one can better concentrate on the contribution of the long ranged solute-solvent interaction to the solute-solute PMF.

As an example to illustrate our definition, for the situation shown in Figure 4.1, the contribution of the B-A long ranged interaction $u_{1,\mathrm{AB}}(r)$ to the B-B PMF is defined as

$$\Delta\omega_{\mathrm{BB}}(r) = \omega_{\mathrm{BB}}(r) - \omega_{\mathrm{B_0B_0}}(r)\,. \tag{4.1}$$

We can represent $\Delta\omega_{\mathrm{BB}}(r)$ as the difference of the reversible work to turn on $u_{1,\mathrm{AB}}(r)$ for a B-B pair with separation r and with separation ∞, which can be mathematically formulated as

$$\Delta\omega_{\mathrm{BB}}(r) = \Delta\Omega_r - \Delta\Omega_\infty\,, \tag{4.2}$$

where the meaning of $\Delta\Omega_r$ and $\Delta\Omega_\infty$ are illustrated in Figure 4.2. By making use of the slowly-varying nature of $u_{1,\mathrm{AB}}(r)$ we can make physical plausible approximations

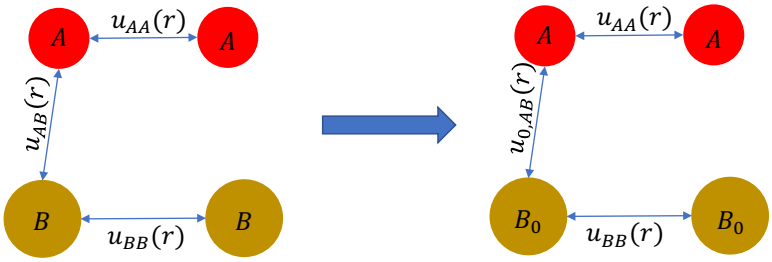

Figure 4.1: The left panel shows full B solutes dissolved in solvent A, with pair interactions $\{u_{\rm AA}(r), u_{\rm AB}(r), u_{\rm BB}(r)\}$. The A-B interaction can be separated into short and long ranged part as $u_{\rm AB}(r) = u_{0,\rm AB}(r) + u_{1,\rm AB}(r)$. The B-B PMF is denoted as $\omega_{\rm BB}(r)$. The right panel shows reference solutes $\rm B_0$ dissolved in A. The $\rm A - B_0$ interaction is just the short ranged part $u_{0,\rm AB}(r)$. The $\rm B_0 - B_0$ interaction is still the full interaction $u_{\rm BB}(r)$. The $\rm B_0 - B_0$ PMF is denoted as $\omega_{\rm B_0B_0}(r)$.

to $\Delta\Omega_r$ and $\Delta\Omega_\infty$ and obtain the following estimation for $\Delta\omega_{\rm BB}(r)$

$$\Delta\omega_{\rm BB}(r) = \int d\boldsymbol{r}' \big\{\delta\rho_{\rm A|B}(r'|0) + \delta\rho_{\rm A|B_0}(r'|0)\big\} u_{1,\rm AB}(|\boldsymbol{r}' - \boldsymbol{r}|)\,, \tag{4.3}$$

where $\rho_{\rm A|B}(r|0)$ represents the density of solvent A given that a full solute B fixed at the origin, $\rho_{\rm A|B_0}(r|0)$ represents the density of solvent A given that a reference solute $\rm B_0$ fixed at the origin, and $\delta\rho_{\rm A|B}(r|0)$ and $\delta\rho_{\rm A|B_0}(r|0)$ are defined as

$$\begin{aligned} \delta\rho_{\rm A|B}(r|0) &= \rho_{\rm A|B}(r|0) - \rho_{b,\rm A} \\ \delta\rho_{\rm A|B_0}(r|0) &= \rho_{\rm A|B_0}(r|0) - \rho_{b,\rm A} \end{aligned} \tag{4.4}$$

where $\rho_{b,\rm A}$ is the bulk density. The derivation needed to get Eq.(4.3) can be found in Chapter 4.1.

It is easy to show that for the PMF between solutes of different species, denoted as B and C, the contribution from B-A long ranged interaction $u_{1,\rm AB}(r)$ and C-A

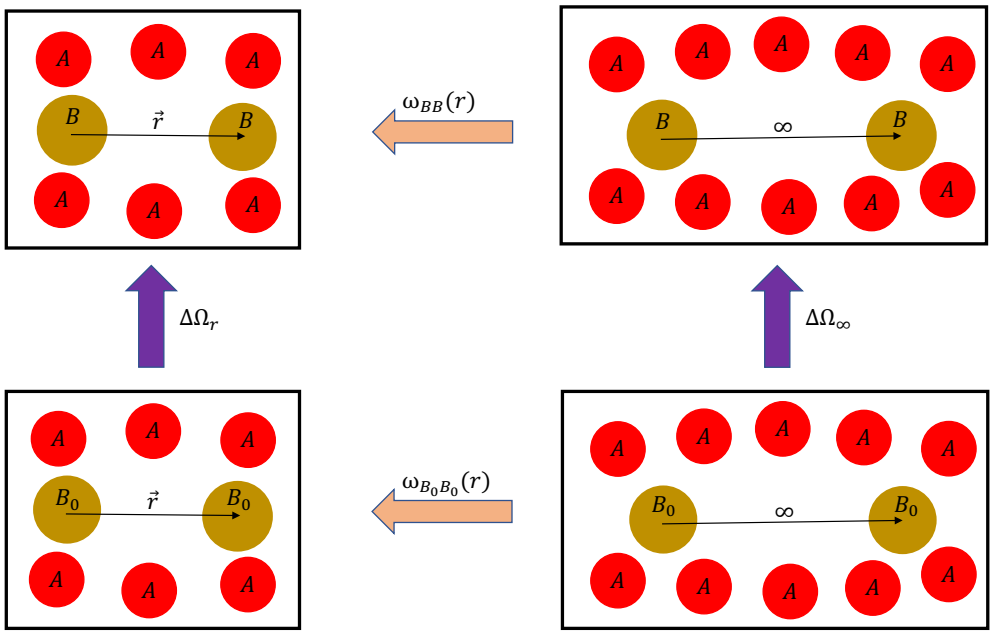

Figure 4.2: This figure shows the relationship of the solute-solute PMF and the reversible work of turning on the solute-solvent long ranged interaction. $\Delta\Omega_r$ is the grand free energy difference between the top left and bottom left panel, which can be interpreted as the reversible work of turning on long ranged solute-solvent interaction $u_{1,\mathrm{AB}}(r)$ given the two solutes are separated at distance r. Similarly, $\Delta\Omega_\infty$ is the grand free energy difference between the top right and bottom right panel, which can be interpreted as the reversible work of turning on long ranged solute-solvent interaction $u_{1,\mathrm{AB}}(r)$ given the two solutes are separated at distance ∞. According to this figure, we have $\omega_{\mathrm{BB}}(r) - \omega_{\mathrm{B_0B_0}}(r) = \Delta\Omega_r - \Delta\Omega_\infty$.

long ranged interaction $u_{1,\mathrm{AC}}(r)$ are approximately

$$\begin{aligned}\Delta\omega_{\mathrm{BC}}(r) =& \frac{1}{2}\int d\boldsymbol{r}'\big\{\delta\rho_{\mathrm{A|B}}(r'|0)+\delta\rho_{\mathrm{A|B_0}}(r'|0)\big\}u_{1,\mathrm{AB}}(|\boldsymbol{r}'-\boldsymbol{r}|)\\ &+\frac{1}{2}\int d\boldsymbol{r}'\big\{\delta\rho_{\mathrm{A|C}}(r'|0)+\delta\rho_{\mathrm{A|C_0}}(r'|0)\big\}u_{1,\mathrm{AC}}(|\boldsymbol{r}'-\boldsymbol{r}|)\,.\end{aligned} \tag{4.5}$$

The derivations to get Eq.(4.5) are similar to the derivations to get Eq.(4.3) and would not be repeated here. Moreover, both Eq.(4.3) and (4.5) are targeting LJ-type interactions, but they can be easily generalized to deal with the Coulomb-type interactions. For example, the contribution from the long ranged ion-solvent Coulomb interaction $v_1(r)$ to the PMF between a ion pair $\xi-\alpha$ can be easily shown to be

$$\begin{aligned}\Delta\omega_{\xi\alpha}(r) =& \frac{1}{2}\int d\boldsymbol{r}'\big\{\rho^q_{\mathrm{A|}\xi}(r'|0)+\rho^q_{\mathrm{A|}\xi_0}(r'|0)\big\}q_\alpha v_1(|\boldsymbol{r}'-\boldsymbol{r}|)\\ &+\frac{1}{2}\int d\boldsymbol{r}'\big\{\rho^q_{\mathrm{A|}\alpha}(r'|0)+\rho^q_{\mathrm{A|}\alpha_0}(r'|0)\big\}q_\xi v_1(|\boldsymbol{r}'-\boldsymbol{r}|)\,,\end{aligned} \tag{4.6}$$

where $\rho^q_{\mathrm{A|}\xi}(r'|0)$ is the charge density of solvent A around the full ion ξ, $\rho^q_{\mathrm{A|}\xi_0}(r'|0)$ is the charge density of solvent A around the reference ion ξ_0, and q_ξ is the charge carried by ion ξ.

4.1 Derivations

In this section we will derive Eq.(4.3) and verify it by study the association of Argon in water.

First let us define some notations. We use B_λ represents a partially coupled solute, as illustrated in Figure 4.3a. Its interaction with solvent A and the other B_λ

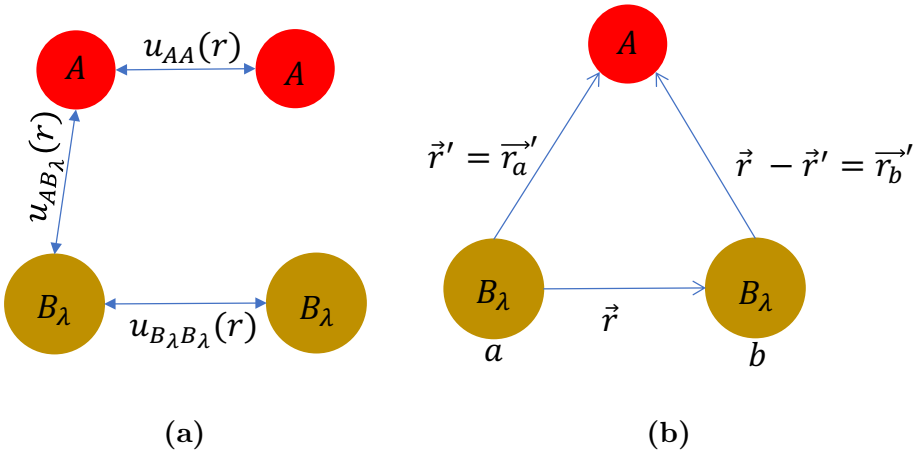

Figure 4.3: Figure (a) illustrates the interactions related to the partially coupled solute B_λ. Figure (b) shows coordinates necessary for the derivation of Equation.(4.3).

is given by

$$u_{\mathrm{AB}_\lambda}(r) = u_{0,\mathrm{AB}}(r) + \lambda u_{1,\mathrm{AB}}(r) \tag{4.7}$$

and

$$u_{\mathrm{B}_\lambda\mathrm{B}_\lambda}(r) = u_{0,\mathrm{BB}}(r) + u_{1,\mathrm{BB}}(r) = u_{\mathrm{BB}}(r)\,. \tag{4.8}$$

Notice that we choose $\mathrm{B}_\lambda - \mathrm{B}_\lambda$ interaction to be the full interaction, and reasons for making this choice have been stated before (See our choice for the interaction between reference solutes).

Ω_λ^r is the grand free energy of the total system when B_λ solutes are at distance r apart as in Figure 4.3b.

In Figure 4.3b solutes B_λ are labeled as a and b. Define $\boldsymbol{r}_a = \boldsymbol{r}$, $\boldsymbol{r}'_a = \boldsymbol{r}'$ and

$\boldsymbol{r}'_b = \boldsymbol{r}' - \boldsymbol{r}$ as in Figure 4.3b. The potential of mean force between B_λ satisfies

$$\omega_{\mathrm{B}_\lambda\mathrm{B}_\lambda}(r) = \Omega^r_\lambda - \Omega^\infty_\lambda \tag{4.9}$$

We have the following exact result using Figure 4.3b notation

$$\begin{aligned}\frac{\partial\big[\Omega^r_\lambda - \Omega^\infty_\lambda\big]}{\partial\lambda} =& \int d\boldsymbol{r}'\delta\rho_{\mathrm{A}|\mathrm{B}_\lambda\mathrm{B}_\lambda}(\boldsymbol{r}'|\boldsymbol{0},\boldsymbol{r})\big\{u_{1,\mathrm{AB}}(r'_a) + u_{1,\mathrm{AB}}(r'_b)\big\} \\ &- \lim_{r\to\infty}\int d\boldsymbol{r}'\delta\rho_{\mathrm{A}|\mathrm{B}_\lambda\mathrm{B}_\lambda}(\boldsymbol{r}'|\boldsymbol{0},\boldsymbol{r})\big\{u_{1,\mathrm{AB}}(r'_a) + u_{1,\mathrm{AB}}(r'_b)\big\}\end{aligned} \tag{4.10}$$

where

$$\delta\rho_{\mathrm{A}|\mathrm{B}_\lambda\mathrm{B}_\lambda} = \rho_{\mathrm{A}|\mathrm{B}_\lambda\mathrm{B}_\lambda} - \rho_{\mathrm{b,A}}\,. \tag{4.11}$$

Eq.(4.10) can be further exactly simplified to

$$\begin{aligned}\frac{\partial\big[\Omega^r_\lambda - \Omega^\infty_\lambda\big]}{\partial\lambda} =& \int d\boldsymbol{r}'_a\big\{\delta\rho_{\mathrm{A}|\mathrm{B}_\lambda\mathrm{B}_\lambda}(\boldsymbol{r}'_a|\boldsymbol{0},\boldsymbol{r}) - \delta\rho_{\mathrm{A}|\mathrm{B}_\lambda}(r'_a|0)\big\}u_{1,\mathrm{AB}}(r'_a) \\ &+ \int d\boldsymbol{r}'_b\big\{\delta\rho_{\mathrm{A}|\mathrm{B}_\lambda\mathrm{B}_\lambda}(\boldsymbol{r}'_b|\boldsymbol{0},\boldsymbol{r}) - \delta\rho_{\mathrm{A}|\mathrm{B}_\lambda}(r'_b|0)\big\}u_{1,\mathrm{AB}}(r'_b) \qquad (4.12) \\ =& 2\int d\boldsymbol{r}'\big\{\delta\rho_{\mathrm{A}|\mathrm{B}_\lambda\mathrm{B}_\lambda}(\boldsymbol{r}'|\boldsymbol{0},\boldsymbol{r}) - \delta\rho_{\mathrm{A}|\mathrm{B}_\lambda}(r'|0)\big\}u_{1,\mathrm{AB}}(r') \qquad (4.13)\end{aligned}$$

Now use the linear approximation for perturbed densities

$$\delta\rho_{\mathrm{A}|\mathrm{B}_\lambda\mathrm{B}_\lambda}(\boldsymbol{r}'|\boldsymbol{0},\boldsymbol{r}) \approx \delta\rho_{\mathrm{A}|\mathrm{B}_\lambda}(r'|0) + \delta\rho_{\mathrm{A}|\mathrm{B}_\lambda}(|\boldsymbol{r}'-\boldsymbol{r}||0) \tag{4.14}$$

in Eq.(4.13). Eq.(4.13) then becomes

$$\begin{aligned}\frac{\partial\big[\Omega^r_\lambda - \Omega^\infty_\lambda\big]}{\partial\lambda} &= 2\int d\boldsymbol{r}'\delta\rho_{\mathrm{A}|\mathrm{B}_\lambda}(|\boldsymbol{r}'-\boldsymbol{r}||0)u_{1,\mathrm{AB}}(r') + u_{1,\mathrm{BB}}(r) \\ &= 2\int d\boldsymbol{r}'\delta\rho_{\mathrm{A}|\mathrm{B}_\lambda}(r'|0)u_{1,\mathrm{AB}}(|\boldsymbol{r}'-\boldsymbol{r}|) + u_{1,\mathrm{BB}}(r)\,,\end{aligned} \tag{4.15}$$

which no longer depends on the 3-body correlation functions.

This linear approximation for the density itself in Eq.(4.14) may not be very accurate in the molecular scale, but since the conditional densities are convoluted with long ranged interaction $u_{1,\mathrm{AB}}(|\boldsymbol{r}' - \boldsymbol{r}|)$ in Eq.(4.13), the error of this approximation will be reduced by the convolution. This is verified by computer simulations when the solute B is Argon. The result is shown in the Figure 4.4. As one can see the linear approximation does not affect the value of the integral in the last line of Eq.(4.13) when the two Argon cores do not overlap.

Now use the Gaussian approximation [41]

$$\delta\rho_{\mathrm{A}|\mathrm{B}_\lambda} = \delta\rho_{\mathrm{A}|\mathrm{B}_0} + \lambda\big\{\delta\rho_{\mathrm{A}|\mathrm{B}} - \delta\rho_{\mathrm{A}|\mathrm{B}_0}\big\} \tag{4.16}$$

and integrate Eq.(4.15) over $\lambda = (0, 1)$. We get

$$(\Omega^r - \Omega_0^r) - (\Omega^\infty - \Omega_0^\infty) = \int d\boldsymbol{r}'\big\{\delta\rho_{\mathrm{A}|\mathrm{B}}(r'|0) + \delta\rho_{\mathrm{A}|\mathrm{B}_0}(r'|0)\big\}u_{1,\mathrm{AB}}(|\boldsymbol{r}' - \boldsymbol{r}|) \tag{4.17}$$

Thus the contribution from $u_{1,\mathrm{AB}}(r)$ to the $B - B$ PMF is

$$\begin{aligned}\Delta\omega_{\mathrm{BB}}(r) =& \omega_{\mathrm{BB}}(r) - \omega_{\mathrm{B}_0\mathrm{B}_0}(r) \\ =& (\Omega^r - \Omega_0^r) - (\Omega^\infty - \Omega_0^\infty) \\ =& \int d\boldsymbol{r}'\big\{\delta\rho_{\mathrm{A}|\mathrm{B}}(r'|0) + \delta\rho_{\mathrm{A}|\mathrm{B}_0}(r'|0)\big\}u_{1,\mathrm{AB}}(|\boldsymbol{r}' - \boldsymbol{r}|)\,,\end{aligned} \tag{4.18}$$

which is just Eq.(4.3).

The accuracy of Eq.(4.3) is verified by studying the effect of the Argon-water vdW attraction on the Argon-Argon PMF. Figure 4.5 compares the $\Delta\omega_{\mathrm{BB}}(r)$ obtained by Eq.(4.3) and by computer simulation when the solute B is Argon. As one can see Eq.(4.3) gives reasonabley accurate results in this case.

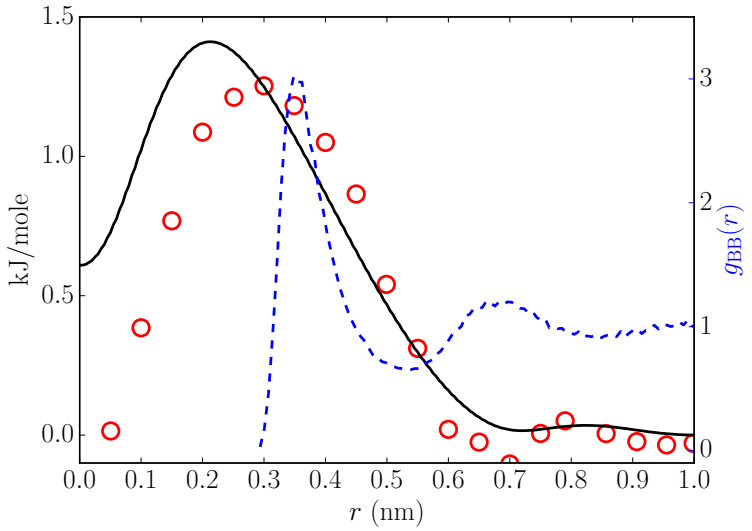

Figure 4.4: In this figure, the curve composed of the red circles corresponds to $\int d\boldsymbol{r}'\big\{\delta\rho_{\rm A|BB}(\boldsymbol{r}'|\boldsymbol{0},\boldsymbol{r}) - \delta\rho_{\rm A|B}(r'|0)\big\}u_{1,\rm AB}(r')$. The solid black curve corresponds to $\int d\boldsymbol{r}'\delta\rho_{\rm A|B}(r'|0)u_{1,\rm AB}(|\boldsymbol{r}'-\boldsymbol{r}|)$. The radial distribution function between two full Argon particles, denoted by $g_{\rm BB}(r)$ is shown as the blue dotted curve, which is put there to illustrate the length scale of the system. As one can see after 0.3nm the difference between the red-circle curve and black solid curve is less than 0.2 kJ/mole ($\sim$0.08kT), which is almost negligible. Both curve goes to 0 after about 0.8nm, after which $g_{\rm BB}(r)$ goes to 1 too. The results are obtained at $T = 300$K and $P = 1$atm.

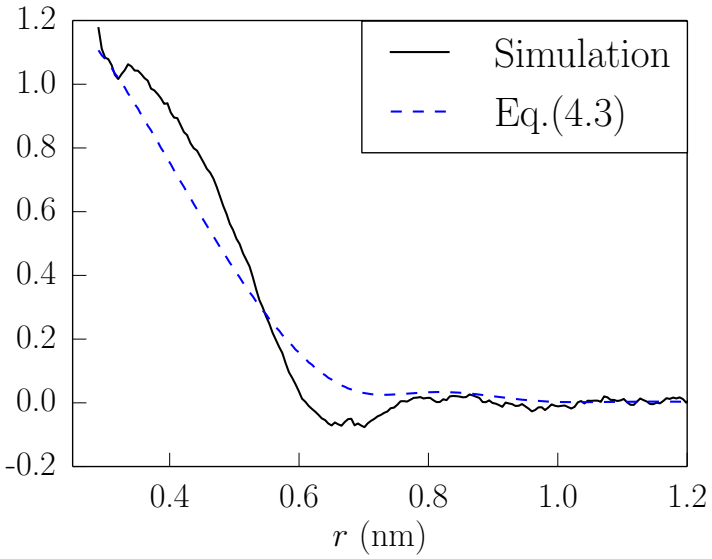

Figure 4.5: In this figure, we compares the $\beta\Delta\omega_{\mathrm{BB}}(r)$ obtained through computer simulation and Eq.(4.3). The computer simulation results(black curve) are obtained by using WHAM method to get $\omega_{\mathrm{BB}}(r)$ and $\omega_{\mathrm{B_0B_0}}(r)$ separately and then taking the difference. The data is obtained at $T = 300\mathrm{K}$ and $P = 1\mathrm{atm}$.

4.2 Conclusions

In this chapter, we have developed a method to quantitatively estimate the effects of long ranged solute-solvent interactions on the solute-solute PMF. This method can be used to calculate the effects of both the vdW attraction and the long ranged Coulomb interaction. Pairing with analytical theories about the cavity-cavity PMF in water, this theory could provide analytical formulas for the PMF between real apolar solutes in aqueous solutions.

Chapter 5

A Short Solvent Model

Solvent molecules usually need to be treated explicitly in computer simulation when one desires accurate description of bioprocesses like folding of biopolymers, protein-ligand binding, etc. In most bio-environments, the concentration of the solutes is much lower than the solvent, which means that a large fraction of computational resources are spent on the solvents. Moreover, the Coulomb interactions between charged molecules need to be taken into account using Ewald summation or related techniques [18, 29, 30], which can become really expensive to be carried out when the size of the system is large. Currently even the fastest implementation of the Ewald-related techniques scales nonlinearly with the size of the system [30]. Also, the long ranged nature of Coulomb interactions shows up in these Ewald algorithms and makes these algorithms less scalable on the massive parallel computing hardwares [42].

People have developed implicit solvent model [20] to tackle these problems. In the implicit solvent model, the solvent degrees of freedom are integrated out and their effects to the structure of the solutes are taken into account as effective interactions between the solutes. These effective interactions are many-body interactions and hard to get exactly. Therefore many approximate ways have been developed

to get the effective solute-solute interactions [43–47]. Famous examples include the Generalized Born model [45] for dielectric effects and the "solvent-exposed surface area model" [44] for nonpolar effects. In many cases one can get qualitatively good results using these approximate methods [48]. However, in many other cases using these approximate methods can give qualitatively incorrect results [49], especially for those cases when the short ranged bonding between the solvent and solute significantly affects the structure of the solutes [50].

To avoid the problems of the implicit solvent model and but still gain substantial computational speed-up compared to the explicit solvent model, in this chapter we propose a truncated or "Short Solvent Model"(SSM). In the SSM, the solvent molecules are presented explicitly in the simulation box, but the long ranged solvent-solvent and solute-solvent interactions are truncated. For example, in the case of the water solvent, the water-water Coulomb interaction and solute-water Coulomb interaction will be truncated in the SSM, and the purpose of doing this is to avoid the necessity of calculating the long tails of these interactions but still make sure that the water-water and solute-water hydrogen bonding are correctly described by the SSM. The effects of truncating the solvent-solvent and solute-solvent interactions on the structure of the solutes are compensated by introducing effective interactions between the solutes. The idea of introducing effective interactions between solutes is similar to what has been done in the implicit solvent model. However, since we only integrate out the slowly-varying long ranged component of the solvent-solvent

and solute-solvent interactions, the effective solute-solute interactions obtained in the SSM will be pairwise to a very good approximation as described below. An illustration of the explicit solvent model, implicit solvent model and the SSM is shown in Figure 5.1. Since the solutes are the dilute species in most bio-simulations, the computational cost to calculate these long ranged solute-solute interactions is negligible and therefore we achieve major speed up by using the SSM comparing to the explicit solvent model. The SSM is also different from the mimic system constructed in Chapter 3. For that mimic system, the solute-solvent interaction could still have non-vanishing long ranged tails (see Chapter 3.3), but in the SSM, the only long ranged interactions are between the solutes. Therefore, the SSM is easier and faster to simulate compared to that mimic system.

In the following sections, we will describe the procedures to get the effective solute-solute interactions for the SSM and verify the accuracy of this model by studying the association of Sodium and Chloride ion in water.

5.1 Effective Solute-Solute Interactions For the SSM

For the SSM, the solute-solute effective interactions are chosen such that the solute-solute PMFs are the same as the corresponding ones of the explicit solvent model or the "target system" using our language. Physically speaking these effective interactions are the contribution from the long ranged solvent-solvent and solute-solvent interactions to the solute-solute PMF. We will show that these solute-solute

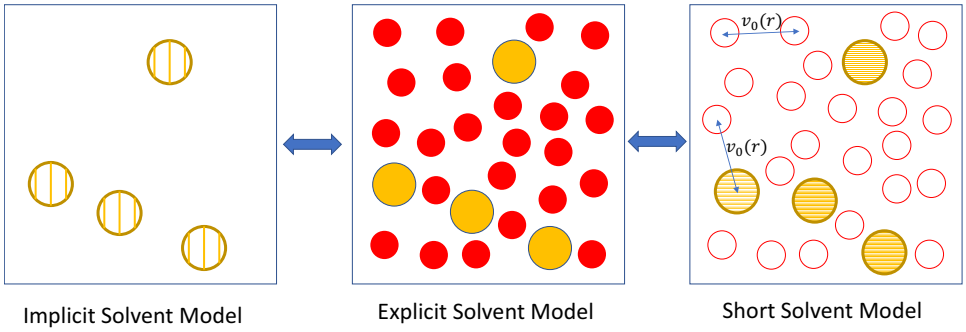

Figure 5.1: This figure compares the explicit solvent model, the implicit solvent model and the SSM. The middle panel, which corresponds to the explicit solvent model, shows a binary solution with full Coulomb interactions between all the species. The left panels shows the corresponding implicit solvent model. In the implicit solvent model, the solvent degrees of freedom are integrated out and effective interactions, which are many-body interactions in principle, are introduced between the solutes. The right panel shows the SSM, which has Gaussian Truncated Coulomb interactions $v_0(r)$ between solvent-solvent and solute-solvent, and long ranged effective interactions between solutes only. The effective solute-solute interactions for the SSM are pairwise to a good approximation.

effective interactions can be obtained by a combination of the techniques used in Chapter 3 and 4.

To get the effective solute-solute interactions in the SSM, one needs to recognize the connection between the mimic system constructed in Chapter 3 and the SSM. In Chapter 3 we have shown that we can simplify the long ranged intermolecular interactions of the target system to get a mimic system which has the same structure as the target system. The mimic system has short ranged solvent-solvent interactions, same as the SSM. But the mimic system has long ranged effective interactions both between solute-solvent and between solute-solute, while the SSM only has long ranged effective interactions between solutes. The additional long ranged effective solute-solvent interactions presented in the mimic system contribute a significant part to the solute-solute PMF and their contributions can be estimated quantitatively using the method developed in Chapter 4. With these additional solute-solvent long tails truncated in the SSM, additional solute-solute interactions should be introduced in the SSM to compensate for this truncation. More precisely, the effective solute-solute interaction in the SSM should equal to the effective solute-solute interaction in the mimic system plus the contribution from the long ranged solute-solvent interactions in the mimic system to the solute-solute PMF.

Let us consider the dilute ion-water solution as an example to illustrate the argument above. Figure 5.2 is also plotted to help understanding. For this dilute solution, the ions are denoted as Greek letters ξ, α etc and the solvents are denoted

as A. We first simplify this target solution to a mimic system, denoted as R. For this mimic system R, the Coulomb interaction between solvents is Gaussian truncated, which means

$$v_{R,\mathrm{AA}}(r) = v_0(r)\,, \tag{5.1}$$

and the effective ion-ion and ion-solvent Coulomb interaction are chosen based on discussions in Chapter 3.3, which have the following expression

$$\begin{aligned} v_{R,\xi A}(r) &= v_0(r) + v_1(r) + \frac{1}{q_\xi}\int d\boldsymbol{r}'\rho^q_{R,A|\xi}(r'|0)v_1(|\boldsymbol{r}-\boldsymbol{r}'|) \\ v_{R,\xi\alpha}(r) &= v_0(r) + v_1(r) - \frac{1}{q_\alpha}\int d\boldsymbol{r}'\rho^q_{R,A|\alpha}(r'|0)(v_{R1,\xi A}(|\boldsymbol{r}-\boldsymbol{r}'|) - v_1(|\boldsymbol{r}-\boldsymbol{r}'|))\,, \end{aligned} \tag{5.2}$$

where $\rho^q_{R,\mathrm{A}|\xi}(r'|0)$ is the conditional charge density of solvent A around ion ξ in the mimic system R. Both $v_{R,\xi A}(r)$ and $v_{R,\xi\alpha}(r)$ can be separated into short and long ranged parts

$$\begin{aligned} v_{R,\xi\mathrm{A}}(r) &= v_0(r) + v_{R1,\xi\mathrm{A}}(r) \\ v_{R,\xi\alpha}(r) &= v_0(r) + v_{R1,\xi\alpha}(r)\,. \end{aligned} \tag{5.3}$$

It can be shown that

$$\begin{aligned} v_{R,\xi\mathrm{A}}(r) &\sim \frac{1}{\epsilon r} \\ v_{R,\xi\alpha}(r) &\sim \frac{2}{\epsilon r} - \frac{1}{\epsilon^2 r} \end{aligned} \tag{5.4}$$

when r is large. To get Eq.(5.4), we assume that the screening charge around an ion is localized and has a total charge of $-(1-\frac{1}{\epsilon})q_\xi$, where q_ξ is the charge of the ion and ϵ is the dielectric constant of the solvent. To put it more precisely, we assume

that

$$\begin{aligned} &\rho^q_{R,A|\xi}(r'|0) = 0 \ \text{ when } r' > \lambda_\xi \\ &\int^{|\boldsymbol{r'}|<\lambda_\xi} d\boldsymbol{r}' \rho^q_{R,A|\xi}(r'|0) = -(1-\frac{1}{\epsilon})q_\xi \,. \end{aligned} \tag{5.5}$$

This assumption is exact when the solvent is a linear dielectric medium [51, 52]. In practice, by calculating the ensemble averaged water charge within a hypothetical sphere around an ion (using the widely accepted charge-based cutoff scheme [53]), we have found Eq.(5.5) to be very accurate, which is possibly due to the fact the singular ion charge is shielded by a harshly repulsive core and would not cause nonlinear dielectric response of the solvent [51]. Given Eq.(5.5), one can show that in the far field regime the electric field generated by $\rho^q_{R,A|\xi}(r'|0)$ is the same as the field generated by a point charge $-(1-\frac{1}{\epsilon})q_\xi$, and this argument can be proved as

$$\begin{aligned} \int d\boldsymbol{r}' \rho^q_{R,A|\xi}(r'|0) v_1(|\boldsymbol{r}-\boldsymbol{r}'|) &= \int^{|\boldsymbol{r'}|<\lambda_\xi} d\boldsymbol{r}' \rho^q_{R,A|\xi}(r'|0) v_1(|\boldsymbol{r}-\boldsymbol{r}'|) \\ &\approx \int^{|\boldsymbol{r'}|<\lambda_\xi} d\boldsymbol{r}' \rho^q_{R,A|\xi}(r'|0) v_1(r) \ \text{ when } r \to \infty \\ &= -(1-\frac{1}{\epsilon}) q_\xi v_1(r) \ \text{ when } r \to \infty \,. \end{aligned} \tag{5.6}$$

Using this argument one can easily get

$$\begin{aligned} v_{R,\xi A}(r) &= v_0(r) + v_1(r) + \frac{1}{q_\xi} \int d\boldsymbol{r}' \rho^q_{R,A|\xi}(r'|0) v_1(|\boldsymbol{r}-\boldsymbol{r}'|) \\ &\approx v_1(r) - (1-\frac{1}{\epsilon}) v_1(r) \ \text{ when } r \to \infty \\ &\approx \frac{1}{\epsilon r} \ \text{ when } r \to \infty \,. \end{aligned} \tag{5.7}$$

Using similar arguments one can get that

$$\begin{aligned} v_{R,\xi\alpha}(r) &= v_0(r) + v_1(r) - \frac{1}{q_\alpha}\int d\boldsymbol{r}'\rho^q_{R,A|\alpha}(r'|0)(v_{R1,\xi A}(|\boldsymbol{r}-\boldsymbol{r}'|) - v_1(|\boldsymbol{r}-\boldsymbol{r}'|)) \\ &\approx v_1(r) + (1-\frac{1}{\epsilon})(v_{R1,\xi A}(r) - v_1(r)) \quad \text{when } r\to\infty \\ &\approx \frac{1}{r} + (1-\frac{1}{\epsilon})(\frac{1}{\epsilon r} - \frac{1}{r}) \quad \text{when } r\to\infty \\ &\approx \frac{2}{\epsilon r} - \frac{1}{\epsilon^2 r} \quad \text{when } r\to\infty\,. \end{aligned} \tag{5.8}$$

The effective Coulomb interaction between ion $\xi-\alpha$ in the SSM is chosen to be the summation of the $\xi-\alpha$ interaction in the mimic system and the contribution from the long ranged ion-solvent interactions to the $\xi-\alpha$ PMF. More precisely, if we use $\tilde{R}$ to denote the SSM, the effective $\xi-\alpha$ Coulomb interaction in the SSM $v_{\tilde{R},\xi\alpha}(r)$ should be

$$v_{\tilde{R},\xi\alpha}(r) = v_{R,\xi\alpha}(r) + \frac{1}{q_\xi q_\alpha}\Delta\omega_{R,\xi\alpha}(r)\,, \tag{5.9}$$

where $\Delta\omega_{R,\xi\alpha}(r)$ is the contribution from $v_{R1,\xi\mathrm{A}}(r)$ and $v_{R1,\alpha\mathrm{A}}(r)$ to the $\xi-\alpha$ PMF. According to the discussions in Chapter 4, $\Delta\omega_{R,\xi\alpha}(r)$ should have the following expression

$$\begin{aligned} \Delta\omega_{\xi\alpha}(r) =& \frac{1}{2}\int d\boldsymbol{r}'\big\{\rho^q_{R,\mathrm{A}|\xi}(r'|0) + \rho^q_{0,\mathrm{A}|\xi}(r'|0)\big\}q_\alpha v_{R1,\alpha\mathrm{A}}(|\boldsymbol{r}'-\boldsymbol{r}|) \\ &+ \frac{1}{2}\int d\boldsymbol{r}'\big\{\rho^q_{R,\mathrm{A}|\alpha}(r'|0) + \rho^q_{0,\mathrm{A}|\alpha}(r'|0)\big\}q_\xi v_{R1,\xi\mathrm{A}}(|\boldsymbol{r}'-\boldsymbol{r}|)\,, \end{aligned} \tag{5.10}$$

where $\rho^q_{R,\mathrm{A}|\xi}(r'|0)$ is the conditional charge density of solvent A around ion ξ in the mimic system, and $\rho^q_{0,\mathrm{A}|\xi}(r'|0)$ is the conditional charge density in the SSM, which is also the conditional charge density of the "Strong Coupling" system where all the Coulomb interactions are Gaussian Truncated.

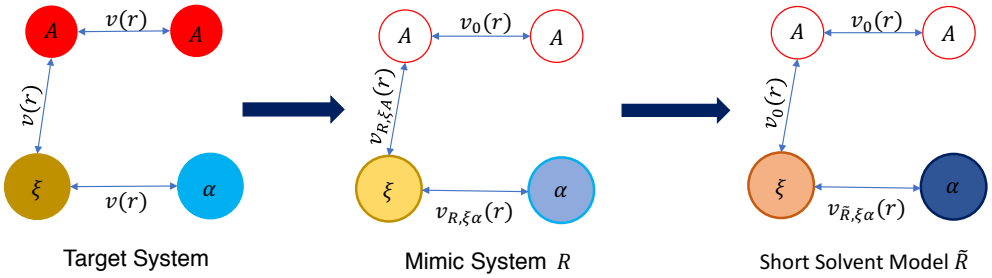

Figure 5.2: This figure illustrates the two-step process to get the effective ion-ion Coulomb interactions of the SSM. The target system is first simplified to the mimic system, in which the solvent-solvent Coulomb interactions is truncated and effective long ranged ion-solvent and ion-ion interactions are introduced. Compared to the mimic system, the ion-solvent Coulomb interactions are truncated in the SSM. We can therefore introduce additional effective interactions between solutes to compensate this truncation, which along with $v_{R,\xi\alpha}(r)$ gives the effective ion-ion interaction $v_{\tilde{R},\xi\alpha}(r)$ in the SSM.

The ion-ion PMF produced by $v_{\tilde{R},\xi\alpha}(r)$ has the correct asymptotic behavior. In the SSM, the ion-solvent and solvent-solvent Coulomb interactions are Gaussian Truncated, which means that the ion charges are not screened at all in the SSM, or more precisely

$$\int d\boldsymbol{r}' \rho^q_{0,\mathrm{A}|\xi}(r'|0) = 0\,. \tag{5.11}$$

Based on Eq.(5.4), (5.5) and (5.11) one can get the asymptotic behavior of $\Delta\omega_{\xi\alpha}(r)$:

$$\begin{aligned}
\Delta\omega_{\xi\alpha}(r) =& \frac{1}{2}\int d\boldsymbol{r}' \big\{\rho^q_{R,\mathrm{A}|\xi}(r'|0) + \rho^q_{0,\mathrm{A}|\xi}(r'|0)\big\} q_\alpha v_{R1,\alpha\mathrm{A}}(|\boldsymbol{r}' - \boldsymbol{r}|) \\
&+ \frac{1}{2}\int d\boldsymbol{r}' \big\{\rho^q_{R,\mathrm{A}|\alpha}(r'|0) + \rho^q_{0,\mathrm{A}|\alpha}(r'|0)\big\} q_\xi v_{R1,\xi\mathrm{A}}(|\boldsymbol{r}' - \boldsymbol{r}|) \\
\approx& -\frac{1}{2}(1-\frac{1}{\epsilon}) q_\xi q_\alpha v_{R1,\alpha\mathrm{A}}(r) - \frac{1}{2}(1-\frac{1}{\epsilon}) q_\alpha q_\xi v_{R1,\xi\mathrm{A}}(r) \quad \text{when } r\to\infty \\
\approx& -q_\xi q_\alpha (1-\frac{1}{\epsilon})\frac{1}{\epsilon r} \quad \text{when } r\to\infty\,,
\end{aligned} \tag{5.12}$$

and to get this we have used again the fact that the conditional charge density distribution around the ion can be viewed as a point charge in the far field regime. Using Eq.(5.4) and Eq.(5.12) we can easily get

$$\begin{aligned}
v_{\tilde{R},\xi\alpha}(r) &= v_{R,\xi\alpha}(r) + \frac{1}{q_\xi q_\alpha}\Delta\omega_{R,\xi\alpha}(r) \\
&\approx \frac{2}{\epsilon r} - \frac{1}{\epsilon^2 r} + \frac{1}{q_\xi q_\alpha}\Big(-q_\xi q_\alpha (1-\frac{1}{\epsilon})\frac{1}{\epsilon r}\Big) \quad \text{when } r\to\infty \\
&= \Big(\frac{2}{\epsilon} - \frac{1}{\epsilon^2} - (1-\frac{1}{\epsilon})\frac{1}{\epsilon}\Big)\frac{1}{r} \text{ when } \quad r\to\infty \\
&= \frac{1}{\epsilon r} \quad \text{when } r\to\infty\,.
\end{aligned} \tag{5.13}$$

Since $v_{\tilde{R},\xi\alpha}(r)$ is the only long ranged interaction in the Short Solvent Model, it determines the asymptotic behavior of the ion-ion PMF when the whole system is

not near the critical point. More precisely

$$\omega_{\tilde{R},\xi\alpha}(r) \sim q_\xi q_\alpha v_{\tilde{R},\xi\alpha}(r) \sim \frac{q_\xi q_\alpha}{\epsilon r} \tag{5.14}$$

when r goes to ∞. This result agrees with the prediction of the dielectric continuum theory.

The ion-ion interactions in the SSM still have non-vanishing long ranged tails as discussed above, but the ion-solvent and solvent-solvent interaction in the SSM are truncated. This means that only the ion-ion interactions needs to be calculated using Ewald sum when doing computer simulations and the computational cost will be $O(N_B^2)$, where N_B is the number of ions in the simulation box. This cost is much smaller compared to the cost of using Ewald sum $O((N_B+N_A)^2)$ or the cost of using Particle Mesh Ewald method $O((N_B + N_A)\log(N_B + N_A))$ in the target system, which means that using the SSM could substantially reduce the computational cost.

5.2 Na-Cl PMF in water

In this section, we try to numerically verify the accuracy of Eq.(5.9) by studying the PMF between Na and Cl in water. In the target system a pair of $Na^+ - Cl^-$ is dissolved in a water box with dimension $2.98\,\text{nm} \times 2.98\,\text{nm} \times 2.98\,\text{nm}$. Periodic boundary conditions are used for this simulation box. In the corresponding SSM, the ion-water and water-water Coulomb interaction are Gaussian Truncated, and the effective ion-ion Coulomb interactions are determined based on Eq.(5.9).

In the SSM, the Na and Cl ion will feel forces from other Na and Cl ions in the

periodic images. Therefore, for the SSM the total energy of ion-ion interactions still need to be calculated by Ewald summation. However, since the only long ranged interactions are between the ions, the Ewald sum for this SSM only involves the ions in the box and is much easier to calculate compared to the Ewald sum in the target system. $\phi^{\text{Ewald}}_{\tilde{R},\text{NaCl}}(\boldsymbol{r})$ is used to denote the total energy of ion-ion interactions in the SSM as a function of the displacement between the Na and Cl ion, and it is defined as

$$\phi^{\text{Ewald}}_{\tilde{R},\text{NaCl}}(\boldsymbol{r}) = \frac{1}{2}\sum_{\boldsymbol{m}}{}' \sum_{\xi}\sum_{\alpha} q_\xi q_\alpha v_{\tilde{R},\xi\alpha}\big(|\boldsymbol{r}_\xi - (\boldsymbol{r}_\alpha + \boldsymbol{m})|\big)\,, \tag{5.15}$$

which sums over the ion-ion interactions coming from the origin box and the periodic images. $\boldsymbol{r}$ is the relative displacement between Na and Cl in the origin box. $\boldsymbol{m} = (i,j,k)L$ represents the center of the periodic boxes, where L is the length of the edge of the box. $\xi, \alpha \in \{\text{Na}^+, \text{Cl}^-\}$. The prime in $\sum'_{\boldsymbol{m}}$ means that the summation omits the $\xi = \alpha$ term when $\boldsymbol{m} = (0,0,0)$. $v_{\tilde{R},\xi\alpha}(r)$ is the effective $\xi - \alpha$ Coulomb interaction in the SSM obtained using Eq.(5.9). This summation is conditionally convergent and calculated using Ewald summation with tin-foil boundary conditions. The meaning of this summation is illustrated in Figure 5.3.

$\phi^{\text{Ewald}}_{\tilde{R},\text{NaCl}}(\boldsymbol{r})$ is in general not a spherically symmetric potential due to the shape of the simulation box. For simplicity, we focus on the situation when Na and Cl are restricted on the z-axis, or in other words $\boldsymbol{r} = (0,0,r)$. With this restriction we use $\phi^{\text{Ewald}}_{\tilde{R},\text{NaCl}}(r)$ as a short-hand notation for $\phi^{\text{Ewald}}_{\tilde{R},\text{NaCl}}(\boldsymbol{r} = (0,0,r))$ in the following context.

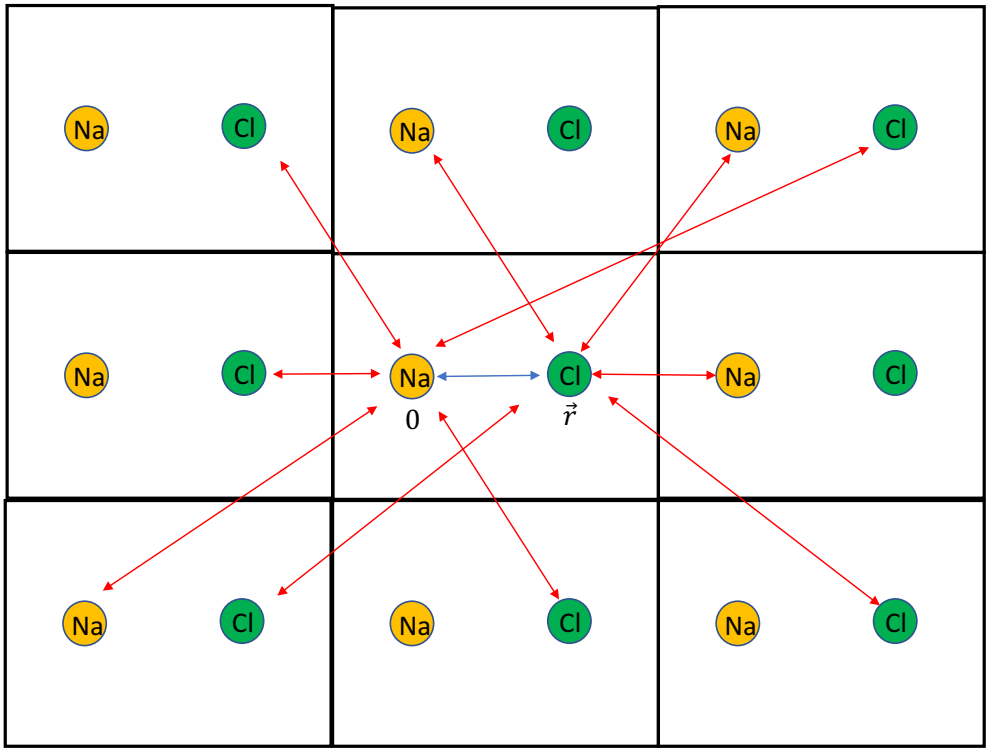

Figure 5.3: $\phi^{\text{Ewald}}_{\tilde{R},\text{NaCl}}(r)$ is a summation of both the Na-Cl interaction in the origin box(blue arrow) and the interactions coming from all the periodic images(red arrow). In the origin box, Na is placed at $\mathbf{0}$, Cl is placed at $\boldsymbol{r} = (0, 0, r)$. To make this figure looks clear, we did not show all the red arrows which are included in $\phi^{\text{Ewald}}_{\tilde{R},\text{NaCl}}(r)$.

$\phi^{\text{Ewald}}_{\tilde{R}1,\text{NaCl}}(r)$, which is the long ranged part of $\phi^{\text{Ewald}}_{\tilde{R},\text{NaCl}}(r)$ and defined as

$$\phi^{\text{Ewald}}_{\tilde{R}1,\text{NaCl}}(r) \coloneqq \phi^{\text{Ewald}}_{\tilde{R},\text{NaCl}}(r) - q_{\text{Na}}q_{\text{Cl}}v_0(r)\,, \tag{5.16}$$

relates Na-Cl PMF in the SSM and the Gaussian Truncated Strong Coupling system by

$$\omega_{\tilde{R},\text{NaCl}}(r) = \omega_{0,\text{NaCl}}(r) + \phi^{\text{Ewald}}_{\tilde{R}1,\text{NaCl}}(r)\,, \tag{5.17}$$

where $\omega_{0,\text{NaCl}}(r)$ is the Na-Cl PMF in the Gaussian Truncated Strong Coupling system.

$\phi^{\text{Ewald}}_{\tilde{R},\text{NaCl}}(r)$ depends on the size of the simulation box. In the limiting situation when the size of the simulation box is infinite, $\phi^{\text{Ewald}}_{\tilde{R},\text{NaCl}}(r)$ only contains the direct interaction energy between the Na-Cl pair in the origin box, or more precisely,

$$\phi^{\text{Ewald}}_{\tilde{R},\text{NaCl}}(r) = q_{\text{Na}}q_{\text{Cl}}v_{\tilde{R},\text{NaCl}}(r) \quad \text{when } L \to \infty. \tag{5.18}$$

To quantitatively show the dependence of $\phi^{\text{Ewald}}_{\tilde{R},\text{NaCl}}(r)$ on L , we compare $\phi^{\text{Ewald}}_{\tilde{R},\text{NaCl}}(r)$ at $L = 2.98$nm, which is our choice of L for the real simulation, and at $L = \infty$ (Figure 5.4). The L-dependence of $\phi^{\text{Ewald}}_{\tilde{R},\text{NaCl}}(r)$ is determined by the contribution from the periodic images. Noticeably, at $L = 2.98$ nm the gradient of $\phi^{\text{Ewald}}_{\tilde{R},\text{NaCl}}(r)$ goes to 0 at the edge of the box (Figure 5.4), which is a constraint imposed by the symmetry of the periodic sum in Eq.(5.15).

The Na-Cl PMF (or equivalently RDF) is expected to be the same in the target system and in the SSM, which is proved to be true by computer simulation as shown in Figure 5.5. The Na-Cl RDF of the target system and the SSM agree

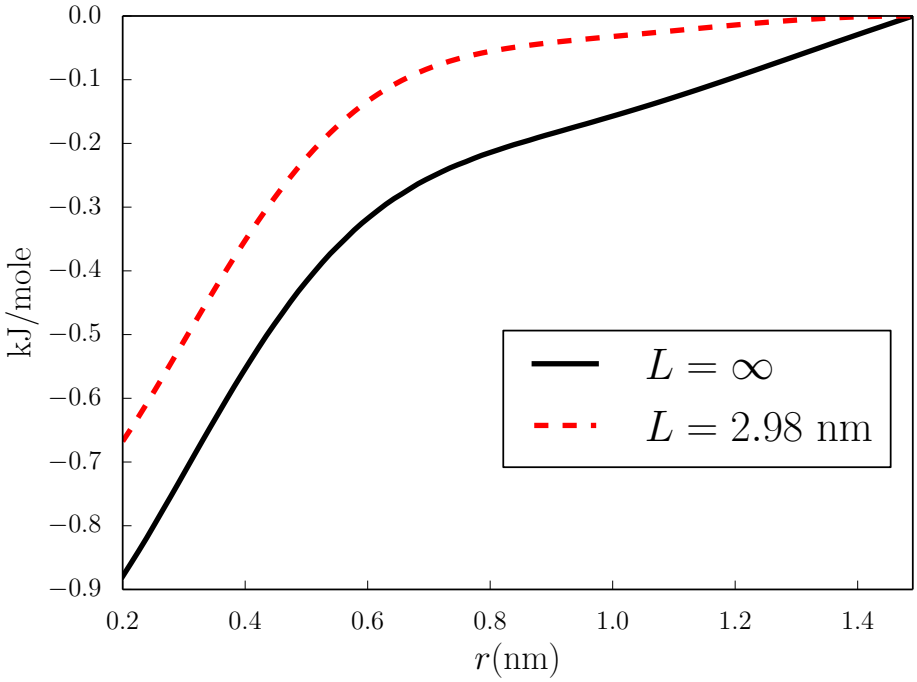

Figure 5.4: This figure compares $\phi^{\text{Ewald}}_{\tilde{R}1,\text{NaCl}}(r)$, which is the long ranged part of $\phi^{\text{Ewald}}_{\tilde{R},\text{NaCl}}(r)$ and defined by Eq.(5.16), at $L = 2.98$nm and at $L = \infty$. Notice that only the long ranged part of $\phi^{\text{Ewald}}_{\tilde{R},\text{NaCl}}(r)$ is compared in this figure since the short ranged part has no L-dependence. Both potential are shifted to 0 at $2.98/2 = 1.49$nm to better show their difference. For the curve corresponding to $L = 2.98$nm, its gradient goes to 0 at the half length of the box(1.49nm), which is a constraint imposed by the symmetry of the periodic sum in Eq.(5.15). As a comparison, for the curve corresponding to $L = \infty$, it decays as $\frac{q_{\text{Na}}q_{\text{Cl}}}{\epsilon r}$ according to Eq.(5.18) and will only have zero gradient at $r = \infty$.

really well, which verifies the accuracy of our theory.

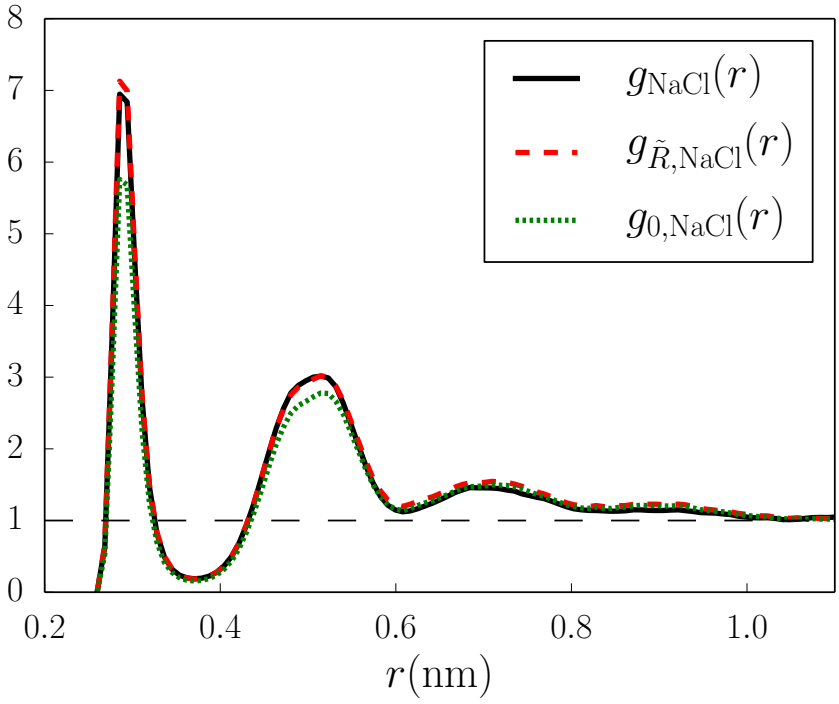

Figure 5.5: This figure compares the Na-Cl RDF of the target system(black curve) and the SSM(red curve). The Na-Cl RDF for the "Strong Coupling" system(green curve), where Coulomb interactions between all the species are truncated, is also shown for comparison. The data is obtained at $P = 1\mathrm{atm}$ and $T = 300\mathrm{K}$.

5.3 Conclusions

In this chapter, we have constructed the Short Solvent Model. The SSM can give an accurate description for the association of $\mathrm{Na}^+ - \mathrm{Cl}^-$ in water. While Ewald summation still needs to be conducted for the SSM, only the ion-ion interactions

need to be calculated using Ewald sum. With the number of long ranged interactions dramatically reduced compared to the explicit solvent model, SSM eliminates the biggest computational bottleneck of simulating large-size systems and therefore could be practically useful for bio-simulations.

Chapter 6

Finite Density Solutions

6.1 Simplifying The Interactions For Phase-Separating and Well-Mixed Solutions

In this chapter we will explore how to manipulate the interactions for finite density solutions. One situation which may occur in finite density solutions is the demixing of different components. When the solution separates into different phases it is challenging to find a single set of manipulated interactions which could preserve the structure of every phase. In this chapter we try to get insight into the well-mixed and phase-separating finite density solutions by studying binary LJ-like mixtures with specially chosen long ranged tails. We will start with the phase separating solutions first.

The phase separated solution studied here is modeled as binary LJ mixture. Let us use A and B to denote the two species. The interactions are denoted as $\{u_{\rm AA}(r), u_{\rm AB}(r), u_{\rm BB}(r)\}$, with the following definition

$$\begin{aligned} u_{\rm AA}(r) &= u_0(r) + u_1(r) \\ u_{\rm AB}(r) &= u_0(r) - u_1(r) \\ u_{\rm BB}(r) &= u_0(r) + u_1(r)\,. \end{aligned} \tag{6.1}$$

$u_0(r)$ is the WCA interaction. $u_1(r)$ is the attractive tail of the LJ interaction. According to the definition, A and B have the same repulsive core u_0. The $A-A$ and $B-B$ interaction has long ranged attractive interaction between them, while $A-B$ has long ranged repulsive interaction between them. According to these interactions, A likes to stay next to A and B likes to stay next to B. Therefore, it is clear that this mixture will phase separate into a A rich phase and B rich phase below a critical demixing temperature T_C. An illustration of the phase diagram for this mixture is shown in Figure 6.1a. Our simulation results show that $T_C^* = k_B T_C/\epsilon$ should be about 10 at a state with total density $\rho* = \rho\sigma^3 = 0.62$. Figure 6.1b shows a typical equilibrium configuration of this system in a MD simulation with periodic boundary conditions at temperature $T^* = 4$, where strong AB phase separation is evident. Due to the symmetry of the interactions between A and B, as shown in Eq.(6.1), the A-rich and B-rich phase occupies the same volume in the simulation box when the mole fraction of B, denoted by χ_B, is 0.5, as shown in Figure 6.1b.

We want to construct a mimic system with the same repulsive cores and appropriately manipulated long range interactions such that it can capture the phase separation behavior. If we want the structure of the mimic system to be exactly the same as the target system, we would have no choice but to make the interactions of the mimic system the same as those of the target system. However, in this case we want to simplify the interactions and still preserve certain particular structural properties which we are interested in, and in this way we can get the freedom to

make meaningful manipulations to the interactions.

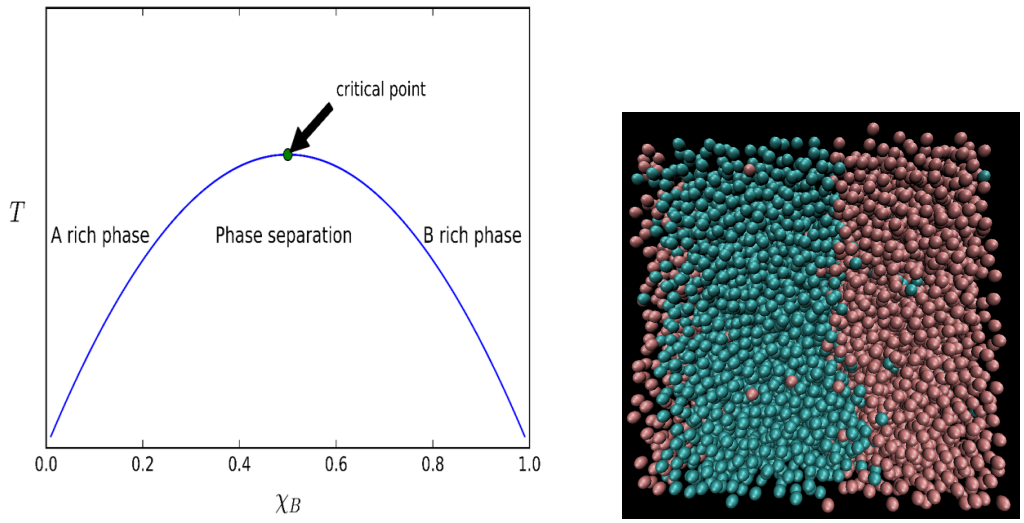

(a) **(b)**

Figure 6.1: Figure (a) is an illustration of the phase diagram for the phase separating mixture mentioned in the main context. χ_B is the mole fraction of species B. Notice that the phase boundary is symmetric about $\chi_B = \frac{1}{2}$, which is due to the symmetry of interactions. Figure (b) shows a snapshot of the phase separating mixture at $\chi_B = \frac{1}{2}$. The state point is $\rho^* = 0.62$ and $T^* = 4$ in LJ units. Notice that ρ^* is the total number density of the two species.

The interactions in the mimic system are denoted as $\{u_{R,\mathrm{AA}}(r), u_{R,\mathrm{AB}}(r), u_{R,\mathrm{BB}}(r)\}$. We choose

$$u_{R1,\mathrm{AA}}(r) = u_{R1,\mathrm{BB}}(r) = 0\,, \tag{6.2}$$

which preserves the A − B symmetry in the mimic system. With A − A and B − B interaction truncated, $u_{R1,\mathrm{AB}}(r)$ in the only effective long ranged in the mimic

system, and is the only interaction able to separate the two phases. Notice that $u_{R1,\mathrm{AB}}(r)$ should in principle depend on the mole fraction χ_B. However, in practice we found that $u_{R1,\mathrm{AB}}(r)$ is not sensitive to χ_B and is only a function of temperature and pressure. Based on this we can very simply determine $u_{R1,\mathrm{AB}}(r)$ in the limit of χ_B goes to zero. The dilute limit has been discussed a lot in the previous chapters and we can take advantage of the results obtained before.

For this special system, we want to choose $u_{R1,\mathrm{AB}}(r)$ such that

$$g_{R,\mathrm{BB}}(r) \approx g_{\mathrm{BB}}(r) \tag{6.3}$$

when B is dilutely solvated in A. We choose to keep the $\mathrm{B}-\mathrm{B}$ correlation function unchanged since it is eventually the clustering of the B particles that drives the phase separating we want to produce. In practice we find to a very good approximation that phase separation occurs only when the average number of nearest neighbors as determined from the first peak of $\mathrm{B}-\mathrm{B}$ correlation function exceeds unity (when two B particles can cluster, on average it seems likely that other B particles can follow and cause phase separation).

$u_{R1,\mathrm{AB}}(r)$ determined from Eq.(6.3) satisfies the following equation, as will be explained in Figure 6.2 and the discussion below following Eq.(6.6)

$$\int d\boldsymbol{r}' \big(\delta\rho_{\mathrm{A|B}}(r'|0)+\delta\rho_{0,\mathrm{A|B}}(r'|0)\big)\big(u_{R1,\mathrm{AB}}(|\boldsymbol{r}'-\boldsymbol{r}|-u_{I1,\mathrm{AB}}(|\boldsymbol{r}'-\boldsymbol{r}|)\big) = u_{I1,\mathrm{BB}}(r) \text{ for } r > d, \tag{6.4}$$

where

$$u_{I1,\mathrm{AB}}(r) = \begin{cases} u_{1,\mathrm{AB}}(r) + \int dr'(\rho_{\mathrm{A|B}}(r'|0) - \rho_{b,\mathrm{A}})u_{1,\mathrm{AA}}(|r-r'|) & \text{for } r \geq d \\ u_{I1,\mathrm{AB}}(d) & \text{for } r < d \end{cases}, \quad (6.5)$$

and

$$u_{I1,\mathrm{BB}}(r) = u_{1,\mathrm{BB}}(r) - \int dr'(\rho_{\mathrm{A|B}}(r'|0) - \rho_{b,\mathrm{A}})(u_{I1,\mathrm{AB}}(|r-r'|) - u_{1,\mathrm{AB}}(|r-r'|)) . \quad (6.6)$$

d is the effective hard sphere distance determined by $u_{0,\mathrm{LJ}}(r)$. $\rho_{\mathrm{A|B}}(r'|0)$ is the $\mathrm{A}-\mathrm{B}$ conditional density in the target system. $\rho_{0,\mathrm{A|B}}(r'|0)$ is the $\mathrm{A}-\mathrm{B}$ conditional density in the repulsive-core system where long ranged interactions between all the species are truncated.

Eq.(6.4) is an integral equation that can be used to determine $u_{R1,\mathrm{AB}}(r)$. To derive it we have used a two-step manipulation which is slightly different than the two-step manipulation used in Figure 5.2. The two-step manipulation is illustrated in Figure 6.2. Notice that Eq.(6.4) only needs to be satisfied for $r > d$ and this gives us freedom to choose $u_{R1,\mathrm{AB}}(r)$ inside the core. Again, we choose $u_{R1,\mathrm{AB}}(r)$ to be constant inside the core such that the approximations we made are more accurate.

Figure 6.3a shows $u_{R1,\mathrm{AB}}(r)$ obtained by Eq.(6.4). As expected, $u_{R1,\mathrm{AB}}(r)$ is more repulsive than the repulsive $\mathrm{A}-\mathrm{B}$ interaction $u_{1,\mathrm{AB}}(r)$ in the target system, since it needs to be stronger to generate essentially the same phase-separation behavior.

Figure 6.3 shows a snapshot of a typical configuration of a simulation of this mimic system when the mole fraction of B is 0.5, and we indeed get very similar

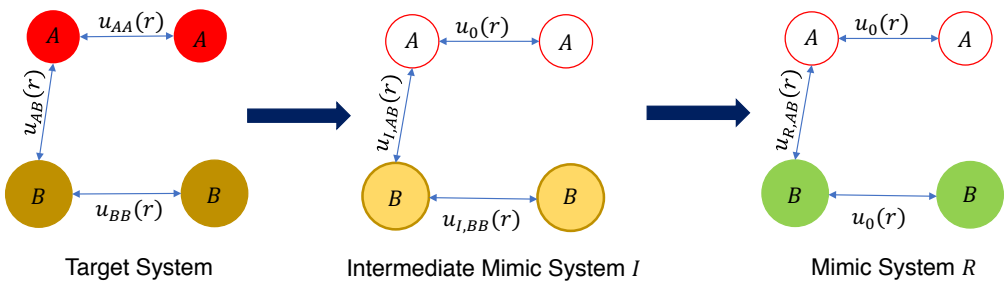

Figure 6.2: The figure illustrates the two-step manipulation which gives us $u_{R1,\mathrm{AB}}(r)$ for the phase separating mixture. The first step is the manipulation defined in Chapter 3.2, which gives us an intermediate mimic system I. The second step is to truncate $u_{I,\mathrm{BB}}(r)$ and choose $u_{R,\mathrm{AB}}(r)$ to compensate the truncation.

phase separation behavior as the target system in Figure 6.1b. In particular we see very similar capillary wave fluctuations at the phase boundaries though these were not targeted when we choose $u_{R1,\mathrm{AB}}(r)$. This shows an important advantage of our new framework compared to the original LMF theory. In previous work on interfaces using LMF theory, phase separation was driven by a static renormalized external field that suppresses capillary wave fluctuations [21]. Moreover standard mean field densities functional treatments of interfaces also suppress these fluctuations and this was thought to be an inherent limitation of mean field ideas as applied to interfaces [22].

The exact same procedure can be used to describe correlation functions in the

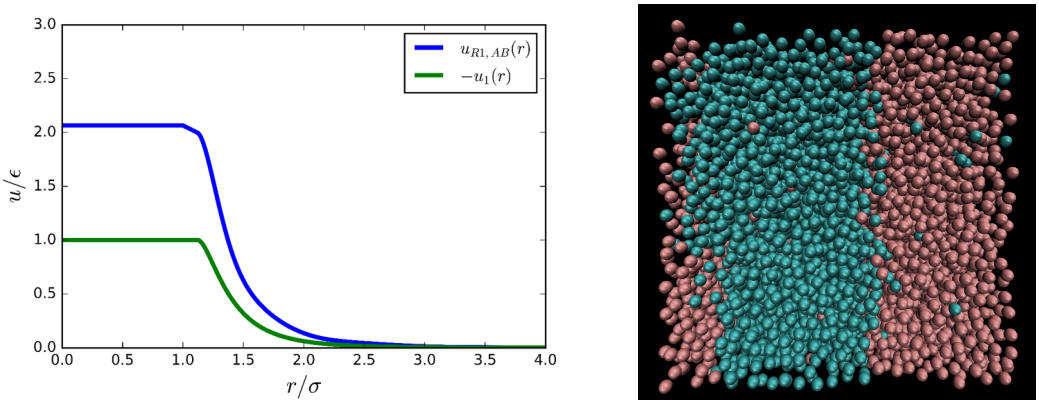

(a) **(b)**

Figure 6.3: Figure (a) shows the $u_{R1,AB}(r)$ in the mimic system of the phase separating mixture. $u_{1,AB}(r) = -u_1(r)$ is shown as a comparison. Figure(b) shows a snapshot of the mimic system with $\chi_B = \frac{1}{2}$.

opposite "Coulomb-like" mixture, where the interactions are defined as

$$\begin{aligned} u_{\mathrm{AA}}(r) &= u_0(r) - u_1(r) \\ u_{\mathrm{AB}}(r) &= u_0(r) + u_1(r) \\ u_{\mathrm{BB}}(r) &= u_0(r) - u_1(r)\,. \end{aligned} \tag{6.7}$$

As one can see, in this Coulomb-like mixture, A likes to stay next to B. This is a typical example of a mixture that mixes completely at all mole fractions but can still exhibit strong $\mathrm{A}-\mathrm{B}$ ordering. This ordering is completely missed in the repulsive-core system.

In the mimic system constructed, again $u_{R1,\mathrm{AA}}(r)$ and $u_{R1,\mathrm{BB}}(r)$ are chosen to be 0. $u_{R1,\mathrm{AB}}(r)$ is the only long ranged interactions in the mimic system and is used to produce the $\mathrm{A}-\mathrm{B}$ ordering in the mimic system. $u_{R1,\mathrm{AB}}(r)$ is chosen according

to Eq.(6.4). The comparison of the radial distribution functions of the target and mimic system is shown in Figure 6.4. As one can see the structure of the mimic system closely matches the target system. Moreover, the successful application of our framework for both the phase separating and well mixed mixture indicates that this framework can be applied to general mixtures, whose phase separation behavior is not known in advance. This could make our framework more useful in practice, though clearly more work will have to be done to fully understand the full implications of these preliminary results.

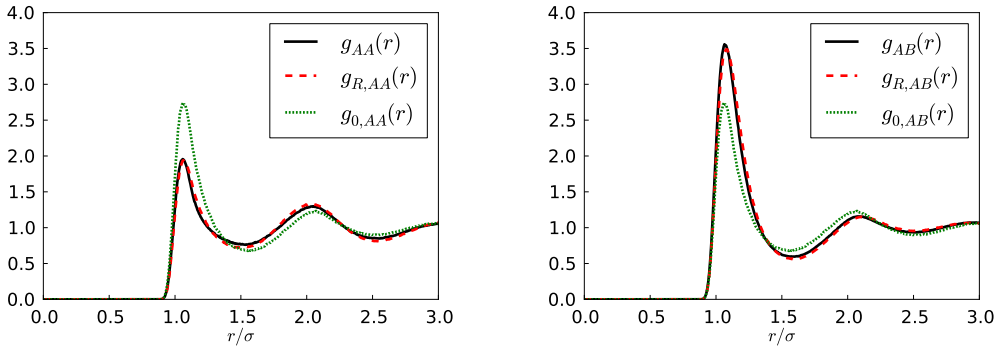

(a) **(b)**

Figure 6.4: This figure compares the RDFs of the Coulomb-like mixture, the corresponding mimic system and the repulsive-core system. Figure (a) shows the $\mathrm{A}-\mathrm{A}$ RDF in the target, mimic and repulsive-core system, denoted by $g_{\mathrm{AA}}(r)$, $g_{R,\mathrm{AA}}(r)$ and $g_{0,\mathrm{AA}}(r)$ respectively. Figure(b) shows the $\mathrm{A}-\mathrm{B}$ RDF in the target, mimic and repulsive-core system, denoted by $g_{\mathrm{AB}}(r)$, $g_{R,\mathrm{AB}}(r)$ and $g_{0,\mathrm{AB}}(r)$ respectively. The state point is $\rho^* = 0.83$ and $T^* = 1$ in LJ units. ρ^* is the total number density of the two species. Notice that the $\mathrm{B}-\mathrm{B}$ RDF is not shown since it is the same as the $\mathrm{A}-\mathrm{A}$ RDF due to the symmetry of interactions.

6.2 Conclusions

In this chapter we have designed a way to simplify the intermolecular interactions for a special type of phase-separating and well-mixed mixtures. The mimic system constructed by us is able to preserve the structural feature of the target mixture. Remarkably, for the phase separating mixture, the mimic system has the same surface tension and capillary wave fluctuations as the target system, which is due to the fact that the phase separation is still driven by pair interactions in the mimic system. With simplified interactions, analytical estimation of the surface tension might be easier in the mimic system. Future work is needed to make the framework described in this chapter applicable to general mixtures.

Chapter 7

Diffusion Dynamics of Solutes in the Target and Mimic System

7.1 Mathematical Framework for Describing the Diffusion Dynamics

In previous chapters we have discussed how to manipulate the long ranged intermolecular interactions without changing the structure of the liquid mixture. In this chapter we will explore how these manipulations affect the diffusion dynamics of the solutes. The diffusion dynamics of solutes has been a central topic in physical chemistry for a long time, and the simplest theory for it is the Stokes-Einstein relationship

$$D = \frac{kT}{c\pi\eta a}\,, \tag{7.1}$$

where $c = 4$ for slip boundary conditions and $c = 6$ for stick boundary conditions. Here D is the diffusion constant of the solute, η is the viscosity of the neat solvent and a is the radius of the solute. A few remarkable implications of the Stokes-Einstein relationship are

1. The diffusion constant is inversely proportional to the size of the solute.

2. The diffusion constant is inversely proportional to the viscosity of the solvent.

3. The diffusion constant is independent of the mass of the solute and solvent.

The Stokes-Einstein relationship is based on continuum hydrodynamic theory, and the contribution of intermolecular interactions is taken into account very implicitly and crudely. In the Stokes-Einstein relationship, the viscosity η is determined by the solvent-solvent interaction, while the radius a and the boundary condition c are determined by solute-solvent interaction. Since the intermolecular interactions are not accurately taken into account, Stokes-Einstein relationship often contradicts experimental facts. A famous example is the diffusion of ions in water [54]. It has been shown that the size dependence of the ion diffusivity violates the Stokes-Einstein relationship. For example, a lithium cation is found to diffuse slower than a potassium cation in water. This behavior is believed to be caused by the electrostatic interactions between ions and water.

The diffusion dynamics can quite sensitively depend on the intermolecular interactions, and many efforts have been made to understand how these interactions can affect the dynamics of a solute. For example, Yamaguchi and his coworkers [55] have studied the effect of attractive solute-solvent and solvent-solvent interactions in LJ solutions. They found that the solute-solvent attractive interaction tend to decrease the diffusion constant of the solute. The solvent-solvent attractive interaction hardly affects the diffusion constant of the solute, but it does alter the shape of the dynamic friction kernel. Wolynes has studied the effects of ion-solvent interactions on the diffusivity of the ion in polar solvent [56]. By partitioning the ion-solvent interactions into harsh short ranged and soft long ranged interactions and consider-

ing their contributions separately, he was able to explain the continuum dielectric friction picture [57] and "solventberg" [58] picture as limiting cases of his theory.

To exactly describe the dynamics of the solutes, one needs the Generalized Langevin Equation [59]. For a spherical solute immersed inside a bulk fluid, the Generalized Langevin Equation has the following form

$$m\frac{d\boldsymbol{v}}{dt} = -\int_0^t d\tau\zeta(t-\tau)\boldsymbol{v}(\tau) + \boldsymbol{R}(t)\,, \tag{7.2}$$

where m and $\boldsymbol{v}$ are the mass and velocity of the solute, respectively. $\zeta(t)$ is called the dynamic friction kernel, memory function or friction kernel in different contexts. $R(t)$ is the random force.

According to Eq.(7.2), the total force on the solute can be divided into two parts. $-\int_0^t d\tau\zeta(t-\tau)\boldsymbol{v}(\tau)$ corresponds to the systematic part, which can be viewed as coming from the "friction" between the moving solute and the solvent. $\boldsymbol{R}(t)$ corresponds to the random part, which comes from the random collisions between the solute and solvent particles. Given that the systematic part and the random part both arise microscopically from the solute-solvent interactions, it is not surprising that they are related to each other. Their relationship is shown in the fluctuation-dissipation theorem

$$\zeta(t) = \frac{1}{3kT}\left\langle \boldsymbol{R}(t)\cdot\boldsymbol{R}(0)\right\rangle\,, \tag{7.3}$$

which can be proved with Mori-Zwanzig theory [59].

The friction kernel $\zeta(t)$ plays a crucial role in the Generalized Langevin Equation. It is related to the velocity auto correlation function(VCF) of the solute $C_v(t)$

by

$$\frac{d}{dt}C_v = -\int_0^t d\tau \zeta(t-\tau)C_v(\tau)\,. \tag{7.4}$$

With $C_v(t)$ known one can determine $\zeta(t)$ using Eq.(7.4), and vice versa. Moreover, the diffusion constant of the solute D can be determined by the friction kernel and velocity auto correlation function with

$$D = \frac{kT}{\int_0^\infty \zeta(t)dt}\,. \tag{7.5}$$

and

$$D = \frac{kT}{m}\int_0^\infty C_v(t)dt\,. \tag{7.6}$$

respectively. In this section velocity auto correlation function $C_v(t)$ is used to characterize the diffusion dynamics of the solutes, and we will analyze how the manipulations of the interactions affects the behavior of $C_v(t)$.

7.2 Short Time Behavior of Diffusion Dynamics

We first analyze the short time behavior the velocity auto correlation function $C_v(t)$ of solute B in solvent A by making a Taylor expansion

$$\begin{aligned}
C_v(t) &= \frac{m_{\rm B}}{3kT}\left\langle \boldsymbol{v}(0)\cdot\boldsymbol{v}(t)\right\rangle \\
&= \frac{m_{\rm B}}{kT}\left\langle v_x(0)\cdot v_x(t)\right\rangle \\
&= \frac{m_{\rm B}}{kT}\Big(\left\langle v_x(0)^2\right\rangle + \frac{1}{2}\left\langle v_x(0)\ddot{v}_x(0)\right\rangle t^2 + \frac{1}{24}\left\langle v_x(0)v_x^{(4)}(0)\right\rangle t^4\ldots\Big) \\
&= \frac{m_{\rm B}}{kT}\Big(\left\langle v_x(0)^2\right\rangle - \frac{1}{2}\left\langle \dot{v}_x(0)\dot{v}_x(0)\right\rangle t^2 + \frac{1}{24}\left\langle \ddot{v}_x(0)\ddot{v}_x(0)\right\rangle t^4\ldots\Big)\,.
\end{aligned} \tag{7.7}$$

m_{B} is the mass of solute B. $\boldsymbol{v}$ represents the velocity of the solute. To get the second line of Eq.(7.7), we have used the fact that the system is spherically symmetric. To get the third line of Eq.(7.7), we have used the fact that $\langle v_x(0)v_x(t)\rangle$ has the time reversal symmetry, which guarantees that there is no odd terms in the time expansion. To get the fourth line of Eq.(7.7), we have used the fact that for any two observable Q and P, we have $\left\langle Q(0)\ddot{P}(t)\right\rangle = -\left\langle \dot{Q}(0)\dot{P}(t)\right\rangle$. A proof of this relationship involves the fact that the Liouville operation $\mathcal{L}$ is anti-self-adjoint. A detailed proof can be found in [60].

The zeroth order term $\frac{m_{\mathrm{B}}}{kT}\langle v_x(0)^2\rangle$ is simply 1. The coefficient of the first order term $\frac{m_{\mathrm{B}}}{2kT}\langle \dot{v}_x(0)^2\rangle$ can be written as

$$\begin{aligned}
\frac{m_{\mathrm{B}}}{2kT}\left\langle \dot{v}_x(0)^2\right\rangle =& \frac{1}{2kT}\left\langle F_x(0)^2\right\rangle \\
=& \frac{1}{2kT}\left\langle \sum_i\sum_j \frac{\partial u_{\mathrm{AB}}(|\boldsymbol{r}_i-\boldsymbol{r}|)}{\partial x}\frac{\partial u_{\mathrm{AB}}(|\boldsymbol{r}_j-\boldsymbol{r}|)}{\partial x}\right\rangle \\
=& \frac{1}{2}\left\langle \sum_i \frac{\partial^2 u_{\mathrm{AB}}(|\boldsymbol{r}_i-\boldsymbol{r}|)}{\partial x^2}\right\rangle \\
=& \frac{1}{2}\frac{\rho_{b,\mathrm{A}}}{3m_{\mathrm{B}}}\int d\boldsymbol{r}\nabla^2 u_{\mathrm{AB}}(r)g_{\mathrm{AB}}(r)\,,
\end{aligned} \tag{7.8}$$

where $u_{\mathrm{AB}}(r)$ is the solute-solvent interaction, the summation of i and j is over all the solvent particles, $F_x = \sum_i \frac{\partial u_{\mathrm{AB}}(|\boldsymbol{r}_i-\boldsymbol{r}|)}{\partial x}$ is the total force on the solute projected to the x-direction, $\boldsymbol{r}$ is the coordinate of the solute, $\boldsymbol{r}_i$ is the coordinate of the solvent particle, the partial derivative $\frac{\partial}{\partial x}$ is with respect to the x coordinate of the solute, $\rho_{b,\mathrm{A}}$ is the bulk density of solvent A. To get the forth line we have used the Yvon theorem [61] .

The coefficient of the second order term is called the Einstein frequency Ω_0^2, which is defined as

$$\begin{aligned}\Omega_0^2 &= \frac{m_{\mathrm{B}}}{kT}\left\langle \dot{v}_x(0)^2 \right\rangle \\ &= \frac{\rho_{b,\mathrm{A}}}{3m_{\mathrm{B}}}\int d\boldsymbol{r}\nabla^2 u_{\mathrm{AB}}(r) g_{\mathrm{AB}}(r)\,.\end{aligned} \tag{7.9}$$

By comparing the Einstein frequency Ω_0^2 between the target and mimic system, we can get insight about how the short time behavior of the velocity autocorrelation function is affected by the manipulation of interactions. In the mimic system, the Einstein frequency $\Omega_{R,0}^2$ is

$$\Omega_{R,0}^2 = \frac{\rho_{b,\mathrm{A}}}{3m_{\mathrm{B}}}\int d\boldsymbol{r}\nabla^2 u_{R,\mathrm{AB}}(r) g_{R,\mathrm{AB}}(r)\,, \tag{7.10}$$

where $u_{R,\mathrm{AB}}(r)$ is the solute-solvent interaction in the mimic system, $g_{R,\mathrm{AB}}(r)$ is the solute-solvent RDF in the mimic system. Take the difference of Eq.(7.9) and (7.11) and we can get

$$\Omega_0^2 - \Omega_{R,0}^2 = \frac{\rho_{b,\mathrm{A}}}{3m_{\mathrm{B}}}\int d\boldsymbol{r}\nabla^2 (u_{1,\mathrm{AB}}(r) - u_{R1,\mathrm{AB}}(r)) g_{R,\mathrm{AB}}(r)\,, \tag{7.11}$$

where we have used the fact that $g_{R,\mathrm{AB}}(r) \approx g_{\mathrm{AB}}(r)$. The difference of the Einstein frequency involves the second derivative of $u_{1,\mathrm{AB}}(r) - u_{R1,\mathrm{AB}}(r)$, which can be expected to be small since both $u_{1,\mathrm{AB}}(r)$ and $u_{R1,\mathrm{AB}}(r)$ are slowly varying. Therefore the short time behavior of the velocity correlation function should be similar for the mimic and target system.

The long time behavior of the velocity autocorrelation function are related to many-body correlation functions [56]. Although the pair correlation functions of

the target and mimic system are similar and the many-body correlation functions are determined by pair correlation functions as discussed in Appendix A, the many-body correlation functions, especially those involving the collective behavior of many particles, could be sensitive to the small differences in the pair correlations functions and can thus be quite different for the target and mimic system. Therefore, there is no guarantee that the long time behavior of the velocity autocorrelation function of the mimic and target system are similar.

To verify our arguments, we computed the velocity autocorrelation function of fullerenes in the target, mimic and repulsive-core system defined in Chapter 3.2.1, and the results are summarized in Figure 7.1. As one can see, the velocity correlation function in the target and mimic system are close to each other. Remember that for this fullerene-water solution we made manipulations to the VdW attractions, which are not slowly varying enough, and this may explain the small discrepancies of the velocity correlation function in the target and mimic system. The velocity correlation function in the repulsive-core system is also close to the velocity correlation function in the target system, which is reasonable since the fullerene-water RDF of the repulsive-core system is not too much different from the corresponding ones in the mimic and target system, as shown in Figure 3.4b. Moreover, one can see that the VCF in the mimic system is closer to the VCF in the target system than the VCF in the repulsive-core system, which is due to the fact that the solute-solvent RDF of the mimic system is closer to the target system.

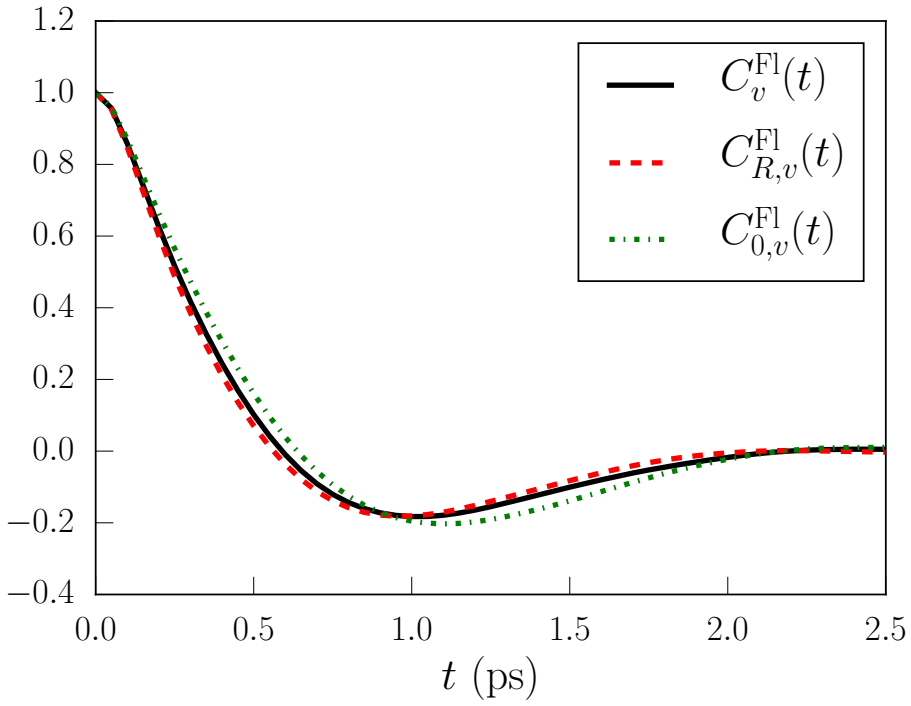

Figure 7.1: This figure shows the velocity autocorrelation function of fullerene in the target, mimic and repulsive-core system defined in Chapter 3.2.1. $C_v^{\mathrm{Fl}}(t)$ represents the velocity autocorrelation function of fullerene in the target system. $C_{R,v}^{\mathrm{Fl}}(t)$ represents the velocity autocorrelation function of fullerene in the mimic system. $C_{0,v}^{\mathrm{Fl}}(t)$ represents the velocity autocorrelation function of fullerene in the repulsive-core system. As one can see, both $C_{R,v}^{\mathrm{Fl}}(t)$ and $C_{0,v}^{\mathrm{Fl}}(t)$ are close to $C_v^{\mathrm{Fl}}(t)$, despite that $C_{R,v}^{\mathrm{Fl}}(t)$ is closer. The data is obtained at NVE ensemble.The average temperature and pressure for this ensemble is $T = 300\mathrm{K}$ and $P = 1\mathrm{atm}$.

To further verify our arguments, we also computed the VCF of the solute in the target, mimic and repulsive-core system when the target system is repulsive core of fullerenes in solution with water, as defined in Chapter 3.2.3. The results are shown Figure 7.2. The VCF in the target and mimic system agrees reasonably well. The discrepancies may due to the fact that VdW attraction is not slowly varying enough, and also due to the fact that the solute-water RDF of the target and mimic system do not match perfectly, as shown in Figure 3.9b. Also, since the solute-water RDF of the repulsive-core system is obviously different compared to the target and mimic system, its VCF is not so close to the solute VCF in the target and mimic system, as shown in Figure 7.2.

We also computed the VCF of Na^+ and Cl^- in the target system, mimic system R defined in Chapter 3.3 and Gaussian-Truncated system where the Coulomb interaction between all the species are truncated , and the results are shown in Figure 7.3. The VCF in all the three systems are basically the same with each other, which indicates that the long ranged Coulomb tail $v_1(r)$ would not affect the diffusion of charged ions, and it is worth further testing whether this fact is generally true for other types of solvents and ions.

7.3 Conclusions

In this chapter, we have analytically shown and verified by simulation that the short time behavior of the diffusion dynamics of the solutes can be well preserved in

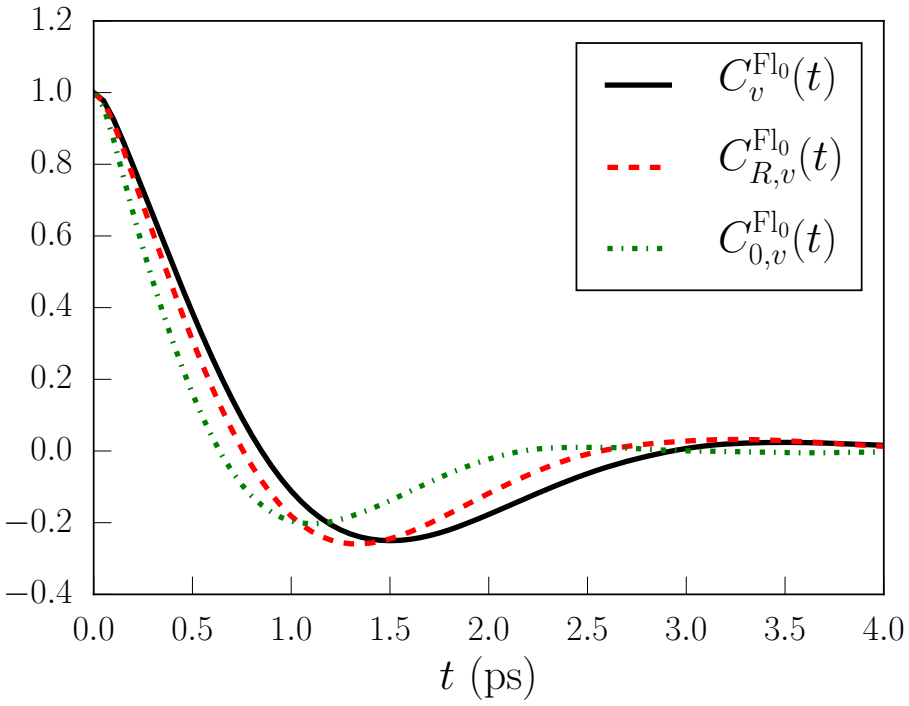

Figure 7.2: This figure shows the velocity autocorrelation function of the solute in the target, mimic and repulsive-core system when the target system is repulsive core of fullerenes in solution with water, as defined in Chapter 3.2.3. Fl_0 is used to define the repulsive core of fullerene. $C_v^{\mathrm{Fl}_0}(t)$ represents the velocity autocorrelation function of solute in the target system. $C_{R,v}^{\mathrm{Fl}_0}(t)$ represents the velocity autocorrelation function of solute in the mimic system. $C_{0,v}^{\mathrm{Fl}_0}(t)$ represents the velocity autocorrelation function of solute in the repulsive-core system. As one can see, both $C_{R,v}^{\mathrm{Fl}_0}(t)$ is close to $C_v^{\mathrm{Fl}_0}(t)$. $C_{0,v}^{\mathrm{Fl}}(t)$ is away from the other two. The data is obtained at NVE ensemble.The average temperature and pressure for this ensemble is $T = 300\mathrm{K}$ and $P = 1\mathrm{atm}$.

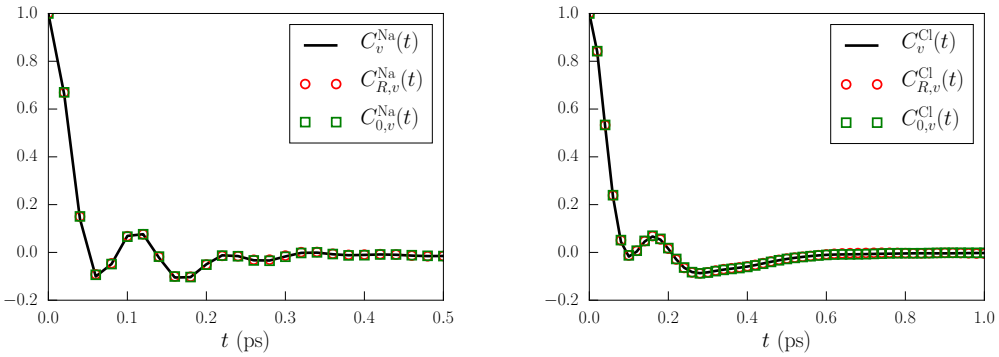

(a) **(b)**

Figure 7.3: This figure shows the velocity autocorrelation function of Na^+ and Cl^- in the target system, mimic system R defined in Chapter 3.3 and Gaussian Truncated system. $C_v^{\mathrm{Na}}(t)$ and $C_v^{\mathrm{Cl}}(t)$ represent the velocity autocorrelation function of Na^+ and Cl^- in the target system. $C_{R,v}^{\mathrm{Na}}(t)$ and $C_{R,v}^{\mathrm{Cl}}(t)$ represent the velocity autocorrelation function of Na^+ and Cl^- in the mimic system R. $C_{0,v}^{\mathrm{Na}}(t)$ and $C_{0,v}^{\mathrm{Cl}}(t)$ represent the velocity autocorrelation function of Na^+ and Cl^- in the Gaussian Truncated system. The data is obtained at NVE ensemble. The average temperature and pressure for this ensemble is $T = 300\mathrm{K}$ and $P = 1\mathrm{atm}$. Notice that in the mimic system, the solute-water interaction has non-vanishing long tails. For the simulation purpose here we just made a cutoff for that solute-water interaction with large enough cutoff distance such that the neglected long tail have no effects on the VCF of the solutes.

the mimic system. Surprisingly, we found out that the diffusion dynamics of Sodium and Chloride ion in water is not affected by the long ranged Coulomb interactions, and it is worthwhile to test whether this is generally true for other type of charged solutes.

Chapter 8

Conclusions and Future work

In this thesis we demonstrated a framework to manipulate the long ranged interactions of liquid mixtures while keeping the structure of the whole system or certain parts essentially unchanged. Within this framework, the unbalanced forces produced by the long ranged interactions are approximated as effective pair interactions between molecules. As a comparison, within the framework of LMF theory the unbalanced forces are usually taken as static effective single-particle fields. Therefore, the new framework can be viewed as a natural generalization of LMF theory by allowing the unbalanced forces to be approximated as more general renormalized pair interactions in the mimic system Hamiltonian.

We have used this framework to manipulate the VdW and Coulomb interactions in dilute solutions. The structure of the mimic systems constructed with the manipulated interactions closely resemble the structure of the target systems, which proves the accuracy of our theory. By manipulating the VdW attractions, we have shown that the inverse temperature behavior of the Argon-Argon hydrophobic interactions is totally an entropic phenomena. Moreover, by manipulating the Coulomb interactions, we have constructed a mimic system with truncated solvent-solvent Coulomb interactions, as shown in Chapter 3.

We have developed a method which tells us how solute-water VdW attraction affects the hydrophobic interactions between apolar solutes, as shown in Chapter 4. A Short Solvent Model, which has long ranged interactions only between solutes, is developed and used to study Na-Cl association in water, as shown in Chapter 5.

We also simplified the interactions of a phase separating mixture and constructed a mimic system which also exhibits the same phase separation behavior and even has the same capillary wave fluctuations at phase boundaries. The manipulations we developed for the phase separating mixture are proved to be a general technique which can apply to well-mixed mixtures, as shown in Chapter 6.

The influence of manipulating interactions on the diffusion dynamics has been explored, with the conclusion that the short-time behavior of the diffusion dynamics is approximately unaffected by the manipulations, as shown in Chapter 7.

In the future we will try to apply the manipulations developed in Chapter 3.3 and the Short Solvent Model developed in Chapter 5 to mixtures containing biomolecules. In the past chapters we have always been focusing on the mixtures composed of rigid small molecules. As we will show in this chapter, some of the ideas and insights gained from dealing with the rigid molecules may help us understand mixtures containing large flexible molecules, like biopolymers and polyelectrolytes in solution with water and mobile co-ions and counter ions. Figure 8.1 schematically depicts a model polyelectrolyte, consisting of nonpolar hydrophobic (H) monomers or beads and charged hydrophilic (P) beads connected by covalent polymer bonds,

in solution with water (W), and charged counter ions (C). (No co-ions are shown in the configuration.) Simulations of such a system incur substantial overhead from conventional Ewald sum and related methods to treat the long ranged Coulomb interactions.

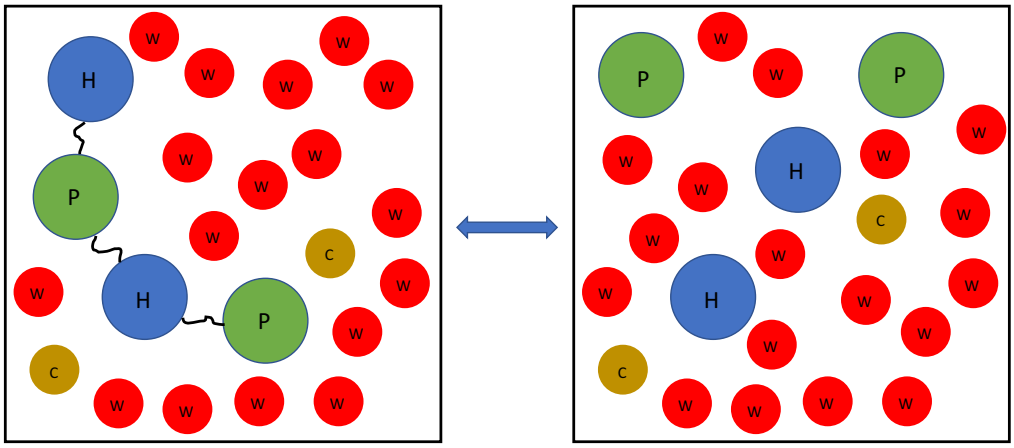

Figure 8.1: In this figure, the left panel schematically shows a polymer consisting of nonpolar hydrophobic (H) beads and charged hydrophilic (P) beads connected by covalent polymer bonds, in solution with water (W), and charged counter ions (C). In the right panel, the covalent bonds connecting the monomers are broken, leaving us a solution containing only small rigid molecules. The system in the right panel is called the broken-bond system in this thesis.

To find out the appropriate mimic system as shown in Chapter 3.3 and the Short Solvent Model as shown in Chapter 5 which could preserve the structure of the polymers, it is beneficial to consider a situation where the covalent bonds connecting the monomers are broken, leaving us a solution containing only small rigid solutes. An illustration of this "breaking bond transformation" is shown in Figure 8.1. In the

following context we will call the solution with free mobile monomers the "broken-bond system". We will assume the broken-bond system still shares the same long ranged intermolecular interactions as the original system, which are denoted as

$$u_{\mathrm{MM'}}(r) = u_{0,\mathrm{MM'}}(r) + u_{1,\mathrm{MM'}}(r)\,, \tag{8.1}$$

M and M′ represents the various types of molecules in the solution, such as the monomers, solvent molecules, co-ions, counter ions, etc.

The broken-bond system contains only rigid molecular monomers, and we already know how to manipulate the intermolecular interactions of this system following the discussions in Chapter 3. Suppose that for the broken-bond system we found a new set of interactions

$$u_{R,\mathrm{MM'}}(r) = u_{0,\mathrm{MM'}}(r) + u_{R1,\mathrm{MM'}}(r) \tag{8.2}$$

which could preserve its structure, then the structure of the original system can also be preserved if switched to this new set of interactions $\{u_{R,\mathrm{MM'}}(r)\}$, based on the discussions in Appendix B. This special connection of the intermolecular interactions in the original and broken-bond system may provide us a convenient way to find out appropriate simplifications of interactions which could preserve the structure of the solution containing polymers. The validity of this argument is to be tested in the future.

Another future development is to further explore the influence of manipulating the long ranged interactions on dynamics. In Chapter 7 we already discussed the

influence on the diffusion dynamics of the single-site solutes in water. When we are studying the diffusion dynamics, the system is still at equilibrium state. In the future we plan to examine the influence of using the effective interactions when the system is undergoing nonequilibirum processes. Some early work shows that the dynamics of the mimic system is different from the dynamics of the target system when undergoing nonequilibirum processes. To be more precise, suppose H is the Hamiltonian of the target system and H_R is the Hamiltonian of the mimic system with effective interactions. Suppose at $t = 0$ the two systems are the same initial condition in the ensemble sense, which means that they have the same probability distribution function

$$f(\Gamma) = f_R(\Gamma) \tag{8.3}$$

at $t = 0$. Γ is a point in phase space. $f(\Gamma)$ is the probability distribution function of the target system. $f_R(\Gamma)$ is the probability distribution function of the mimic system. Early work shows that even if these two systems are subject to the same external perturbations or "protocols", they still might have different "ensemble of trajectories", in the trajectory space, which means that

$$f(\Gamma, t) \neq f_R(\Gamma, t)\,. \tag{8.4}$$

$f(\Gamma, t)$ is the probability distribution function of the target system at time t. $f_R(\Gamma, t)$ is the corresponding one in the mimic system.

Early work of a current member of Weeks group–Teddy Baker, shows that one might need an additional time dependent field $\phi_R(\boldsymbol{r}, t)$ added to the mimic system to

make sure the mimic system has the same trajectories as the target system. Since it is technically complicated to implement a time-dependent field in MD simulations, we have generalized the linear response theory such that it could be applied to a nonequilibrium reference systems. By making use of the generalized linear response theory, we might be able take in to account the time-dependent field $\phi_R(\boldsymbol{r}, t)$ as a perturbation to the mimic system. The details about the generalized linear response theory are shown in Appendix C. Collaborating with Teddy Baker, we will further pursue this idea in the future.

Appendix A

The correspondence between the interactions and correlation functions for mixtures

If we know the temperature, volume, number of particles and the interactions between the particles, we are able to uniquely determine the thermodynamic state of a system. All the other thermodynamics observables, including pair correlation functions, 3-body correlation functions etc, can be determined based on these information. An inverse question is that if we know the spatial correlation functions between particles instead of the interactions between particles, can we still uniquely determine the thermodynamics state of a system? In a paper by Zwicker and Lovett, it is shown that this argument is true for a pure system. It is proved in that paper that one can use T, V, N, $\rho^{(1)}(\boldsymbol{r})$ and $\rho^{(2)}(\boldsymbol{r}, \boldsymbol{r'})$ to uniquely specify the state of a system. To prove this, Lovett has used the fact that the free energy is a convex function of the interactions $\phi(\boldsymbol{r})$ and $u(\boldsymbol{r}, \boldsymbol{r'})$. I have found this idea of using convexity to be generalizable to mixtures and will show it in the following part.

I will demonstrate the idea using binary mixtures. I will also assume that the mixture is uniform, which means no external fields. However, notice that the conclusions obtained in the following part can be easily generalized to mixtures with many species and nonuniform cases.

Let's consider a uniform binary mixture consisting of specie A and specie B with pairwise intermolecular interactions. The Hamiltonian for this mixture is

$$H = \sum_{i=1}^{N_{\mathrm{A}}} \sum_{j=1}^{N_{\mathrm{B}}} u_{\mathrm{AB}}(\boldsymbol{r}_i, \boldsymbol{r}_j) + \sum_{i=1}^{N_{\mathrm{A}}-1} \sum_{j=i+1}^{N_{\mathrm{A}}} u_{\mathrm{AA}}(\boldsymbol{r}_i, \boldsymbol{r}_j) + \sum_{i=1}^{N_{\mathrm{B}}-1} \sum_{j=i+1}^{N_{\mathrm{B}}} u_{\mathrm{BB}}(\boldsymbol{r}_i, \boldsymbol{r}_j)\,. \tag{A.1}$$

u_{AB} is the pair interaction between A and B. Similarly, u_{AA} is the pair interaction between A and A. u_{BB} is the pair interaction between B and B.

In many thermodynamics textbooks, the Helmholtz free energy is considered to be a function of temperature T, volume V and number of particles N. However, it is in fact also a functional of the interactions u, if we allow the interactions to vary. For example, for this binary mixture mentioned above, the Helmholtz free energy is

$$A = A(T, V, N_{\mathrm{A}}, N_{\mathrm{B}}, u_{\mathrm{AB}}, u_{\mathrm{AA}}, u_{\mathrm{BB}}) = -kT \ln \int e^{-\beta H} d\tau\,, \tag{A.2}$$

where H is defined in Eq (A.1).

We can take the partial derivative of A with respect to T, V, N_{A} and N_{B} respectively and get

$$\begin{aligned} \frac{\partial A}{\partial T} &= -S \\ \frac{\partial A}{\partial V} &= -P \\ \frac{\partial A}{\partial N_{\mathrm{A}}} &= \mu_{\mathrm{A}} \\ \frac{\partial A}{\partial N_{\mathrm{B}}} &= \mu_{\mathrm{B}}\,, \end{aligned} \tag{A.3}$$

which are classic textbook results.

We can also take functional derivatives of A with respect to $u_{\mathrm{AB}}(\boldsymbol{r},\boldsymbol{r'})$, $u_{\mathrm{AA}}(\boldsymbol{r},\boldsymbol{r'})$ and $u_{\mathrm{BB}}(\boldsymbol{r},\boldsymbol{r'})$. It can be shown that we get the following results

$$\begin{aligned}
\frac{\delta A}{\delta u_{\mathrm{AB}}(\boldsymbol{r},\boldsymbol{r'})} &= \rho^{(2)}_{\mathrm{AB}}(\boldsymbol{r},\boldsymbol{r'}) \\
\frac{\delta A}{\delta u_{\mathrm{AA}}(\boldsymbol{r},\boldsymbol{r'})} &= \frac{1}{2}\rho^{(2)}_{\mathrm{AA}}(\boldsymbol{r},\boldsymbol{r'}) \\
\frac{\delta A}{\delta u_{\mathrm{BB}}(\boldsymbol{r},\boldsymbol{r'})} &= \frac{1}{2}\rho^{(2)}_{\mathrm{BB}}(\boldsymbol{r},\boldsymbol{r'})
\end{aligned} \tag{A.4}$$

The procedures for doing these functional derivatives are long but not hard. A pedagogical description can be found in Ref [62]. $\rho^{(2)}_{\mathrm{AB}}(\boldsymbol{r},\boldsymbol{r'})$ is the probability density of finding one A particle at position $\boldsymbol{r}$ and another B particle at position $\boldsymbol{r'}$. Similarly, $\rho^{(2)}_{\mathrm{AA}}(\boldsymbol{r},\boldsymbol{r'})$ is the probability density of finding one A particle at position $\boldsymbol{r}$ and another A particle at position $\boldsymbol{r'}$. $\rho^{(2)}_{\mathrm{BB}}(\boldsymbol{r},\boldsymbol{r'})$ is the probability density of finding one B particle at position $\boldsymbol{r}$ and another B particle at position $\boldsymbol{r'}$. They are directly related to radial distribution functions when the pair interactions are spherically symmetric, which are shown as follows

$$\begin{aligned}
\rho^{(2)}_{\mathrm{AB}}(\boldsymbol{r},\boldsymbol{r'}) &= \frac{N_{\mathrm{A}}}{V}\frac{N_{\mathrm{B}}}{V}g_{\mathrm{AB}}(|\boldsymbol{r}-\boldsymbol{r'}|) \\
\rho^{(2)}_{\mathrm{AA}}(\boldsymbol{r},\boldsymbol{r'}) &= \frac{N_{\mathrm{A}}}{V}\frac{N_{\mathrm{A}}}{V}g_{\mathrm{AA}}(|\boldsymbol{r}-\boldsymbol{r'}|) \\
\rho^{(2)}_{\mathrm{BB}}(\boldsymbol{r},\boldsymbol{r'}) &= \frac{N_{\mathrm{B}}}{V}\frac{N_{\mathrm{B}}}{V}g_{\mathrm{BB}}(|\boldsymbol{r}-\boldsymbol{r'}|)\,.
\end{aligned} \tag{A.5}$$

It is known that $A(T,V,N_{\mathrm{A}},N_{\mathrm{B}},u_{\mathrm{AB}},u_{\mathrm{AA}},u_{\mathrm{BB}})$ is a convex function of T, V, N_{A} and N_{B}. The convexity guarantees us that we can do the Legendre transform with respect to T, V, N_{A} and N_{B} and get new free energies, which can also specify the state of a system just as the Helmholtz free energy A does but use different

variables as arguments. For example, we can define a new free energy as

$$G(T, P, N_{\mathrm{A}}, N_{\mathrm{B}}, u_{\mathrm{AB}}, u_{\mathrm{AA}}, u_{\mathrm{BB}}) = A + PV\,, \tag{A.6}$$

which is just the Gibbs free energy of this system. As you can see it uses pressure P instead of volume V as its argument. However, we are still able to recover V from G with the following relationship

$$V = \frac{\partial G}{\partial P}\,. \tag{A.7}$$

This shows that G does contain same amount of information as A.

In the following part, we are going to show that $A(T, V, N_{\mathrm{A}}, N_{\mathrm{B}}, u_{\mathrm{AB}}, u_{\mathrm{AA}}, u_{\mathrm{BB}})$ is a convex functional of $u_{\mathrm{AB}}(\boldsymbol{r}, \boldsymbol{r'})$, $u_{\mathrm{AA}}(\boldsymbol{r}, \boldsymbol{r'})$ and $u_{\mathrm{BB}}(\boldsymbol{r}, \boldsymbol{r'})$. To prove this convexity, we need to use the following theorem, which is found in the paper by Lovett.

Theorem A.0.1 (Zwicker and Lovett) *Let $A(T, V, N, H)$ denote the Helmholtz free energy of a system with Hamiltonian H at state $\{T, V, N\}$. We have the following inequality*

$$A(T, V, N, H + \Delta H) \leq A(T, V, N, H) + \langle \Delta H \rangle\,. \tag{A.8}$$

ΔH is a perturbation over the Hamiltonian H. $\langle \Delta H \rangle$ is defined as

$$\langle \Delta H \rangle = \frac{\int d\tau \Delta H e^{-\beta H}}{\int d\tau e^{-\beta H}}\,, \tag{A.9}$$

which is the ensemble average of ΔH in the ensemble defined at $\{T, V, N, H\}$.

The proof for this theorem is as follows.

Proof Let's begin the proof by defining $\tilde{A}(T, V, N, H, f)$ as

$$\tilde{A}(T, V, N, H, f) = \int d\tau f(H + k_B T \ln f) \,. \tag{A.10}$$

As you can see, $\tilde{A}(T, V, N, H, f)$ is a functional of f, which maps any normalized distribution function $f(\boldsymbol{r}_1, \cdots, \boldsymbol{r}_N, \boldsymbol{p}_1, \cdots, \boldsymbol{p}_N)$ to a real number.

$\tilde{A}(T, V, N, H, f)$ is related to the Helmholtz free energy $A(T, V, N, H)$ by the following relationship

$$\tilde{A}(T, V, N, H, f) - A(T, V, N, H) = k_B T \int d\tau f \ln \frac{f}{f_{eq}} \,, \tag{A.11}$$

where

$$f_{eq}(\boldsymbol{r}_1, \cdots, \boldsymbol{r}_N, \boldsymbol{p}_1, \cdots, \boldsymbol{p}_N) = e^{\beta(A - H(\boldsymbol{r}_1, \cdots, \boldsymbol{r}_N, \boldsymbol{p}_1, \cdots, \boldsymbol{p}_N))} \tag{A.12}$$

is the equilibrium distribution function. To prove Eq (A.11) one just needs to substitute the definition of f_{eq} in and do some algebraic manipulations. The right hand side of Eq (A.11) is usually called the relative entropy.

Based on Eq (A.11) and using the fact that f and f_{eq} are normalized, we can further get

$$\begin{aligned} \tilde{A}(T, V, N, H, f) - A(T, V, N, H) &= k_B T \int d\tau (f \ln \frac{f}{f_{eq}} - f + f_{eq}) \\ &= k_B T \int d\tau f_{eq} (\frac{f}{f_{eq}} \ln \frac{f}{f_{eq}} - \frac{f}{f_{eq}} + 1) \\ &= k_B T \langle x \ln x - x + 1 \rangle \,, \end{aligned} \tag{A.13}$$

where $x = \frac{f}{f_{eq}}$. For $x \geq 0$, $x \ln x - x + 1 \geq 0$ and equality obtains only at $x = 1$. Thus

$$\tilde{A}(T, V, N, H, f) \geq A(T, V, N, H) \tag{A.14}$$

with equality realized only be $f = f_{eq}$.

If two distinct Hamiltonians H and $\bar{H} = H + \Delta H$ have equilibrium distributions f_{eq} and $\bar{f}_{eq}$,

$$\begin{aligned} A(T,V,N,H) &= \int d\tau f_{eq}(H + k_B T \ln f_{eq}) \\ &= \int d\tau f_{eq}(H - \bar{H}) + \int d\tau f_{eq}(\bar{H} + k_B T \ln f_{eq}) \\ &= -\langle \Delta H \rangle + \tilde{A}(T,V,N,\bar{H},f_{eq}) \\ &\geq -\langle \Delta H \rangle + A(T,V,N,\bar{H}) \,. \end{aligned} \tag{A.15}$$

Now, we have proved that

$$A(T,V,N,H+\Delta H) \leq A(T,V,N,H) + \langle \Delta H \rangle \,. \quad \blacksquare \tag{A.16}$$

Theorem A.0.1 focuses on case when the system has only one species. However, if one goes through the proof, one can easily see that Theorem A.0.1 is also applicable to mixtures. For example, for binary mixture, we can get

$$A(T,V,N_{\rm A},N_{\rm B},H+\Delta H) \leq A(T,V,N_{\rm A},N_{\rm B},H) + \langle \Delta H \rangle \,. \tag{A.17}$$

Now come back to the question about the convexity of $A(T,V,N_{\rm A},N_{\rm B},u_{\rm AB},u_{\rm AA},u_{\rm BB})$ over of $u_{\rm AB}(\boldsymbol{r},\boldsymbol{r'})$, $u_{\rm AA}(\boldsymbol{r},\boldsymbol{r'})$ and $u_{\rm BB}(\boldsymbol{r},\boldsymbol{r'})$. Suppose we change

$$\begin{aligned} u_{\rm AB}(\boldsymbol{r},\boldsymbol{r'}) &\to u_{\rm AB}(\boldsymbol{r},\boldsymbol{r'}) + \Delta u_{\rm AB}(\boldsymbol{r},\boldsymbol{r'}) \\ u_{\rm AA}(\boldsymbol{r},\boldsymbol{r'}) &\to u_{\rm AA}(\boldsymbol{r},\boldsymbol{r'}) + \Delta u_{\rm AA}(\boldsymbol{r},\boldsymbol{r'}) \\ u_{\rm BB}(\boldsymbol{r},\boldsymbol{r'}) &\to u_{\rm BB}(\boldsymbol{r},\boldsymbol{r'}) + \Delta u_{\rm BB}(\boldsymbol{r},\boldsymbol{r'}) \,. \end{aligned} \tag{A.18}$$

The Hamiltonian of the system will change from H to $H + \Delta H$ correspondingly. According to Eq (A.17) we have

$$\begin{aligned}
&A(T, V, N_{\mathrm{A}}, N_{\mathrm{B}}, u_{\mathrm{AB}} + \Delta u_{\mathrm{AB}}, u_{\mathrm{AA}} + \Delta u_{\mathrm{AA}}, u_{\mathrm{BB}} + \Delta u_{\mathrm{BB}}) \\
\leq &A(T, V, N_{\mathrm{A}}, N_{\mathrm{B}}, u_{\mathrm{AB}}, u_{\mathrm{AA}}, u_{\mathrm{BB}}) + \langle \Delta H \rangle \\
= &A(T, V, N_{\mathrm{A}}, N_{\mathrm{B}}, u_{\mathrm{AB}}, u_{\mathrm{AA}}, u_{\mathrm{BB}}) + \int d\boldsymbol{r} d\boldsymbol{r'} \rho^{(2)}_{\mathrm{AB}}(\boldsymbol{r}, \boldsymbol{r'}) \Delta u_{\mathrm{AB}}(\boldsymbol{r}, \boldsymbol{r'}) \\
&+ \frac{1}{2} \int d\boldsymbol{r} d\boldsymbol{r'} \rho^{(2)}_{\mathrm{AA}}(\boldsymbol{r}, \boldsymbol{r'}) \Delta u_{\mathrm{AA}}(\boldsymbol{r}, \boldsymbol{r'}) + \frac{1}{2} \int d\boldsymbol{r} d\boldsymbol{r'} \rho^{(2)}_{\mathrm{BB}}(\boldsymbol{r}, \boldsymbol{r'}) \Delta u_{\mathrm{BB}}(\boldsymbol{r}, \boldsymbol{r'}) \,.
\end{aligned} \tag{A.19}$$

From Eq (A.19), one can see that $A(T, V, N_{\mathrm{A}}, N_{\mathrm{B}}, u_{\mathrm{AB}}, u_{\mathrm{AA}}, u_{\mathrm{BB}})$ is a convex functional of $u_{\mathrm{AB}}(\boldsymbol{r}, \boldsymbol{r'})$, $u_{\mathrm{AA}}(\boldsymbol{r}, \boldsymbol{r'})$ and $u_{\mathrm{BB}}(\boldsymbol{r}, \boldsymbol{r'})$. Based on the convexity we can do Legendre transforms of A to get new free energies. For example, one can do the following Legendre transform

$$\begin{aligned}
&B(T, V, N_{\mathrm{A}}, N_{\mathrm{B}}, \rho^{(2)}_{\mathrm{AB}}, \rho^{(2)}_{\mathrm{AA}}, \rho^{(2)}_{\mathrm{BB}}) \\
= &A - \int d\boldsymbol{r} d\boldsymbol{r'} \rho^{(2)}_{\mathrm{AB}}(\boldsymbol{r}, \boldsymbol{r'}) u_{\mathrm{AB}}(\boldsymbol{r}, \boldsymbol{r'}) \\
&- \frac{1}{2} \int d\boldsymbol{r} d\boldsymbol{r'} \rho^{(2)}_{\mathrm{AA}}(\boldsymbol{r}, \boldsymbol{r'}) u_{\mathrm{AA}}(\boldsymbol{r}, \boldsymbol{r'}) - \frac{1}{2} \int d\boldsymbol{r} d\boldsymbol{r'} \rho^{(2)}_{\mathrm{BB}}(\boldsymbol{r}, \boldsymbol{r'}) u_{\mathrm{BB}}(\boldsymbol{r}, \boldsymbol{r'}) \,.
\end{aligned} \tag{A.20}$$

The new defined free energy B is a function of $T, V, N_{\mathrm{A}}, N_{\mathrm{B}}$ and a functional of $\rho^{(2)}_{\mathrm{AB}}, \rho^{(2)}_{\mathrm{AA}}, \rho^{(2)}_{\mathrm{BB}}$. This tells us that we can use the pair correlation functions to specify the state of mixture. The pair interactions are still recoverable from B according to

$$\begin{aligned}
\frac{\delta B}{\delta \rho^{(2)}_{\mathrm{AB}}(\boldsymbol{r}, \boldsymbol{r'})} &= u_{\mathrm{AB}}(\boldsymbol{r}, \boldsymbol{r'}) \\
\frac{\delta B}{\delta \frac{1}{2} \rho^{(2)}_{\mathrm{AA}}(\boldsymbol{r}, \boldsymbol{r'})} &= u_{\mathrm{AA}}(\boldsymbol{r}, \boldsymbol{r'}) \\
\frac{\delta B}{\delta \frac{1}{2} \rho^{(2)}_{\mathrm{BB}}(\boldsymbol{r}, \boldsymbol{r'})} &= u_{\mathrm{BB}}(\boldsymbol{r}, \boldsymbol{r'}) \,.
\end{aligned} \tag{A.21}$$

The unique existence of B guarantees that there exists and only exists one set of pair interactions $\{u_{\mathrm{AB}}, u_{\mathrm{AA}}, u_{\mathrm{BB}}\}$ corresponding to the pair correlation functions $\{\rho^{(2)}_{\mathrm{AB}}, \rho^{(2)}_{\mathrm{AA}}, \rho^{(2)}_{\mathrm{BB}}\}$.

We can construct another free energy C as follows

$$\begin{aligned} &C(T, V, N_{\mathrm{A}}, N_{\mathrm{B}}, \rho^{(2)}_{\mathrm{AB}}, u_{\mathrm{AA}}, \rho^{(2)}_{\mathrm{BB}}) \\ =&A - \int d\boldsymbol{r} d\boldsymbol{r'} \rho^{(2)}_{\mathrm{AB}}(\boldsymbol{r}, \boldsymbol{r'}) u_{\mathrm{AB}}(\boldsymbol{r}, \boldsymbol{r'}) - \frac{1}{2} \int d\boldsymbol{r} d\boldsymbol{r'} \rho^{(2)}_{\mathrm{BB}}(\boldsymbol{r}, \boldsymbol{r'}) u_{\mathrm{BB}}(\boldsymbol{r}, \boldsymbol{r'}) \,. \end{aligned} \tag{A.22}$$

As you can see, C uses both pair correlation functions and pair interactions as its arguments. Although it may seem strange, C is still a valid free energy which could completely specify the state of a system. More importantly, C is very closely related to our framework of manipulating the long ranged interactions.

In our framework, we want to construct a mimic system, whose solvent-solvent interaction $u_{R,\mathrm{AA}}(r)$ has freely a chosen long tail, while the solute-solute interaction $u_{R,\mathrm{BB}}(r)$ and solute-solvent interaction $u_{R,\mathrm{AB}}(r)$ are are chosen such that $g_{R,\mathrm{AB}}(r) = g_{\mathrm{AB}}(r)$ and $g_{R,\mathrm{BB}}(r) = g_{\mathrm{BB}}(r)$. In other words, we are using $\{u_{R,\mathrm{AA}}(r), g_{\mathrm{AB}}(r), g_{\mathrm{BB}}(r)\}$ to specify the mimic system, and these three arguments are the same arguments used by free energy C. $u_{R,\mathrm{AB}}(r)$ and $u_{R,\mathrm{BB}}(r)$ can be obtained directly from C

$$\begin{aligned} \frac{\delta C}{\delta \rho^{(2)}_{\mathrm{AB}}(\boldsymbol{r}, \boldsymbol{r'})} &= \frac{\delta C}{\delta \frac{N_{\mathrm{A}}}{V} \frac{N_{\mathrm{B}}}{V} g_{\mathrm{AB}}(\boldsymbol{r}, \boldsymbol{r'})} = u_{R,\mathrm{AB}}(|\boldsymbol{r} - \boldsymbol{r'}|) \\ \frac{\delta C}{\delta \frac{1}{2} \rho^{(2)}_{\mathrm{BB}}(\boldsymbol{r}, \boldsymbol{r'})} &= \frac{\delta C}{\delta \frac{1}{2} \frac{N_{\mathrm{B}}}{V} \frac{N_{\mathrm{B}}}{V} g_{\mathrm{BB}}(\boldsymbol{r}, \boldsymbol{r'})} = u_{R,\mathrm{BB}}(|\boldsymbol{r} - \boldsymbol{r'}|) \,. \end{aligned} \tag{A.23}$$

The unique existence of C guarantees the unique existence of $u_{R,\mathrm{AB}}(r)$ and $u_{R,\mathrm{BB}}(r)$.

Although in principle $u_{R,\mathrm{AB}}(r)$ and $u_{R,\mathrm{BB}}(r)$ can be obtained from C, it is

really hard to get the explicit form of C. So we still need the formulas described in Chapter 3 to get $u_{R,\mathrm{AB}}(r)$ and $u_{R,\mathrm{BB}}(r)$ approximately.

Appendix B

Deriving the interactions in the mimic system from a free energy perspective

Based on the previous work of Remsing, Liu and Weeks [23], I have been able to rederive the results shown in Chapter 3 from the free energy perspective. We will focus on the manipulation of Coulomb interactions in this appendix but the method developed in this appendix can be generalized to manipulate other slowly varying long ranged interactions.

Let us consider a system where N solutes, labeled as $1, 2, 3, \cdots, i, \cdots, N$, are in solution with solvent A. We want to manipulate the long ranged tail of the Coulomb interactions between these species in the following way.

$$\left\{ \begin{array}{c} v_{\mathrm{AA}}(r) = v_0(r) + v_1(r) \\ v_{i\mathrm{A}}(r) = v_0(r) + v_1(r) \\ v_{ij}(r) = v_0(r) + v_1(r) \end{array} \right\} \Rightarrow \left\{ \begin{array}{c} v_{R,\mathrm{AA}}(r) = v_0(r) + v_{R1,\mathrm{AA}}(r) \\ v_{R,i\mathrm{A}}(r) = v_0(r) + v_{R1,i\mathrm{A}}(r) \\ v_{R,ij}(r) = v_0(r) + v_{R1,ij}(r) \end{array} \right\} \tag{B.1}$$

The new set of Coulomb interaction $\{v_{R,\mathrm{AA}}(r), v_{R,i\mathrm{A}}(r), v_{R,ij}(r)\}$, which defines the mimic system, should be chosen such that the structure of the mimic system is the same as the target system. Since A is the dominant species, we could manipulate $v_{R1,\mathrm{AA}}(r)$ freely without affect the $\mathrm{A}-\mathrm{A}$ radial distribution function. $v_{R1,i\mathrm{A}}(r)$ and $v_{R1,ij}(r)$ are chosen to match the following two conditions.

- Condition 1:

$$\rho^q_{\mathrm{A}}(\boldsymbol{r}|\{\boldsymbol{r}_1\cdots\boldsymbol{r}_N\}) \approx \rho^q_{R,\mathrm{A}}(\boldsymbol{r}|\{\boldsymbol{r}_1\cdots\boldsymbol{r}_N\}) \tag{B.2}$$

- Condition 2:

$$\omega(\boldsymbol{r}_1,\boldsymbol{r}_2\cdots\boldsymbol{r}_N) \approx \omega_R(\boldsymbol{r}_1,\boldsymbol{r}_2\cdots\boldsymbol{r}_N) \tag{B.3}$$

Condition 1 means that the charge density generated by solvent A given the solutes are fixed in configuration $\boldsymbol{R} = \{\boldsymbol{r}_1\cdots\boldsymbol{r}_N\}$ should be the same in the target and mimic system. Condition 2 means that the N-solutes potential of mean force should be the same in the target and mimic system. Notice that we are demanding the match of many-body correlation functions in Condition 1 and 2, which is a much stronger requirement than just matching the pair correlation function. The implications of this stronger requirement is discussed at the end of this appendix.

Let us consider how to satisfy Condition 1 first. According to LMF theory, to satisfy Condition 1 we need an external LMF field

$$\begin{aligned}\phi_R(\boldsymbol{r}) &= \sum_{i=1}^{N} q_i v_0(|\boldsymbol{r}-\boldsymbol{r}_i|) + \phi_{R1}(\boldsymbol{r}) \\ &= \sum_{i=1}^{N} q_i v_0(|\boldsymbol{r}-\boldsymbol{r}_i|) + \sum_{i=1}^{N} q_i v_1(|\boldsymbol{r}-\boldsymbol{r}_i|) \\ &\quad + \int d\boldsymbol{r}'\rho^q_{R|\mathrm{A}}(\boldsymbol{r}'|\{\boldsymbol{r}_1\cdots\boldsymbol{r}_N\})\big(v_1(|\boldsymbol{r}-\boldsymbol{r}'|) - v_{R1,\mathrm{AA}}(|\boldsymbol{r}-\boldsymbol{r}'|)\big)\end{aligned} \tag{B.4}$$

This external field acts on the solvent particles. The solutes are fixed in configuration $\boldsymbol{R} = \{\boldsymbol{r}_1\cdots\boldsymbol{r}_N\}$, which is viewed as external perturbation in the framework of LMF theory. q_i is the charge of solute i.

In our mimic system, there is no external fields, but we have manipulated interactions. We want to choose the manipulated solute-solvent Coulomb interactions $v_{R,i\mathrm{A}}(r)$ such that they will produce the LMF field shown in Eq.(B.4). More precisely, we want

$$\sum_{i=1}^{N} q_i v_{R,i\mathrm{A}}(|\boldsymbol{r}-\boldsymbol{r}_i|) = \phi_R(\boldsymbol{r})\,. \tag{B.5}$$

To solve the equation above, we need to make the following linear approximation of charge densities

$$\rho^q_{\mathrm{A}}(\boldsymbol{r}|\{\boldsymbol{r}_1\cdots\boldsymbol{r}_N\}) \approx \sum_{i=1}^{N} \rho^q_{\mathrm{A}|i}(|\boldsymbol{r}-\boldsymbol{r}_i|)\,, \tag{B.6}$$

where $\rho^q_{\mathrm{A}|i}(|\boldsymbol{r}-\boldsymbol{r}_i|)$ is the charge density of A when a single ion i is solvated. This approximation may not be very accurate in the molecular scale, but in our derivation the charge density of the solvent is always convoluted with the slowly varying long ranged potential, which smoothes the charge density over the molecular scale. Therefore the possible error in using this approximation will be greatly reduced by the convolution.

Based on this approximation Eq.(B.5) can be rewritten as

$$\sum_{i=1}^{N} q_i v_{R,i\mathrm{A}}(|\boldsymbol{r}-\boldsymbol{r}_i|) = \sum_{i=1}^{N} \Big(q_i v(|\boldsymbol{r}-\boldsymbol{r}_i|) + \int d\boldsymbol{r}' \rho^q_{\mathrm{A}|i}(|\boldsymbol{r}'-\boldsymbol{r}_i|)\big(v_1(|\boldsymbol{r}-\boldsymbol{r}'|) - v_{R1,\mathrm{AA}}(|\boldsymbol{r}-\boldsymbol{r}'|)\big)\Big) \tag{B.7}$$

which further gives

$$v_{R,i\mathrm{A}}(r) = v(r) - \frac{1}{q_i}\int d\boldsymbol{r}' \rho^q_{\mathrm{A}|i}(|\boldsymbol{r}'-\boldsymbol{r}|)\big(v_{R1,\mathrm{AA}}(|\boldsymbol{r}-\boldsymbol{r}'|) - v_1(|\boldsymbol{r}-\boldsymbol{r}'|)\big)\,. \tag{B.8}$$

As you can see by matching Condition 1 we have derived the expression for $v_{R1,i\mathrm{A}}(r)$.

The result is the same as what we obtained by making use of YBG hierarchy, as shown in Eq.(3.31).

Now let us consider how to match Condition 2. First of all, I will define the free energy difference between the target and mimic system given the solutes fixed at $\boldsymbol{R} = \{\boldsymbol{r}_1 \cdots \boldsymbol{r}_N\}$ as $\Omega_{\boldsymbol{R}}$, which is illustrated by the Figure B.1.

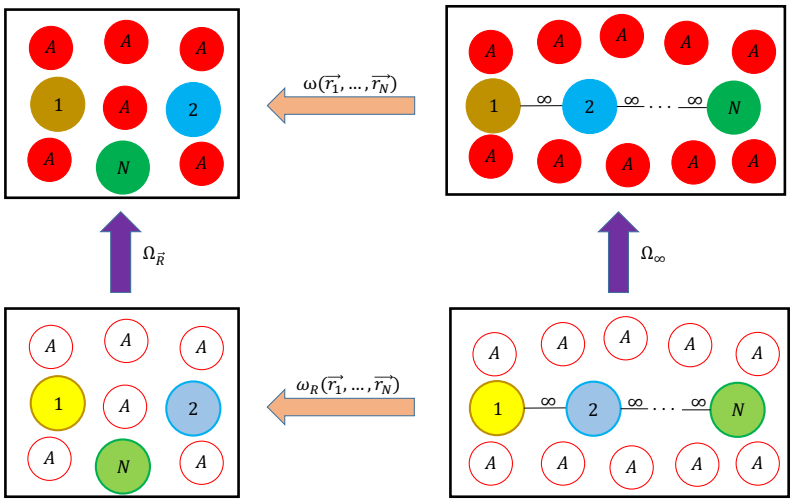

Figure B.1: In this figure the top left panel represents the target system with the solutes fixed at configuration $\boldsymbol{R} = \{\boldsymbol{r}_1 \cdots \boldsymbol{r}_N\}$. The top right panel represents the target system with the solutes separated infinitely far away. The bottom left panel represents the mimic system with the solutes fixed at configuration $\boldsymbol{R} = \{\boldsymbol{r}_1 \cdots \boldsymbol{r}_N\}$. The bottome right panel represents the mimic system with the solutes separated infinitely far away. $\Omega_{\boldsymbol{R}}$ is the free energy difference between the top left and bottom left panel. Similarly, Ω_∞ is the free energy difference between the top right and bottom right panel. $\omega(\boldsymbol{r}_1 \cdots \boldsymbol{r}_N)$ is the free energy difference between top left and top right panel, which can also be interpreted as the N-solutes potential of mean force of the target system. Similarly, $\omega_R(\boldsymbol{r}_1 \cdots \boldsymbol{r}_N)$ is the N-solutes potential of mean force of the mimic system.

Also, let us define the free energy difference between the bulk A fluid interacting with $v(r)$ and the bulk A fluid interacting with $v_{R,\mathrm{AA}}(r)$ as Ω_{ref}, which is illustrated in Figure B.2. Based on the Ref [23], we have the following expression

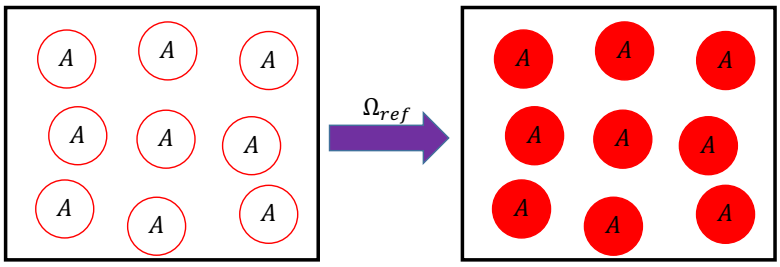

Figure B.2: The left panel shows the bulk A fluid interacting with $v_{R,\mathrm{AA}}(r)$. The right panel shows the bulk A fluid interacting with $v(r)$. Their free energy difference is Ω_{ref}. The bulk A fluid shown in this figure has the same bulk density and temperature as the A solvent in the dilute solution shown in Figure B.1.

$$\begin{aligned}\Omega_{\boldsymbol{R}} - \Omega_{ref} = &-\frac{1}{2}\int d\boldsymbol{r}\rho^{q}_{\mathrm{A}}(\boldsymbol{r}|\{\boldsymbol{r}_1\cdots\boldsymbol{r}_N\})\sum_{i=1}^{N} q_i\big(v_{R,i\mathrm{A}}(|\boldsymbol{r}-\boldsymbol{r}_i|) - v(|\boldsymbol{r}-\boldsymbol{r}_i|)\big) \\ &-\sum_{i<j} q_i q_j\big(v_{R,ij}(|\boldsymbol{r}_j-\boldsymbol{r}_i|) - v(|\boldsymbol{r}_j-\boldsymbol{r}_i|)\big)\,,\end{aligned} \tag{B.9}$$

which can be simplified using the linear approximation shown in Eq.(B.6), which will give us

$$\begin{aligned}\Omega_{\boldsymbol{R}} - \Omega_{ref} = &-\frac{1}{2}\sum_{i=1}^{N}\sum_{j=1}^{N}\int d\boldsymbol{r}\rho^{q}_{\mathrm{A}|j}(|\boldsymbol{r}-\boldsymbol{r}_j|)q_i\big(v_{R,i\mathrm{A}}(|\boldsymbol{r}-\boldsymbol{r}_i|) - v(|\boldsymbol{r}-\boldsymbol{r}_i|)\big) \\ &-\sum_{i<j} q_i q_j\big(v_{R,ij}(|\boldsymbol{r}_j-\boldsymbol{r}_i|) - v(|\boldsymbol{r}_j-\boldsymbol{r}_i|)\big)\,.\end{aligned} \tag{B.10}$$

Now consider the special case where the solute particles are infinitely far apart. In this case, the free energy difference between the target and mimic system is defined

as Ω_∞, which is illustrated in Figure B.1.

It is easy to show that

$$\Omega_\infty - \Omega_{ref} = -\frac{1}{2}\sum_{i=1}^{N}\int d\boldsymbol{r}d\boldsymbol{r}'\rho^q_{\mathrm{A}|i}(|\boldsymbol{r}-\boldsymbol{r}_i|)q_i\big(v_{R,i\mathrm{A}}(|\boldsymbol{r}-\boldsymbol{r}_i| - v(|\boldsymbol{r}-\boldsymbol{r}_i|)\big)\,, \quad \text{(B.11)}$$

which is basically Eq.(B.10) without the coupling terms between different i and j, since they are infinitely far away.

Based on Eq.(B.10) and Eq.(B.11), we are able to match Condition 2. From Figure B.1 it is easy to see that

$$\begin{aligned}\omega(\boldsymbol{r}_1\cdots\boldsymbol{r}_N) - \omega_R(\boldsymbol{r}_1\cdots\boldsymbol{r}_N) = \Omega_{\boldsymbol{R}} - \Omega_\infty &= (\Omega_{\boldsymbol{R}} - \Omega_{ref}) - (\Omega_\infty - \Omega_{ref}) \\ &= -\sum_{i<j}\int d\boldsymbol{r}\rho^q_{\mathrm{A}|j}(|\boldsymbol{r}-\boldsymbol{r}_j|)q_i\big(v_{R,i\mathrm{A}}(|\boldsymbol{r}-\boldsymbol{r}_i| - v(|\boldsymbol{r}-\boldsymbol{r}_i|) \\ &\quad - \sum_{i<j} q_iq_j\big(v_{R,ij}(|\boldsymbol{r}_j-\boldsymbol{r}_i| - v(|\boldsymbol{r}_j-\boldsymbol{r}_i|)\big)\,.\end{aligned} \quad \text{(B.12)}$$

Condition 2 requires that $\omega(\boldsymbol{r}_1,\boldsymbol{r}_2\cdots\boldsymbol{r}_N) \approx \omega_R(\boldsymbol{r}_1,\boldsymbol{r}_2\cdots\boldsymbol{r}_N)$, which would be satisfied if

$$v_{R,ij}(r) = v(r) - \frac{1}{q_j}\int d\boldsymbol{r}'\rho^q_{\mathrm{A}|j}(r')\big(v_{R,i\mathrm{A}}(|\boldsymbol{r}-\boldsymbol{r}'| - v(|\boldsymbol{r}-\boldsymbol{r}'|)\big)\,. \quad \text{(B.13)}$$

This is the same as what we obtained from YBG hierarchy, as shown in Eq.(3.32).

Now we have found the $v_{R,i\mathrm{A}}(r)$ and $v_{R,ij}(r)$ which satisfy Condition 1 and 2. This mimic system R can also be simplified to the Short Sovlent Model, following steps shown in Chapter 5. It can be shown that t $v_{\tilde{R},ij}(r)$ have the same expression as what is obtained in Chapter 5. The derivations are basically the same as the derivations made previously and therefore will not be repeated here.

Condition 1 and 2 means that the probability for any configuration of the N solutes to occur is the same in the target and mimic system. Now consider a case when the N solutes are covalently bonded to form a polymer. The configurational space of the polymer will be just a subspace of the configurational space of the N free mobile solutes. Since we have found potentials which will preserve the structure of the N solutes over the whole configurational space, these potentials will certainly also preserve the structure of the polymer formed by the N solutes. This implies that when we are trying to find appropriate manipulation of interactions for polymers, we can dissect the polymer into single-site beads or monomers, and the same interactions which will preserve the structure of monomers will also preserve the structure of polymer. Notice that this implication is much stronger than what is implied by the "YBG hierarchy derivation" shown in Chapter 3. This is due to the fact that we have used the linear approximation of the charge density(Eq.(B.6)), which is not used by "YBG hierarchy derivation". Using this additional approximation does enable us to make a stronger conclusion, but it may also bring extra error. Therefore, this stronger conclusion may not be as accurate as expected in some scenarios.

Appendix C

Linear response theory for nonequilibrium reference systems

The linear response theory, which tells us how a system responds to an external perturbation, has been proved to be a very useful tool in understanding the statistics of liquids. The importance of linear response theory for liquid simulation is that all the statistical quantities of the perturbed system can be obtained from the correlation functions of the reference system. Thus the simulation for the perturbed system can be avoid, and only the simulation for the reference system is necessary. Based on this nice simplification, it has been used in many scenarios. For example, the famous Green-Kubo formula, which is derived by making use of linear response theory, can give us various transport coefficients of liquids. However, one requirement for the linear response theory is that the reference system has to be in an equilibrium state. This requirement restricts the application of linear response theory, because in some cases one needs to perturb a nonequilibrium system. Various efforts have been made to generalize linear response theory so that it can be used with the nonequilibrium reference system. Evans [63] has successfully generalized linear response theory to systems which are in steady state. However, how to generalize linear response theory so that it can be applied to a system that is in general nonequilibrium state is still a problem. In this appendix I will explore

this problem and try to apply linear response theory to nonequilibrium reference systems which satisfy the local equilibrium assumption.

C.1 Review of Linear Response Theory

In this section, I will give a review of the original linear response theory. The linear response theory is based on the famous Liouville equation

$$\frac{\partial f(\Gamma)}{\partial t} = \mathcal{L} f(\Gamma)\,, \tag{C.1}$$

where $\mathcal{L}$ is the Liouville operator, Γ is a point in phase space, $f(\Gamma)$ is the probability distribution function in phase space. For a system that follows Hamiltonian dynamics, $\mathcal{L} = \{H,\ \}$, where H is the Hamiltonian of the system. If a Langevin thermostat is applied to the system, $\mathcal{L} = \{H,\ \} + \mathcal{L}_{diffuse}$. You can see that along with the Hamiltonian term there is an additional diffusion term in the Liouville operator for the Langevin thermostat.

To understand the linear response theory, assume that we have a reference system which is in equilibrium and its distribution function is $f_0(\Gamma)$, where Γ denotes a point in phase space. If we turn on a perturbation at $t = 0$, the system will be driven away from the equilibrium. The distribution function of the system under perturbation will become $f(\Gamma, t) \approx f_0(\Gamma) + f_1(\Gamma, t)$, where $f_1(\Gamma, t)$ represents the leading order effect of the perturbation. Basically, what linear response theory does is that it tells us how to express $f_1(\Gamma, t)$ in terms of $f_0(\Gamma)$. Let us use H_0 to denote the Hamiltonian of the reference system and use H_1 to denote the perturbation

Hamiltonian. When H_1 is much smaller than H_0, linear response theory gives the following result

$$f_1(\Gamma, t) = \int_0^t ds e^{(t-s)\mathcal{L}_0}\{H_1, f_0\}\,. \tag{C.2}$$

If the perturbation is an external field, denoted as $\phi(\boldsymbol{r}, t)$, we will have $H_1 = \sum_{i=1}^n \phi(\boldsymbol{r}_i, t)$, where $\boldsymbol{r}_i$ is the coordinate of particle i. In that case, we will have

$$\{H_1, f_0\} = (\beta \sum_{i=1}^n \boldsymbol{F}_{ext}(\boldsymbol{r}_i, t) \cdot \boldsymbol{v}_i) f_0 \coloneqq P(\Gamma, t) f_0\,, \tag{C.3}$$

where I have made the definition that $P(\Gamma, t) = \beta \sum_{i=1}^n \boldsymbol{F}_{ext}(\boldsymbol{r}_i, t) \cdot \boldsymbol{v}_i$.

If we consider the ensemble average of an observable $A(\Gamma)$, we can get

$$\begin{aligned} < A >_t &= \int d\Gamma f(\Gamma, t) A(\Gamma) \\ &= < A >_{ref} + \int d\Gamma f_1(\Gamma, t) A(\Gamma) \\ &= < A >_{ref} + \int_0^t ds < P_s A_t >_{ref}\ . \end{aligned} \tag{C.4}$$

I did not give the complete derivation above since the derivation needed here is a special case of the more general derivation shown below. Notice that the perturbation part of $< A >_t$ can be obtained by integrating the time correlation function $< P_s A_t >_{ref}$, where the subscripts indicate that the time correlation function is for the reference system.

After all, we reached the conclusion that the ensemble average of an observable in the perturbed system can be obtained from the corresponding time correlation function in the reference system.

C.2 Nonequilibrium Reference System And Local Equilibrium

As I mentioned before, the classic linear response theory only applies when the reference system is in equilibrium. However, what will happen when the reference system is not in equilibrium? For example, suppose that we have a reference system which is not in equilibrium at $t = 0$, whose distribution function $f_0(\Gamma, t = 0) \neq f_{eq}(\Gamma)$. After $t = 0$ the system will gradually relax to the equilibrium state. Now suppose that we put a perturbation to this system during this relaxation process. How will the relaxing system respond to the perturbation? Do we have some theory similar to linear response theory? This is the question I want to answer in this appendix.

The nonequilibrium processes are generally very complicated. However, the local equilibrium hypothesis can help us understand it. The local equilibrium hypothesis states that for a system in the local equilibrium state, the movements of particles are equilibrated locally, due to the collisions between the neighbor particles. The local equilibrium state can be described by local variables. For example, a pure liquid in local equilibrium state can be described by density field $\rho(\boldsymbol{r}, t)$, velocity field $\boldsymbol{v}(\boldsymbol{r}, t)$, temperature field $T(\boldsymbol{r}, t)$ and so on. Based on the local equilibrium hypothesis, people have brought out many macroscopic theories, like the Fick's law, Fourier's law, ect, to describe the evolution of these fields. These macroscopic theories are quite successful, but have ignored the fluctuations of the system. For this work, these local fields will be obtained by the ensemble average. For example, if

you want to get the velocity field for a pure fluid at a given time, you need to do the following ensemble average.

$$\boldsymbol{v}(\boldsymbol{r},t)=\frac{<\sum_i \boldsymbol{v}_i\delta(\boldsymbol{r}-\boldsymbol{r}_i)>_t}{<\sum_i \delta(\boldsymbol{r}-\boldsymbol{r}_i)>_t}\,, \tag{C.5}$$

and if you want the temperature field, you need

$$T(\boldsymbol{r},t)=\frac{m}{3k}\frac{<\sum_i(\boldsymbol{v}_i-\boldsymbol{v}(\boldsymbol{r},t))^2\delta(\boldsymbol{r}-\boldsymbol{r}_i)>_t}{<\sum_i \delta(\boldsymbol{r}-\boldsymbol{r}_i)>_t}\,, \tag{C.6}$$

from where you can see the meaning of the temperature field is actually the variance field of the Maxwell distribution.

The local equilibrium hypothesis can help us a lot when we try to develop the linear response theory for the nonequilibrium refernce system. Based on the discussions above, we know that the state of a local equilibrium liquid can be described by local variables. Based on this, I want to make the following statement.

For a simple pure liquid, its distribution function at local equilibrium will have the following form

$$f(\boldsymbol{r}_1,...,\boldsymbol{r}_n,\boldsymbol{v}_1,...,\boldsymbol{v}_n,t)=\prod_{i=1}^{n} e^{-\frac{m}{2kT(\boldsymbol{r}_i,t)}(\boldsymbol{v}_i-\boldsymbol{v}(\boldsymbol{r}_i,t))^2} g(\boldsymbol{r}_1,...,\boldsymbol{r}_n,t)\,. \tag{C.7}$$

Its physical meaning is that the velocity distribution for each particle satisfies Maxwell distribution locally. The width and the mean of the Maxwell distribution are determined by the temperature field and velocity field respectively.

For complex fluids, like glasses, polymers and colloids, the local equilibrium hypothesis may not be true [64]. So in this appendix, we will only focus on the simple pure liquid, which is good enough to illustrate our idea.

C.3 Linear response theory for nonequilibrium reference system

In this section, I derive the linear response theory for reference systems which are undergoing nonequilibrium processes.

First of all, suppose that we have a reference system, which is undergoing a nonequilibrium process. The nonequilibrium process starts at $t = 0$. To simplify our discussions, the reference system is assumed to be a simple pure liquid. To develop our "generalized" linear response theory, we need to make the assumption that the nonequilibrium reference system is *always* in local equilibrium, which is to say that the distribution function of the reference system $f_0(\Gamma, t)$ satisfies

$$f_0(\boldsymbol{r}_1, ..., \boldsymbol{r}_n, \boldsymbol{v}_1, ..., \boldsymbol{v}_n, t) = \prod_{i=1}^{n} e^{-\frac{m}{2kT(\boldsymbol{r}_{i,t})}(\boldsymbol{v}_i - \boldsymbol{v}(\boldsymbol{r}_{i,t}))^2} g(\boldsymbol{r}_1, ..., \boldsymbol{r}_n, t), \quad t > 0\,. \quad \text{(C.8)}$$

Of course this is an approximation. The reference fluid needs some relaxation time τ_{le} to relax to the local equilibrium state. So the equation above should only be true for $t > \tau_{le}$. However, the time scale of the macroscopic dynamics of the fluid is usually larger than τ_{le}. So Eq. (C.8) will be a good approximation if one is interested in the macroscopic dynamics of the liquid.

Now, suppose that we put a perturbation on this nonequilibrium reference system at $t = 0$. The perturbation is assumed to be an external potential $\phi_{ext}(\boldsymbol{r}, t)$. The system with the external potential turned on is called the perturbed system. Its distribution function is denoted by $f(\Gamma, t)$, which coincides with $f_0(\Gamma, 0)$ at $t = 0$

$$f(\Gamma, 0) = f_0(\Gamma, 0)\,. \quad \text{(C.9)}$$

The Liouville operator for the perturbed system is $\mathcal{L} = \mathcal{L}_0 + \mathcal{L}_1$, where $\mathcal{L}_0$ is the Liouville operator for the reference system and $\mathcal{L}_1$ is the Liouville operator of the perturbed part

$$\mathcal{L}_1 = \{H_1, \ \}\,. \tag{C.10}$$

$H_1 = \sum_{i=1}^{n} \phi_{ext}(\boldsymbol{r}_i, t)$ is the perturbation Hamiltonian.

When the perturbation is small, we can expand the distribution function of the perturbed system

$$f(\Gamma, t) \approx f_0(\Gamma, t) + f_1(\Gamma, t)\,, \tag{C.11}$$

where $f_0(\Gamma, t)$ is the distribution function for the relaxing reference system and $f_1(\Gamma, t)$ is the leading order effect of the response to the perturbation.

The Liouville equation for the perturbed system is

$$\frac{\partial f}{\partial t} = \mathcal{L} f\,. \tag{C.12}$$

If we put $f = f_0 + f_1$ and $\mathcal{L} = \mathcal{L}_0 + \mathcal{L}_1$ into it and rearrange the terms by their orders, we can get

$$\begin{aligned} \frac{\partial f_0}{\partial t} &= \mathcal{L}_0 f_0 \\ \frac{\partial f_1}{\partial t} &= \mathcal{L}_0 f_1 + \mathcal{L}_1 f_0\,. \end{aligned} \tag{C.13}$$

By solving the second equation we can get the expression of f_1

$$\begin{aligned} f_1(\Gamma, t) &= \int_0^t ds\, T[e^{\int_s^t d\tau \mathcal{L}_0(\tau)}] \mathcal{L}_1 f_0(\Gamma, s) \\ &= \int_0^t ds\, T[e^{\int_s^t d\tau \mathcal{L}_0(\tau)}] \{H_1(\Gamma, s), f_0(\Gamma, s)\}\,. \end{aligned} \tag{C.14}$$

Notice that $\{H_1, f_0\}$ is evaluated at position Γ and time s. $T[...]$ means time ordered product since we assume that $\mathcal{L}_0$ can vary with time.

Eq. (C.14) is our basis for the following derivation. Assume that the local equilibrium hypothesis is always true for the relaxing reference system, which means that f_0 satisfies

$$f_0(\boldsymbol{r}_1, ..., \boldsymbol{r}_n, \boldsymbol{v}_1, ..., \boldsymbol{v}_n, t) = \prod_{i=1}^{n} e^{-\frac{m}{2kT(\boldsymbol{r}_i,t)}(\boldsymbol{v}_i - \boldsymbol{v}(\boldsymbol{r}_i,t))^2} g(\boldsymbol{r}_1, ..., \boldsymbol{r}_n, t)\,. \tag{C.15}$$

With the help of Eq.(C.15) we are able to evaluate $\{H_1, f_0\}$

$$\begin{aligned} \{H_1(\Gamma, s), f_0(\Gamma, s)\} &= \sum_{i=1}^{n} \frac{\partial \phi_{ext}(\boldsymbol{r}_i, s)}{\partial \boldsymbol{r}_i} \cdot \frac{\partial f_0(\Gamma, s)}{\partial \boldsymbol{v}_i} \\ &= \sum_{i=1}^{n} \frac{1}{kT(\boldsymbol{r}_i, s)} \boldsymbol{F}_{ext}(\boldsymbol{r}_i, s) \cdot (\boldsymbol{v}_i - \boldsymbol{v}(\boldsymbol{r}_i, s)) f_0(\Gamma, s) \end{aligned} \tag{C.16}$$

Let's define $P(\Gamma, s)$ as

$$P(\Gamma, s) = \sum_{i=1}^{n} \frac{1}{kT(\boldsymbol{r_i}, s)} \boldsymbol{F}_{ext}(\boldsymbol{r}_i, s) \cdot (\boldsymbol{v}_i - \boldsymbol{v}(\boldsymbol{r}_i, s))\,. \tag{C.17}$$

Thus, we have

$$\{H_1(\Gamma, s), f_0(\Gamma, s)\} = P(\Gamma, s) f_0(\Gamma, s)\,. \tag{C.18}$$

Thus, f_1 can be further simplified

$$\begin{aligned} f_1(\Gamma, t) &= \int_0^t ds\, T[e^{\int_s^t d\tau \mathcal{L}_0(\tau)}] P(\Gamma, s) f_0(\Gamma, s) \\ &= \int_0^t ds \int d\Gamma'\, T[e^{\int_s^t d\tau \mathcal{L}_0(\tau)}] \delta(\Gamma - \Gamma') P(\Gamma', s) f_0(\Gamma', s) \\ &= \int_0^t ds \int d\Gamma' P(\Gamma', s) f_0(\Gamma', s) T[e^{\int_s^t d\tau \mathcal{L}_0(\tau)}] \delta(\Gamma - \Gamma') \\ &= \int_0^t ds \int d\Gamma' P(\Gamma', s) f_0(\Gamma', s) K_0(\Gamma, t | \Gamma', s)\,, \end{aligned} \tag{C.19}$$

where $K_0(\Gamma, t|\Gamma', s) = T[e^{\int_s^t d\tau \mathcal{L}_0(\tau)}]\delta(\Gamma - \Gamma')$ is the propagator of the reference system.

Now if we consider the ensemble average of observable $A(\Gamma)$ at time t for the perturbed system, we can get

$$\begin{aligned} < A >_t &= \int d\Gamma f(\Gamma, t) A(\Gamma) \\ &= < A >_{ref,t} + \int d\Gamma f_1(\Gamma, t) A(\Gamma) \\ &= < A >_{ref,t} + \int_0^t ds d\Gamma d\Gamma' A(\Gamma) K_0(\Gamma, t|\Gamma', s) P(\Gamma', s) f_0(\Gamma', s) \\ &= < A >_{ref,t} + \int_0^t ds < P_s A_t >_{ref} , \end{aligned} \tag{C.20}$$

Thus, for the nonequilibrium reference system, we obtained a similar expression as for the equilibrium reference system (see Section 1). The perturbation part of $< A >_t$ can still be expressed as an integral of the time correlation function of the reference system. The only difference is the definition of the observable $P(\Gamma, s)$. For the equilibrium reference system

$$P(\Gamma, s) = \frac{1}{kT} \sum_{i=1}^{n} \boldsymbol{F}_{ext}(\boldsymbol{r}_i, s) \cdot \boldsymbol{v}_i , \tag{C.21}$$

and for the nonequilibrium reference system

$$P(\Gamma, s) = \sum_{i=1}^{n} \frac{1}{kT(\boldsymbol{r_i}, s)} \boldsymbol{F}_{ext}(\boldsymbol{r}_i, s) \cdot (\boldsymbol{v}_i - \boldsymbol{v}(\boldsymbol{r}_i, s)) . \tag{C.22}$$

You can see that the nonequilibrium formula will become the equilibrium formula when $T(\boldsymbol{r}, s) = T_0$ and $\boldsymbol{v}(\boldsymbol{r}, s) = 0$. So what we get for the nonequilibrium reference system is a natural generalization of the equilibrium case.

As I mentioned before, the classic linear response theory tells us how an equilibrium reference system responds to a perturbation. Similarly, the generalized

linear response theory tells us how a nonequilibrium reference system responds to a perturbation. So the meaning of the generalized linear response theory is that it gives us more flexibility in choosing the reference systems. This can be useful when we want to put a strong perturbation on the equilibrium reference system. When the perturbation is strong, the classic linear response theory will fail. However, if we use a nonequilibrium reference system which is close enough to the perturbed system, the generalized linear response theory may be able to predict the properties of the perturbed system.

C.4 Simulation Result

In this section I am going to verify the generalized linear response theory by computer simulation. The system I studied is WCA pure fluid, which is the most simple model of simple liquid. A large WCA core is fixed inside the WCA fluid. As we know, if we change the WCA fluid surrounding the large core into a LJ fluid, there will be drying effect around the surface of the large core, which is due to the attractions between LJ particles. This effect can be taken account in by LMF theory. LMF theory proposes that one can put an effective field around the large core to represent the drying effect. Meanwhile the surrounding fluid keeps as the WCA fluid. The effective drying potential can be calculated by LMF theory. Now, to verify the generalized linear response formula, suppose that the drying potential $\phi_{dry}(\boldsymbol{r})$ is turned on at $t = 0$. The system will be driven from the non-drying state

to the drying state. To get the properties of this drying process, we could take the non-drying state as our reference system and apply the classic linear response theory formula. However, because the drying potential is too big, the classic linear response theory wouldn't work very well. A better choice is to take a "half-drying" process as our reference. By "half-drying" I mean to turn on a portion of the drying potential. The "half-drying" process is closer to the drying process. So we can take it as our reference of perturbation. The other portion of the drying potential is taken account in by the generalized linear response formula, as described in previous sections.

Here are the parameters for the simulation and the results. The simulation temperature and density for the WCA fluid is $\rho^* = 0.72$ and $T^* = 0.92$. The diameter of the large WCA core is fixed in the origin, which is twice as large as the surrounding WCA fluid. The drying potential $\phi_{dry}(\boldsymbol{r})$ is shown in Figure (C.1) . The relaxing reference system is constructed by turning on the external potential $\phi_{ext} = 0.7\phi_{dry}(\boldsymbol{r})$, which is a large portion of the drying potential. The initial state for the reference system is the non-drying state. The other portion of the the drying potential is taken as the perturbation and is taken account it by the generalized linear response theory we developed. The direct simulation of the perturbed system is also done, so that we can compare it with the results obtained from generalized linear response theory.

In Figure C.2 , the density of the WCA fluid around the large core during the nonequilibrium process is plotted. From Figure C.2, we can see that the generalized

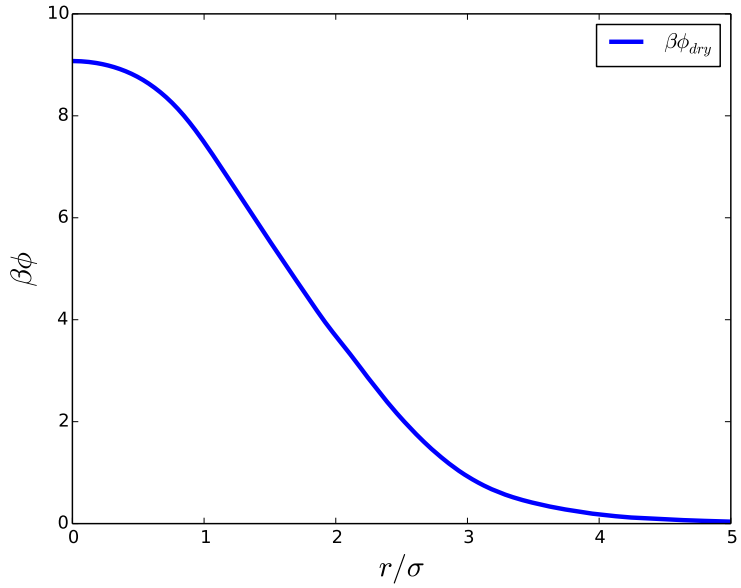

Figure C.1: This figure shows the drying potential obtained by LMF theory which drives the WCA particles away from the large WCA core.

linear response theory is able to correct the density of the reference system to the density of the perturbed system.

C.5 Conclusion

In this chapter, we developed the generalized linear response theory, which is the perturbation theory for the nonequilibrium reference system. Our new formula relies on the local equilibrium hypothesis. Computer simulation results have been given to verify the generalized linear response theory. The limitation of the generalized linear response theory is the same as the classic linear response theory, which is that the reference system has be be close enough to the perturbed system. Further developments involve how to develop the linear response theory to complex fluids and stronger perturbations.

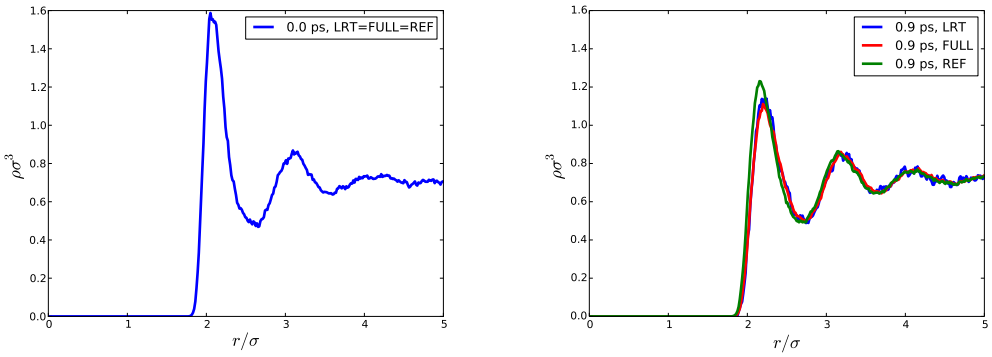

(a)

(b)

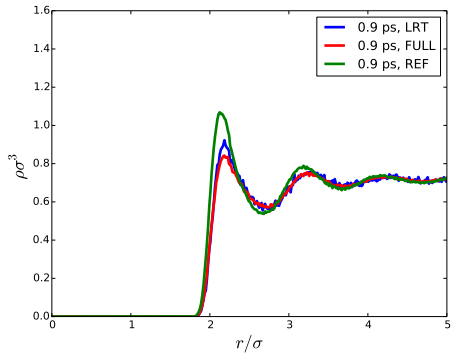

(c)

Figure C.2: This figure shows the density distribution around the large core at different times. "REF" represents the relaxing reference system. "FULL" represents the perturbed system. "LRT" represents the results obtained by generalized linear response theory. At $t = 0$ the three curves coincide because they have the same initial condition. "LRT" basically matches "FULL" in these graphs, which means that the generalized linear response theory is able to predict the perturbed system.

Bibliography

[1] Van der Waals. J. D. Thesis. *Leiden*, 1873.

[2] B Widom. Intermolecular forces and the nature of the liquid state. *Science*, 157:375–382, 1967.

[3] J D Weeks, D Chandler, and Hans C Andersen. Role of repulsive forces in determining the equilibrium structure of simple liquids. *The Journal of Chemical Physics*, 54(12):5237–5247, 1971.

[4] Jocelyn M. Rodgers, Zhonghan Hu, and John D. Weeks. On the efficient and accurate short-ranged simulations of uniform polar molecular liquids. *Molecular Physics*, 109:1195–1211, 2011.

[5] Jocelyn M. Rodgers and John D. Weeks. Accurate thermodynamics for short-ranged truncations of coulomb interactions in site-site molecular models. *The Journal of Chemical Physics*, 131, 2009.

[6] John D. Weeks, K Vollmayr, and K Katsov. Intermolecular forces and the structure of uniform and nonuniform fluids. *Physica A*, 244(1-4):461–475, 1997.

[7] Yng-gwei Chen, Charanbir Kaur, and John D Weeks. Connecting systems with short and long ranged interactions: Local molecular field theory for ionic fluids. *The Journal of Physical Chemistry B*, 108:19874–19884, 2004.

[8] Yng-Gwei Chen and John D. Weeks. Local molecular field theory for effective attractions between like charged objects in systems with strong coulomb interactions. *Proceedings of the National Academy of Sciences*, 103:7560–7565, 2006.

[9] Jocelyn M. Rodgers, Charanbir Kaur, Yng-Gwei Chen, and John D. Weeks. Attraction between like-charged walls: Short-ranged simulations using local molecular field theory. *Phys. Rev. Lett.*, 97:097801, 2006.

[10] Jocelyn M Rodgers and John D Weeks. Local molecular field theory for the treatment of electrostatics. *Journal of Physics: Condensed Matter*, 20:494206, 2008.

[11] Jocelyn M. Rodgers and John D. Weeks. Interplay of local hydrogen-bonding and long-ranged dipolar forces in simulations of confined water. *Proceedings of the National Academy of Sciences*, 105:19136–19141, 2008.

[12] Zhonghan Hu and John D. Weeks. Efficient solutions of self-consistent mean field equations for dewetting and electrostatics in nonuniform liquids. *Phys. Rev. Lett.*, 105:140602, 2010.

[13] Shule Liu, Zhonghan Hu, John D Weeks, and John T Fourkas. Structure of liquid propionitrile at interfaces. 1. molecular dynamics simulations. *The Journal of Physical Chemistry C*, 116:4012–4018, 2012.

[14] K Lum, D Chandler, and JD Weeks. Hydrophobicity at small and large length scales. *Journal Of Physical Chemistry B*, 103(22):4570–4577, 1999.

[15] David Chandler. Interfaces and the driving force of hydrophobic assembly. *Nature*, 437(7059):640–647, September 2005.

[16] Katharina Vollmayr-Lee, Kirill Katsov, and John D. Weeks. Using mean field theory to determine the structure of uniform fluids. *The Journal of Chemical Physics*, 114:416–425, 2001.

[17] Richard C Remsing and John D Weeks. Dissecting hydrophobic hydration and association. *The Journal of Physical Chemistry B*, 117:15479–15491, 2013.

[18] Mahfoud Belhadj, Howard E. Alper, and Ronald M. Levy. Molecular dynamics simulations of water with ewald summation for the long range electrostatic interactions. *Chemical Physics Letters*, 179:13–20, 1991.

[19] L R Pratt and D Chandler. Effects of solute-solvent attractive forces on hydrophobic correlations. *J. Chem. Phys.*, 73:3434 – 41, 1980.

[20] B. Roux and T. Simonson. Implicit solvent models. *Biophysical chemistry*, 78:1–20, 1999.

[21] Kirill Katsov and John D Weeks. Incorporating molecular scale structure into the van der waals theory of the liquid-vapor interface. *The Journal of Physical Chemistry B*, 106:8429–8436, 2002.

[22] R. Evans. *Density functionals in the theory of nonuniform fluids. Fundamentals of Inhomogeneous Fluids.* Number 85-175. Dekker, New York, 1992.

[23] Richard C Remsing, Shule Liu, and John D Weeks. Long-ranged contributions to solvation free energies from theory and short-ranged models. *Proceedings of the National Academy of Sciences*, 113:2819–2826, 2016.

[24] J.-P. Hansen and I. R. McDonald. *Theory of Simple Liquids.* Academic Press, 1976.

[25] H. J. C. Berendsen, J. R. Grigera, and T. P. Straatsma. The missing term in effective pair potentials. *J Phys Chem*, 91(24):6269–6271, 1987.

[26] Michael W. Mahoney and William L. Jorgensen. A five-site model for liquid water and the reproduction of the density anomaly by rigid, nonpolarizable potential functions. *The Journal of Chemical Physics*, 112, 2000.

[27] Richard C. Remsing, Jocelyn M. Rodgers, and John D. Weeks. Deconstructing classical water models at interfaces and in bulk. *Journal of Statistical Physics*, 145:313–334, 2011.

[28] Richard C. Remsing. From structure to thermodynamics with local molecular field theory. *PhD thesis University of Maryland*, 2013.

[29] In-Chul Yeh and Max L. Berkowitz. Ewald summation for systems with slab geometry. *The Journal of Chemical Physics*, 111:3155–3162, 1999.

[30] Ulrich Essmann, Lalith Perera, Max L. Berkowitz, Tom Darden, Hsing Lee, and Lee G. Pedersen. A smooth particle mesh ewald method. *The Journal of Chemical Physics*, 103:8577–8593, 1995.

[31] Lawrence R. Pratt and D. Chandler. Effects of solute-solvent attractive forces on hydrophobic correlations. *The Journal of Chemical Physics*, 73:3434, 1980.

[32] David M. Huang and D. Chandler. The hydrophobic effect and the influence of solute-solvent attractions. *The Journal of Physical Chemistry B*, 106:2407–2053, 2002.

[33] D. Asthagiri, S. Merchant, and L. R. Pratt. Role of attractive methane-water interactions in the potential of mean force between methane molecules in water. *J. Chem. Phys.*, 128:244512, 2008.

[34] L. A. Girifalco. Molecular properties of c_{60} in the gas and solid phase. *The Journal of Physical Chemistry*, 96:858–861, 1992.

[35] N. Choudhury. A molecular dynamics simulation study of buckyballs in water: Atomistic versus coarse-grained models of c_{60}. *The Journal of Chemical Physics*, 125:034502, 2006.

[36] L. R. Pratt and D. Chandler. Theory of the hydrophobic effect. *J. Chem. Phys.*, 67:3683–3704, 1977.

[37] L. R. Pratt. Theory of hydrophobic effects. *Ann. Rev. Phys. Chem.*, 36:433 –449, 1985.

[38] Mangesh I Chaudhari, Susan B Rempe, D Asthagiri, L Tan, and L R Pratt. Molecular Theory and the Effects of Solute Attractive Forces on Hydrophobic Interactions. *J. Phys. Chem. B*, 120:1864–1870, 2016.

[39] D. Asthagiri, S. Merchant, and L. R. Pratt. Role of attractive methane-water interactions in the potential of mean force between methane molecules in water. *J. Chem. Phys.*, 128:244512, 2008.

[40] F H Stillinger. Structure in aqueous solutions of nonpolar solutes from the standpoint of scaled-particle theory. *J. Soln. Chem.*, 2:141, 1973.

[41] C Chipot, Pohorille A, and eds. *Free Energy Calculations: Theory and Applications in Chemistry and Biology*. Springer, Berlin, 2007.

[42] Roland Schulz, Benjamin Lindner, Loukas Petridis, and Jeremy C. Smith. Scaling of multimillion-atom biological molecular dynamics simulation on a petascale supercomputer. *Journal of Chemical Theory and Computation*, 5:2798–2808, 2009.

[43] Robert Pierotti. A scaled particle theory of aqueous and nonaqueous solutions. *Chemical Reviews*, pages 717–726, 1976.

[44] Charles Tanford. Interfacial free energy and the hydrophobic effect. *Proceedings of the National Academy of Sciences*, 76:4175–4176, 1979.

[45] W Clark Still, Anna Tempczyk, Ronald C Hawley, and Thomas Hendrickson. Semianalytical treatment of solvation for molecular mechanics and dynamics. *Journal of the American Chemical Society*, 112:6127–6129, 1990.

[46] Di Qiu, Peter S Shenkin, Frank P Hollinger, and W Clark Still. The gb/sa continuum model for solvation. a fast analytical method for the calculation of approximate born radii. *The Journal of Physical Chemistry A*, 101:3005–3014, 1997.

[47] Michael Schaefer and Martin Karplus. A comprehensive analytical treatment of continuum electrostatics. *The Journal of Physical Chemistry*, 100:1578–1599, 1996.

[48] Jianhan Chen, Charles L. Brooks, and Jana Khandogin. Recent advances in implicit solvent-based methods for biomolecular simulations. *Current Opinion in Structural Biology*, 18:140–148, 2008.

[49] Ruhong Zhou. Free energy landscape of protein folding in water: Explicit vs. implicit solvent. *Proteins: Structure, Function, and Bioinformatics*, 53:148?161, 2003.

[50] Jianhan Chen and Charles L. Brooks. Critical importance of length-scale dependence in implicit modeling of hydrophobic interactions. *Journal of the American Chemical Society*, 129:2444–2445, 2007.

[51] Richard C Remsing and John D Weeks. Role of local response in ion solvation: Born theory and beyond. *The Journal of Physical Chemistry B*, 120:6238–6249, 2016.

[52] David Chandler. Dielectric constant and related equilibrium properties of molecular fluids: Interaction site cluster theory analysis. *Journal of Chemical Physics*, 67:1113–1124, 1977.

[53] G Hummer, L R Pratt, A E Garcia, B J Berne, and S W Rick. Electrostatic potentials and free energies of solvation of polar and charged molecules. *Journal of Physical Chemistry B*, 101:3017–3020, 1997.

[54] S. Koneshan, Jayendran C. Rasaiah, R. M. Lynden-Bell, and S. H. Lee. Sovlent structure, dynamics, and ion mobility in aqueous solutions at 25 c. *The Journal of Physical Chemistry B*, 102:4193–4204, 1998.

[55] T. Yamaguchi and Y. Kimura. Effects of solute-solvent and solvent-solvent attractive interactions on solute diffusion. *Molecular Physics*, 2000.

[56] Peter G. Wolynes. Molecular theory of solvated ion dynamics. *The Journal of Chemical Physics*, 1978.

[57] Robert Zwanzig. Dielectric friction on a moving ion. *The Journal of Chemical Physics*, 1963.

[58] P. W. Atkins. *Physical Chemistry*. Oxford University Press, 5th edition, 1994.

[59] Mark E. Tuckerman. *Statistical Mechanics: Theory and Molecular Simulation*. Oxford University Press, 2010.

[60] Robert Zwanzig. *Nonequilibrium Statistical Mechanics*. Oxford University Press, 2001.

[61] J P Hansen and I R McDonald. *Theory of Simple Liquids*. Academic Press, 3rd edition, 2005.

[62] J.-P. Hansen and I. R. McDonald. *Theory of Simple and Liquids*. Academic Press, 3rd edition edition, 2006.

[63] Denis J. Evans and Gray Morriss. *Statistical Mechanics of Nonequilibrium Liquids*. Cambridge University Press, 2nd edition, 2008.

[64] J.M.G. Vilar and J.M. Rubi. Thermodynamics "beyond" local equilibrium. *Proceedings Of The National Academy Of Sciences Of The United States Of America*, 98:11081–4, 2001.